Master of Science Thesis

A Study of Free Edge Stresses and Delamination Initiation in Fibre Reinforced Composite Laminates

Priyanshu Anand

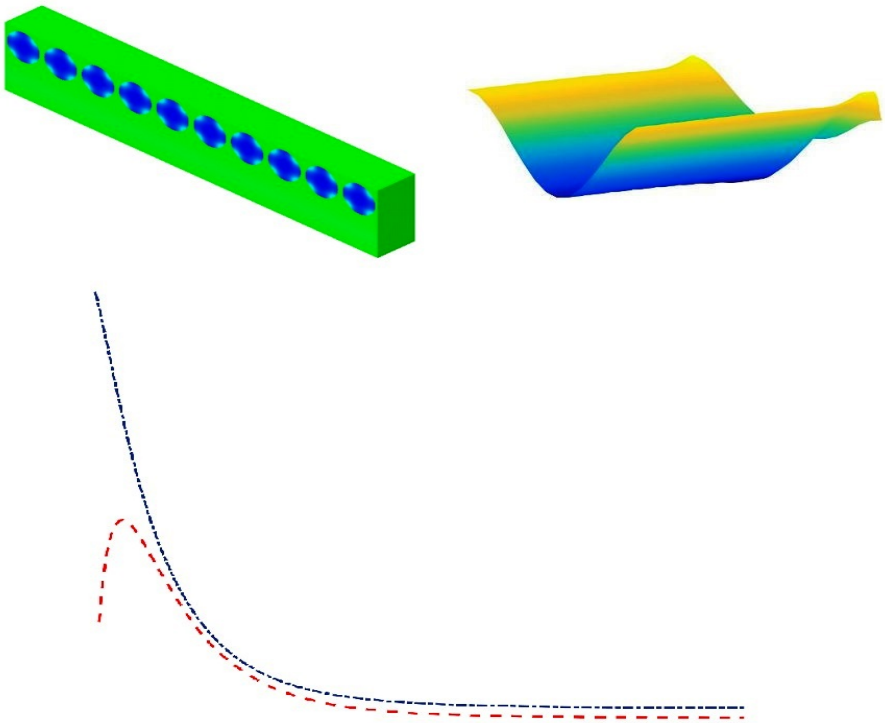

Faculty of Aerospace Engineering · Delft University of Technology

TU Delft Delft University of Technology

A Study of Free Edge Stresses and Delamination Initiation in Fibre Reinforced Composite Laminates

Master of Science Thesis

For obtaining the degree of Master of Science in Aerospace Engineering
at Delft University of Technology

Priyanshu Anand

28th August 2017

Faculty of Aerospace Engineering · Delft University of Technology

Delft University of Technology
Faculty of Aerospace Engineering
Department of Aerospace Structures and Materials

GRADUATION COMMITTEE

Dated: 28th August 2017

Chair holder:

Dr. Sergio R. Turteltaub

Committee members:

Dr. Boyang Chen

Dr. Daniël Peeters

Dr.ir. F.P. van der Meer

Abstract

Near free edges of fibre reinforced composite laminates modelled with homogeneous material layers, the presence of high gradient interlaminar stresses has been found by theoretical means. The steep gradient in stresses has come to be known as the free edge effect. Over a span of nearly 50 years, the free edge stresses have been studied through various methods. The high gradient stresses, sometimes to an extent of a singularity, have been found to be a mathematical artefact. Hence, the analysis of such high gradient stresses near free edges could be computationally expensive. At the same time, it is imperative that an estimate of interlaminar stresses at the free edge be made because the interlaminar stresses play a part in initiating delamination and hence, to be able to predict delamination initiation through a convenient criterion for prediction of delamination initiation, their values in the free edge region need to be known.

The abrupt material discontinuity at the interface between dissimilar layers when laminates are modelled with homogeneous layers is identified as a reason for generation of such high gradient interlaminar stresses. Therefore, the concept of taking constituent material properties of fibre and matrix into account while modelling layers of a laminate might mitigate the problem of high gradient stresses near free edges and hence, is interesting. Modelling the laminate heterogeneously would eliminate abrupt material discontinuity between dissimilar layers and hence could eliminate the high gradient stresses, the convergence study of which is found to be computationally expensive. This idea of modelling heterogeneous composite laminates with explicit definition of fibres and matrix in an attempt to analyse free edge stresses has inspired the execution of this thesis project.

Investigations of interlaminar stresses have been carried out at interfaces of $[0/90]_s$ cross-ply laminate on both, homogeneous layer and heterogeneous layer models. Correspondingly equivalent stresses in both models have been compared with a view to understand the difference in their profiles at interface between layers near free edges. The use of average stresses obtained by averaging of interlaminar stresses up to a characteristic distance from free edge has been reported in literature to predict delamination initiation effectively with reference to experimental findings. Hence, the average of interlaminar stresses along the interface between layers has been investigated in both homogeneous and heterogeneous models. The study of average stresses has been carried out with an intention to find an averaging distance for a

given material which could be incorporated with a suitable criterion for prediction of delamination initiation. Further, investigation of average stresses would allow the comparison of computational expenses while studying convergence of high gradient interlaminar stresses and convergence of their averages.

The laminates are loaded under longitudinally extensional strain and linear Finite Element Analysis (FEA) has been conducted throughout the course of this work. In case of homogeneous layer laminates, uniform displacement boundary condition is simulated. Whereas, in case of heterogeneous layer model, strain loading has been simulated through Periodic Boundary Condition (PBC). To be able to compare the results from homogeneous and heterogeneous layer models, homogenisation on heterogeneous Unit Cell (UC) has been conducted through PBCs. Upon obtaining relevant results from both models, the comparison of results has been made to form the basis for correlation between average stresses from homogeneous and heterogeneous layer models to arrive at the averaging distance from free edge.

It is found that compared to stresses in homogeneous layer models, no such high gradient free edge stresses exist in heterogeneous layer model. The analysis on heterogeneous model helps in determining definite values at free edge unlike in the case of homogeneous layer model in which the high gradient stresses either require computationally expensive convergence studies or are sometimes even singular in nature. Further, the overall profile of corresponding stresses in two models is found to be similar except near the free edge. An approach has been proposed for correlation of average stresses between the homogeneous and heterogeneous layer models and an averaging distance of 0.125 mm has been found for T300/934 material. This averaging distance when incorporated in criterion for prediction of delamination initiation results in predicting delamination initiation successfully in the range of experimentally reported delamination initiating strain for $[\pm 25/90]_s$ laminate made of T300/934 material. Finally, a comparison of computational time required for convergence of high gradient interlaminar stress and computational time required for convergence of average of the high gradient interlaminar stress in homogeneous layer $[\pm 25/90]_s$ laminate reveals that convergence of average stress could be computationally less expensive. This highlights an efficient prediction of delamination initiation through use of average stresses in vicinity of free edges.

Table of Contents

List of Figures

List of Tables

Nomenclature

List of Acronyms

UC	Unit Cell
QDC	Quadratic Delamination Criterion
RoM	Rule of Mixtures
FEA	Finite Element Analysis
FEM	Finite Element Method
CLT	Classical Laminate Theory
RVE	Representative Volume Element
DoF	Degree of Freedom
PBC	Periodic Boundary Condition
3D	Three-Dimensional
2D	Two-Dimensional

List of Symbols

$\boldsymbol{\epsilon}$	Strain tensor (macroscopic)
$\boldsymbol{\sigma}$	Stress tensor (macroscopic)
$\boldsymbol{\varepsilon}$	Strain tensor (microscopic)
$\boldsymbol{\Sigma}$	Stress tensor (microscopic)
ν	Poisson's ratio
x, y, z	Cartesian coordinate axes
d	Laminate thickness
θ	Ply orientation angle
$\mathbf{u}$	Displacement vector (microscopic)
$\mathbf{F}$	Force vector
u, v, w	Displacement components in x, y and z directions
α	Power of singularity
A_1	Strength of singularity
R	Radial distance from point of singularity
b	Half width of laminate
v_f	Volume fraction
P	Effective property of lamina
P_f	Fibre property
P_m	Matrix property
ξ	Scaling factor in Halpin-Tsai relation
χ	Reduced properties of components in Halpin-Tsai relation
c_1, c_2	Fraction of concentration by volume of phases
$\mathbf{C}$	Stiffness tensor for periodic displacement (macroscopic)
$\hat{\mathbf{C}}$	Stiffness tensor for homogeneous traction (macroscopic)
$\tilde{\mathbf{C}}$	Stiffness tensor for homogeneous displacement (macroscopic)
$\mathbf{c}$	Stiffness tensor (microscopic)
$\mathbf{S}$	Compliance tensor (macroscopic)
v	Voigt's notation
r	Reuss's notation
k	Bulk modulus
G	Shear Modulus
E	Young's modulus
$\mathbf{x}$	Position vector (microscopic)
$\mathbf{y}$	Position vector (macroscopic)
$<>$	Averaging notation
V	Volume of RVE
∂V	Boundary of RVE
$\mathbf{n}$	Normal vector on RVE boundary
$\mathbf{D}$	Localisation tensor
A	Cross-sectional area of unit cell
L	Length of unit cell
Z^t, Z^c, Z^{s1}, Z^{s2}	Strength corresponding to σ_z(tensile), σ_z (compressive), τ_{xz} and τ_{yz}
h	Ply thickness
ρ	Fibre radius

a	Smallest dimension between fibre and unit cell's edge
c	Arbitrary constant
W	Work done on unit cell
s	Interval size in trapezoidal integration
T	Transpose
π	Pi constant
i, j, k	Indices for representing tensor components
Δx_k	Length of side of cubic RVE
y_{avg}	Averaging distance
f	Continuous function
$T_n(f)$	Integration of f
n	Arbitrary integer
N	Total number of points in domain of f
K	Material stiffness

Acknowledgements

I extend my sincere thanks to my supervisors Dr. Boyang Chen Dr. Daniël Peeters and Dr. Mostafa Abdalla for their continuous guidance and support during the execution and writing of this thesis. Discussions on the topic through the course of this work have been highly enriching to me. Going forward, I shall immensely cherish the ideas and approaches I got to learn.

I thank my family for their love and for constantly being a source of inspiration.

Lastly but importantly, thanks to my friends within and outside the university with whom I have had the opportunity to learn together and to make this experience a memorable one.

Delft, University of Technology — Priyanshu Anand
28th August 2017

"Imagination is more important than knowledge. For knowledge is limited, whereas imagination embraces the entire world, stimulating progress, giving birth to evolution."

— *Albert Einstein*

Chapter 1

Introduction

Since the discovery of interlaminar stresses near the free edge of composite laminates, a vast amount of research has been done over the years in an attempt to investigate the nature of these stresses. The assumption of homogeneous material layers while modelling of composite laminae introduces sudden differences in material properties between layers of different material orientations at their interfaces. The deformation compatibility of the laminate at these interfaces introduces interlaminar stresses. Some of these interlaminar stresses have been theoretically found to be high gradient stresses near the free edges [2]. This high gradient in stress is a matter of concern as the danger of delamination initiation in laminates arises due to such stress states.

A simple force equilibrium state of a laminate under linear elastic tensile loading is introduced for a description of the stress states near the free edge.

Interlaminar stresses in vicinity of laminate's free edges at interface of two layers

To understand the effect of homogeneous laminate layers towards generation of free edge stresses, the force equilibrium condition of a laminate is studied. *Mittlestedt et al* [1] provide a comprehensive study of a laminate's equilibrium under longitudinal tensile displacement. Since the difference in adjacent layers is most contrasting between the zero and ninety degree layers of a cross-ply laminate, the force equilibrium is illustrated conveniently with the help of a cross-ply laminate.

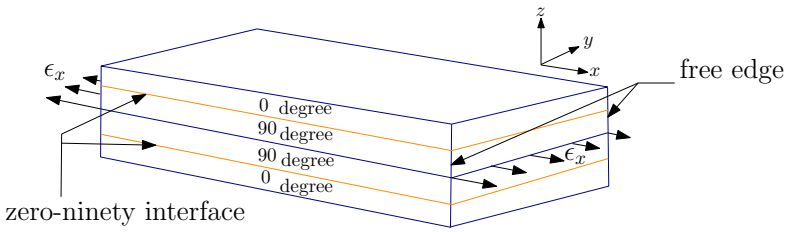

Figure 1.1: Longitudinal extensional strain in a $[0/90]_s$ cross-ply laminate [1]

In figure 1.1, fibres in the zero degree layers are aligned with the x axis and that of the ninety degree layers are aligned with y axis. For once, let's consider the layers of the laminate to not be bonded to each other. The displacement is applied in the x direction to provide a tensile load in the laminate. It is notable that the zero degree layers have lower stiffness in the transverse (y) direction. Contrastingly, the ninety degree layers have higher stiffness in the transverse direction. This difference in stiffnesses is abrupt at the interface of zero and ninety degree layers (highlighted in orange). This results in greater contraction of zero degree layers in comparison to contraction of ninety degree layers in the y direction due to Poisson's effect (ν_{xy}). Essentially in a de-bonded laminate, the in-plane displacement in y direction would be comparatively higher in the zero degree layer. This suggests a discontinuous displacement at the zero-ninety degree layers' interface. However, in reality, the layers of a laminate are completely bonded to each other and this strain compatibility at interface results in generation of transverse normal stress σ_y in both zero and ninety degree layers. Since the zero degree ply contracts more than the ninety degree ply, transverse tensile stress is introduced in the zero degree ply and transverse compressive stress is introduced in the ninety degree ply. Transverse normal stress σ_y vanishes at free edges because of traction free edge condition.

Since, the overall resultant stress σ_y must vanish through the laminate's thickness direction (z) , the following could be inferred for a laminate of thickness d as shown in figure 1.2.

$$\int_{-d/2}^{d/2} \sigma_y dz = 0 \tag{1.1}$$

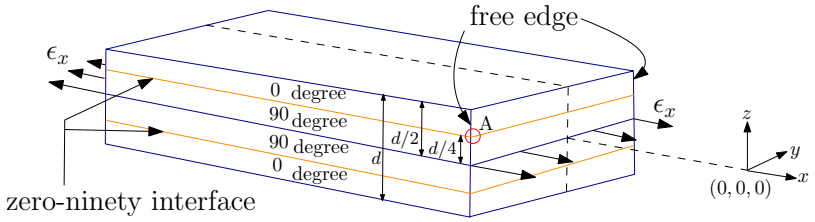

Figure 1.2: Schematic geometry of $[0/90]_s$ laminate [1]

Since the boundary conditions require the free edges to be traction free, the equilibrium of forces in the y direction must be satisfied. In order to achieve this, interlaminar shear stress τ_{yz} arises at the zero-ninety degree layers' interface i.e. at $z = \pm d/4$ as shown in detailed view in figure 1.3.

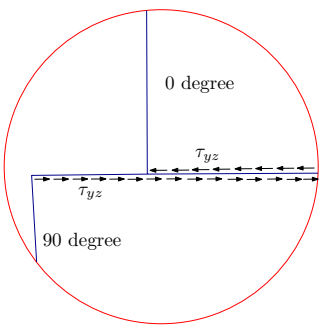

Figure 1.3: Detail A: Generation of shear stress σ_{yz} at zero-ninety degree layers' interface [1]

Thus, the following condition holds true for a high enough value of y [1]:

$$\int_0^y \tau_{yz} dy = \int_{d/4}^{d/2} \sigma_y dz \tag{1.2}$$

The stress resultants of σ_y and τ_{yz} discussed above do not act along a common line of action and thus a moment is generated about the x axis. In order to maintain an equilibrium of moments about the x axis, interlaminar normal stress σ_z is generated at the zero-ninety degree layers' interface. The tendency of σ_z is to counter the moment generated by σ_y.

The region at zero-ninety degree layers' interface suggests the presence of stresses as shown in figure 1.4. The stress state is shown before the free edge at an interior location of upper zero degree layer.

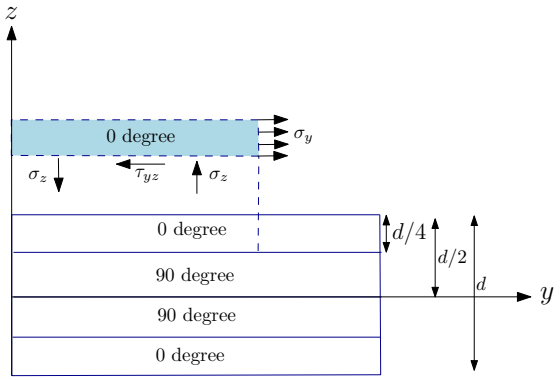

Figure 1.4: State of stresses at interface between zero and ninety degree layers of $[0/90]_s$ cross-ply laminate [1]

This results in the following equation to hold true:

$$\int_0^y \sigma_z y dy = -\int_{d/4}^{d/2} \sigma_y (z - \frac{d}{4}) dz \tag{1.3}$$

Since, σ_z acts alone in z direction, for a sufficiently wide laminate, the resultant stress in z direction must vanish. Hence, the equation 1.4 must also hold true.

$$\int_0^y \sigma_z dy = 0 \tag{1.4}$$

The equilibrium of forces and moments suggests the presence of a three-dimensional (3D) stress state in the vicinity of laminate's free edge. Further, a study of the nature of these stresses reveals an intriguing finding. Strictly speaking of the interlaminar normal stress σ_z, it has been observed that the highest point of the stress occurs at the free edge. However, since there is no other force in the z direction, σ_z must be self-equilibrated and hence it is expected to change its sign across the width of the laminate i.e. along y direction. Further, theoretical studies highlighted in the following chapters, have revealed the presence of a high gradient at the intersection of the free edge and interface of layers in laminates with homogeneous layer models. The difference of material properties is most contrasting at the interface of zero-ninety layers of a cross-ply laminate and thus, the presence of steep gradient could be studied

conveniently at the zero-ninety interface of a cross-ply laminate. The findings at this stage open the doors for studying the nature of free edge stresses in laminates with homogeneous material layers.

Therefore, the analysis of stress fields at free edge vicinity becomes imperative to laminate designing. Several analysis methods ranging from analytical to numerical have been employed over the years to get as close an estimate as possible of free edge region stress fields and to find the peak value of these stresses [1]. Delamination initiation has been cited as a potential mode of failure at the free edges and therefore accurate prediction of interlaminar stresses which are responsible for initiating delamination, has been an area of concentration. The application of methods for delamination initiation prediction often involve free edge region stresses. However, a high gradient stress profile results in high computational investment for convergence studies of these stresses and sometimes these stresses might show a singular tendency as well which makes prediction of peak stress values cumbersome. One of the methods used to determine a definite stress value near the free edge region is the averaging of high gradient stresses over a characteristic distance from the free edge along the laminate's width in an attempt to represent the peak stress value with an equivalent averaged value of interlaminar stress components. Over the years, several approaches have been followed to determine the characteristic averaging distance for a given combination of material properties and laminate layup. Some of these approaches include experimental procedures and determination of strain energy release rate.

An approach to arriving at an averaged interlaminar stress value near free edge region has been proposed in the course of this thesis. The main hurdle in mitigating steep stress gradients at free edge is the consideration of homogeneous layer laminates. To overcome this hurdle, heterogeneous model of cross-ply laminate is built to study the nature of stresses near the free edge region through Finite Element Method (FEM). The FEA of stresses on both homogeneous and heterogeneous models allows a correlation of stresses on models with equivalent stiffness. Thereafter, an effort has been made to propose an approach for determination of averaging distance by taking into consideration the high gradient free edge stresses from homogeneous layer laminates and free edge stresses obtained from detailed modelling of laminate's constituent materials. Through determination of averaged stresses, delamination initiation prediction could be done by employment of a suitable delamination initiation criterion. This leads us to defining the title of the project as

'A Study of Free Edge Stresses and Delamination Initiation in Fibre Reinforced Composite Laminates.'

Linear FEM analysis has been carried out throughout this research on Abaqus FEA software tool. Upon analysis, the obtained averaging distance is found to be predicting delamination initiation in the reported experimental range for $[\pm 25/90]_s$ laminate which is reported to be susceptible to delamination initiation [9] through the use of average stress based Quadratic Delamination Criterion (QDC) [12]. Delamination initiation index of the QDC is found based on the determined averaging distance. The applicability of averaging distance on different layups for a given material system has been reported [12]. This encourages the use of the proposed averaging distance on suitable laminates for predicting delamination initiation. Since FEM modelling and analysis of detailed constituent elements of a laminate could be a time consuming and computationally expensive task, determination of the averaging distance once through this approach for a given material, enables an application on a range of layups. This

enables saving computational time and modelling effort while making a judicious use of FEA codes.

In the following chapters of this thesis report, literatures studied, the results obtained for various analyses and the conclusions derived from the research are discussed. Chapter 2 deals with the state of the art methods on analysis of high gradient free edge stress fields, modelling of detailed constitutive elements of composite laminates, application of suitable boundary conditions, application of a suitable delamination initiation criterion and layup suitable for verification of averaging distance has been highlighted. Following this, chapter 3 is about modelling and analysis of homogeneous layer models and determination of free edge stresses. Further in chapter 4, modelling and analysis of stress states in heterogeneous layer models has been reported. Following this, in chapter 5, an approach for homogenisation of heterogeneous laminate to model a homogeneous laminate with equivalent stiffness is highlighted. Chapter 6 illustrates the approach for correlation and verification of proposed approach on a suitable homogeneous layer composite model. Finally in chapter 7, the conclusion of results has been reported along with recommendations for future works on the topic.

Chapter 2

State of the Art

2.1 Background

A long-standing area of research in composite laminate design is the study of nature and consequences of the free edge effect. The free edge stresses may exhibit high gradients near free edges of homogeneous layer models and could be a potential source for causing delamination initiation. This chapter aims at covering a range of state of the art literatures proposed over a span of nearly 50 years on the various methods for detection and analysis of the free edge stresses in composite laminates. Further, study of heterogeneous model with constituent materials of composite laminates is done. This includes the use of appropriate modelling approaches and application of suitable boundary conditions. This enables determination of the stress state without imposing material homogeneity in a lamina. Further, delamination criteria are studied which provide a framework for determining the initiation of delamination due to the stresses with high gradient near free edges of equivalent layer models. This is followed by study of methods to extract engineering properties from Representative Volume Element (RVE) of a composite lamina. Finally, a study related to laminates prone to delamination due to high gradient free edge stresses is done.

Before moving to the next section, it is worth highlighting that for laminates made of orthotropic laminae, the implication of Saint Venant's principle suggests that at a far-off distance from the location of load application, the displacements in the directions y and z become independent of the longitudinal (x) coordinate in a laminate of sufficient length with reference to figure 1.1. Thereby making the strain and hence the stress at a far-off distance from point of load application, independent of x coordinate. This understanding could be important to reduce computational effort by avoiding unnecessary modelling of the entire laminate where possible. Sometimes, a mid-section along the laminate's transverse direction could be good enough to analyse free edge effect in transverse (y) direction under uniform extensional loading in linear deformation regime.

2.2 Study of free edge stresses: Their detection and nature

This section deals with major works carried out on the discovery and analysis of free edge interlaminar stresses. Since the discovery of the presence of interlaminar stresses in the free edge region in the work of *Puppo et al* [4] and the pioneering work of *Pipes et al* [2] on highlighting the presence interlaminar stresses near free edges possibly to an extent of a singularity, various methods including analytical, semi-analytical and numerical have been employed over the years for their further analysis. The existence of 3D stress fields due to interlaminar stresses has been explained in chapter 1. The presence of interlaminar stresses is mostly confined to the free edge region and their presence becomes negligible away from the vicinity of the free edge.

The methods through which the free edge interlaminar stresses have been analysed can be broadly categorised into numerical and analytical methods along with approximately closed form and closed form solutions. Particularly with respect to numerical methods, FEM has been widely used and hence, major works related to the use of FEM have been highlighted until 2016.

2.2.1 Numerical studies on free edge effect

One of the landmark works related to the analysis of free edge stresses can be traced to the work of *Pipes et al* [2] in which finite difference solution methods are employed to study the free edge stresses. The fact that Classical Laminate Theory (CLT) assumes the existence of in-plane stresses in response to in-plane tractions in symmetric laminates, implies boundary traction on the free edge when the laminate consists of differently oriented layers, which cannot be possible. Hence, the nature of the stress field in the free edge region in this paper is studied. A schematic laminate geometry has been shown in the figure 2.1.

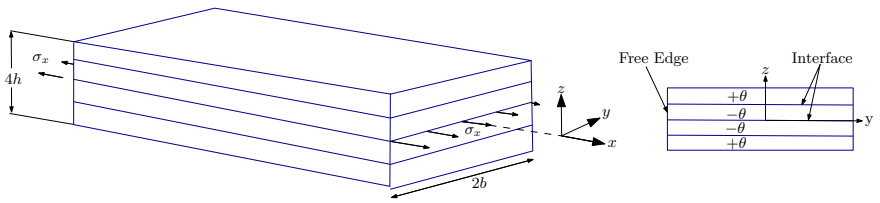

Figure 2.1: Schematic laminate geometry as shown in Pipes et al (1970) [2]

Symmetry boundary conditions are applied at the $x-y$ and $x-z$ planes. Material properties of a typically high modulus graphite-epoxy material (listed in table 3.1) is used to carry out analyses in this paper, the results of which are shown in figure 2.2. It has been indicated through the reported plots in figure 2.2 that while the results correlate well for τ_{xy} and σ_x with *Puppo et al* (1970) [4] (results described in section 2.2.2), the presence of a possible singularity is indicated for τ_{xz} unlike in *Puppo et al* (1970) [4] wherein τ_{xz} is shown to have a finite value at free edge. Thus, the study suggests the requirement of significant amount of interlaminar shear for shear transfer between layers of the laminate. Moreover, the possibility of existence of singularity in interlaminar shear stress in a region equal to laminate's thickness from free edge has been proposed.

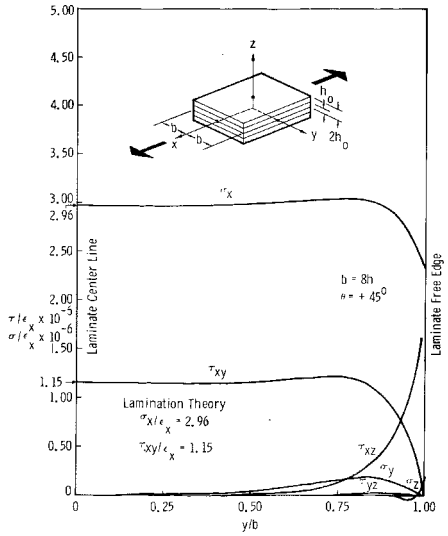

(a) Rise in τ_{xz} and σ_z stresses near free edge at interface $z = h$ $(h = h_0)$ [2]

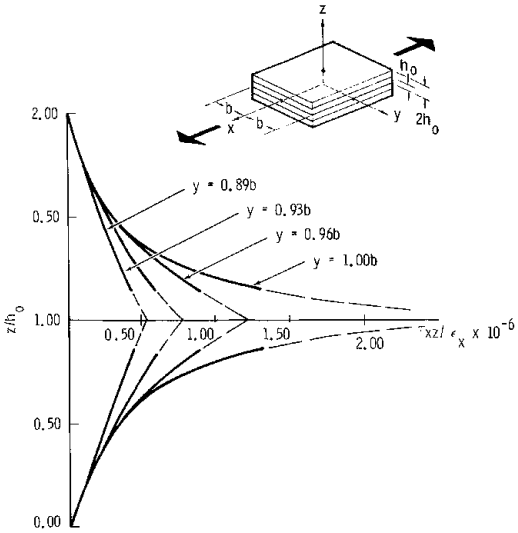

(b) Shear stress τ_{xz} distribution through laminate's thickness [2]

Figure 2.2: Interlaminar stress distribution along laminate's interfacial width and through thickness along free edge [2]

In the work of *Rybicki* (1971) [13], an approximate solution has been proposed using FEA based on complementary energy formulation for a laminate under in-plane loading. The method satisfies all equilibrium conditions and stress boundary conditions exactly but the compatibility and displacement boundary conditions are satisfied approximately. An analysis on a [90/0/0/90] laminate shows that the sign of σ_z at the free edge is negative like that of σ_y of the top ply. It is indicated that σ_z reaches its maximum value at the free edge and has the same sign as that of σ_y in the top laminate. The reason behind this is cited to be the equilibrium of moment at centre section. Further, it is reported that a significant value of τ_{yz} is found at the ends of the laminate.

One of the most highly cited works using FEA in the field of free edge analysis has come from *Wang et al* (1977) [14]. This paper proposes an approach using displacement based multi-purpose finite elements. For carrying out the analysis, plane strain triangular elements are used near the free edge region. A total of 392 elements with 226 nodes are used with substantial mesh biasing towards the free edge region. The material used for analysis is same as the one used in Pipes et al (1970) [2]. The result of σ_z along the zero-ninety degree ply interface shows a rise in the stress levels as the free edge is approached. Further, it has been reported that while in case of $[0/90]_s$ laminate σ_z shows a sharp rise near free edge and hence a possible singularity, σ_z in case of $[90/0]_s$ laminate attains a finite value at free edge. This noticeable difference in the nature of the two plots makes the author to remark that the two laminates behave fundamentally differently.

Quasi 3D FEA has been carried out by *Raju et al* (1981) [15] on $[\theta/\theta - 90]_s$ laminate family. In the analysis, eight node isoparametric elements have been used to model homogeneous elastic orthotropic plies of four-ply laminates. With regard to the meshing strategy, it is considered that the singularity exists along the radial line from the singular point. Therefore, radial/polar meshing strategy is adopted to capture the singularity. If R is considered to be

the radial distance from the singular point, then for regions close to the singularity or for smaller R values the stress distribution could be approximated as:

$$\sigma_{ij} \simeq A_1 R^{-\alpha} \tag{2.1}$$

or

$$\log \sigma_{ij} = \log A_1 - \alpha \log(R) \tag{2.2}$$

where α is the power of singularity and A_1 is the strength of singularity. Thus, if the equation is fitted well to the computed stresses on a log scale plot, then the nature of stress near free edge could be studied. With respect to cross-ply laminates, near intersection of dissimilar layers and free edge, σ_z is reported to be tensile for both $[0/90]_s$ and $[90/0]_s$ laminates while τ_{xz} at the same location is found to be zero for both laminates.

A work by *Whitcomb et al* (1982) [16] highlights that upon analysing $[\pm 45]_s$ graphite/epoxy laminate through FEM for free edge stresses, the stress σ_z is found to be compressive in nature at intersection of interface between +45 and -45 degree plies and free edge as opposed to the tensile nature showed by other studies through finite difference method and perturbation solution. A displacement formulated FEM is incorporated using 8 node isoparametric elements and a converged solution is found with the exception of two elements closest to the free edge. Upon further comparison with known problems of exact solution, it is indicated that the displacement formulated FEM shows the same behaviour in case of $[\pm 45]_s$ laminates. Also for symmetric cross-ply laminates, the stress distribution agrees qualitatively and hence, FEM is indicated to be a highly accurate method for calculating interlaminar stresses in laminates.

The next study suggests an effective approach to FEM based analysis of the free edge problem. This work by *Lessard et al* (1996) [3] deals with 3D analysis of edge effect in symmetric cross-ply laminates under uniaxial tensile loading. For the analysis, a slice model has been created with a view to optimise mesh refinement and computational time. 20 node 3D quadratic brick elements are used for finite element meshing. Thus, an approach has been taken for simulating the actual stress state near free edge. The figure 2.3 shows the slice model set up and the meshing of the model using aforementioned brick elements.

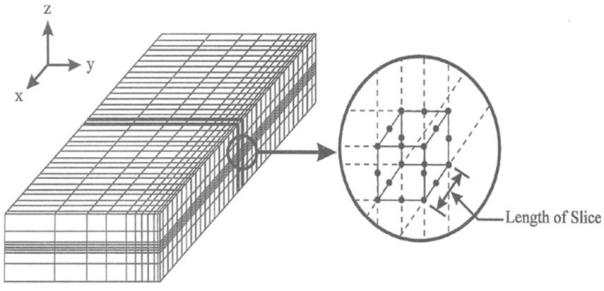

Figure 2.3: Slice model set up using quadratic brick elements [3]

A quarter of the laminate is modelled using the transverse slice of length 0.0156 mm. A uniaxial tensile load is applied to the nodes on one side of the elements while constraining the other side's Degree of Freedom (DoF) longitudinally. A total of 856 elements have been created

using 6225 nodes for a fine mesh while not exceeding the element aspect ratio of 2:1 near the free edge. Use of this model could be extended to analyse 8 layered laminates effectively. Further this model is indicated to behave better than quasi 3D models. A comparative analysis of interlaminar normal σ_z stress has been shown in figure 2.4. The figure suggests a higher peak stress compared to the peak stresses observed in some of the earlier studies on σ_z at the free edge of zero-ninety interface. The study uses the same material as used in [2].

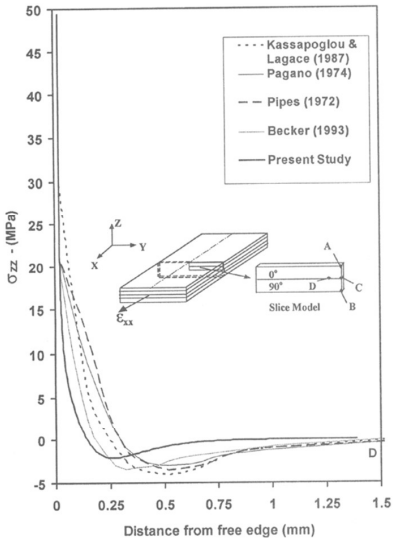

Figure 2.4: Comparative analysis of σ_z along $0/90$ interface of $[0/90]_s$ laminate [3]

Figures 2.5 and 2.6 show the distribution of σ_z and τ_{yz} stresses along the free edge and zero-ninety layers' interface of $[0/90]_s$ laminate.

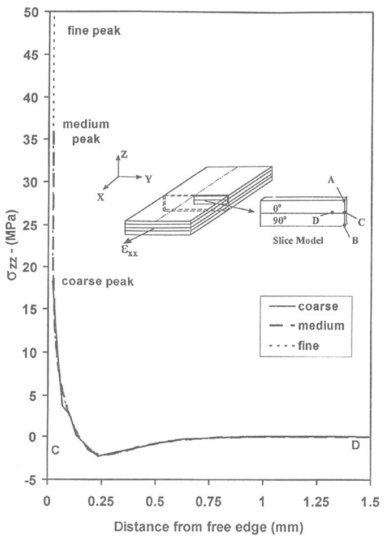

(a) Distribution of σ_z along interface of $[0/90]_s$ laminate [3]

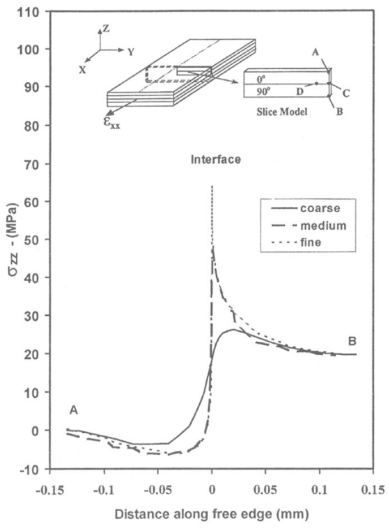

(b) Distribution of σ_z along free edge of $[0/90]_s$ laminate [3]

Figure 2.5: Distribution of interlaminar tensile stress along interface and along the free edge

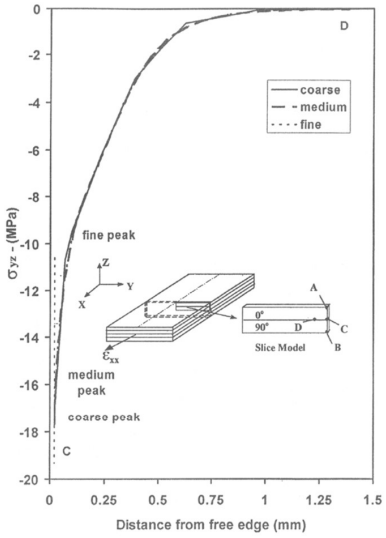

(a) Distribution of τ_{yz} along interface of $[0/90]_s$ laminate [3]

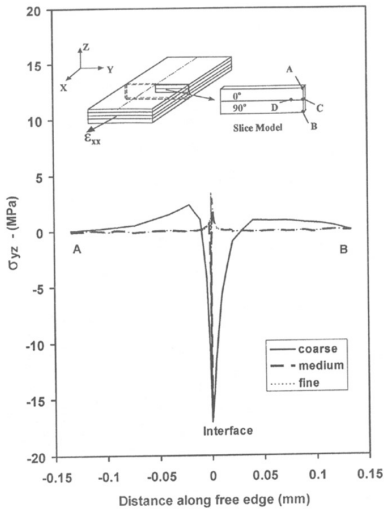

(b) Distribution of τ_{yz} along free edge of $[0/90]_s$ laminate [3]

Figure 2.6: Distribution of interlaminar shear stress along interface and free edge

In the work of *Kant et al* (2000) [17] a review of the methods adopted for interlaminar stress determination is done. While referring to the work of *Salamon* (1980) [18], it has been shown that while two-dimensional (2D) elements can predict accurate results away from the free edge, they cannot predict complex stress states near any geometric or material discontinuities or near traction free edges, accurately.

Work by *Lindemann et al* (2000) [19] is based on boundary finite element method. This method combines the boundary element method and FEM for analysing the free edge effect by taking an example of symmetric cross-ply laminate. Analogous to the boundary element method, only the boundary needs to be discretised while the element formulation is finite element based. The analysis result is suggested to be in good agreement qualitatively and quantitatively with σ_z and τ_{yz} results obtained from FEM.

In a paper by *Nailadi* (2002) [20], free edge effect has been analysed using numerical method (FEM) and experimental results using a $[+45_4/-45_4]_s$ angle-ply laminate subjected to uniform axial strain. Singular finite elements are used in regions close to free edge and interface regions with element length in the order of 2.54 microns in singular region, whereas, 8 node quadrilateral elements had are used at other locations. A quasi 3D approach is followed and it is found that an agreement between the FEM analysis and experimental data exists.

Paper by *Nguyen et al* (2006) [21] suggests that the accurate prediction of interlaminar stresses is not possible with two-dimensional finite elements. Thus, a need for the use of 3D elements or layer wise 2D finite elements is highlighted. In this proposal, an eight node isoparametric multi-particle quadrilateral element is developed. The result is indicated to be valid by comparison with 3D finite element results. In a work of *Ramesh et al* (2009) [22], a higher order triangular plate element is used. It is suggested that transverse shear stresses are not predicted effectively using 3D finite elements at the free surfaces because the shear stresses do not vanish completely after discretisation and the stresses are still speculated to appear.

As a result, the proposed element is suggested to be more effective in terms of providing DoF and in handling complex problems involving stress singularities efficiently.

Other numerical studies on free edge effect

In a work by *Spilker et al* (1980) [23], a special single purpose element has been incorporated which is reported to exactly satisfy the traction free free-edge conditions. A multi-layered element formulation is used that complies to conditions of equilibrium and compatibility at the interfaces as well as at traction free edges and surfaces. The versatility of hybrid finite elements is due to allowance of an independent stress distribution in the interior of the element. As a result, interlaminar traction continuity and traction free upper and lower surfaces could be obtained. It is reported that high gradients are observed in interlaminar normal stress (likewise in interlaminar shear stress) near the traction-free edges which is in agreement with FEA of *Wang et al* [14].

For the analysis of traction free straight boundaries, 3D hybrid stress elements with traction free planar surface has been proposed by *Tian et al* (2004) [24]. It is mentioned that boundary conditions and continuity conditions along with material property changes, lead to singularity. Further, it has been mentioned that for general 3D elements, increasing the order of interpolation polynomial does not improve the rate of convergence of results and hence, while dealing with smaller aspect ratios at free edge region, computational difficulties are encountered. The results obtained are suggested to be as efficient and effective as with a coarse mesh and an agreement in results with existing elasticity solutions could be found.

2.2.2 Analytical studies on free-edge effects

One of the earliest literatures on findings related to interlaminar stress near the free edge was based on analytical method. Since then, several analytical and semi-analytical studies have been proposed on the topic over the years of which a few are reported herein chronologically. *Puppo et al* (1970) [4] propose an analysis on the interlaminar shear stresses (stresses distributed on faces of laminate layers) subjected to generalised plane stresses. The laminates are modelled with anisotropic layers bonded by isotropic adhesive layers. In this paper, an analytical approach based on simple equilibrium based method has been adopted and solutions have been obtained for infinite and finite width laminates. The adhesive layer is assumed to be developing only shear stresses while the anisotropic layers are assumed to be under generalised plane stress state. Using constitutive relations for anisotropic layers and isotropic adhesive layer, the equilibrium equations have been solved by applying tensile displacement boundary conditions in longitudinal (x) direction.

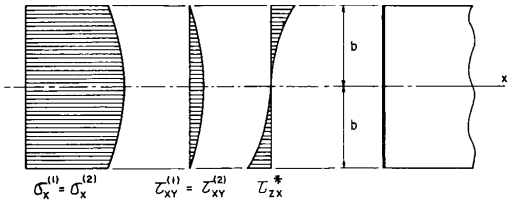

Figure 2.7: Stress distribution across the laminate's width in transverse direction [4]

Figure 2.7 gives an overview of the obtained results (b is the half width of the laminate). Zero interlaminar shear stresses are obtained for infinite width laminate at the edges along transverse (y) direction, but finite interlaminar shear stresses depending on y coordinate are reported for a finite width laminate.

Pipes et al (1974) [25] propose an approximate elasticity solution for a finite width angle-ply laminate loaded under uniform axial strain. The displacements are expanded as Fourier series. During solution formulation, considerably large number of terms are used to arrive at sufficiently accurate results. This tendency indicates the possibility of an existence of singularity in the interlaminar shear stresses in the free edge region. In a study by *Kassapoglou et al* (1986) [26], an analytical approach towards studying interlaminar stresses under uniaxial loading is proposed. Stress shape functions represented as product of functions dependent on transverse an interlaminar coordinates, is solved. Force balance method and minimisation of complementary energy of entire laminate are used to obtain the solutions which are compared with FEM based results by *Wang et al* [14]. The free edge stresses are reported to be higher in magnitude compared to those by *Wang et al* [14].

An analytical work by *Tahani et al* (2003) [27] investigates the free edge stresses in a general cross-ply laminate. A quasi-3D problem is considered. The approach is based on providing more kinematic freedom across thickness of a layer. A comparison is drawn with results obtained from FEA results of *Wang et al* [14] and the results have been shown to correlate closely. Another study by *Dhanesh et al* (2016) [28] proposes a new 3D elasticity based analytical solution which satisfies all boundary conditions and interfacial continuity conditions exactly. The results are suggested to successfully capture singularity at free edge. The results show a rise in interlaminar normal stress near the free edge and a tendency of interlaminar shear stress to approach zero in the free edge region of zero-ninety degree layers' interface of $[0/90]_s$ laminate. Through a semi-analytical approach, *Peng et al* (2016) [29] present the potential of mechanics of structure genome for free edge stress analysis of composite laminates. The results obtained are suggested to be in good agreement with 3D FEA results.

An equilibrium based approximate closed form analysis is carried out by *Pagano et al* (1971) [30]. The interlaminar normal and shear stresses are investigated and it is indicated that these stresses have a significant effect in precipitating delamination initiation and strength reduction. It has been shown in the study that in a cross-ply laminate, the sequence of arrangement of zero degree and ninety degree plies has an effect on the interlaminar normal strength of the laminate. In a paper by *Kassapoglou et al* (1987) [31], a closed form solution based on force balance method and minimisation of complementary energy has been proposed which shows that interlaminar normal stress σ_z in a cross-ply laminate have a pronounced rise in peak stress at the zero-ninety ply interface of a $[0/90]_s$ laminate.

2.3 Heterogeneous modelling of cross-ply composite laminates

The objective of heterogeneous modelling in this study is to represent the state of constituent materials i.e. the fibre and matrix of the considered cross-ply laminate. In a periodic medium, a UC can form a Representative Volume Element (RVE). These UCs by periodic repetition represent the entire structure of the composite. The RVEs are statistically homogeneous representation of a heterogeneous medium which can be used to derive macroscopic (homog-

enized) law for the composite [6]. Further details about requirements of choice of UC is highlighted in section 2.5. UC of a cross-ply laminate has been shown in the figure 2.8.

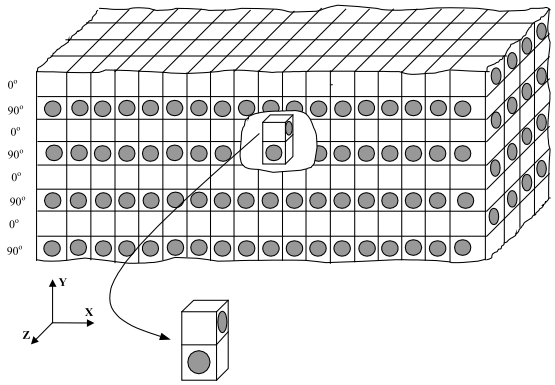

Figure 2.8: Unit Cell of a cross-ply laminate [5]

It might be noted in figure 2.8 that every zero and ninety degree ply has been represented by a combination of only one fibre along the laminate's thickness direction. However, to represent the heterogeneous state of a lamina at micro scale, a combination of single fibre cubes could be stacked in the thickness direction. Considering a nominal fibre diameter to be 7 microns and fibre volume fraction of 0.6, the size of a unit cell would be around 8.018 microns using the relation for ratio of fibre diameter to unit cell side to be $2\sqrt{\frac{v_f}{\pi}}$, where v_f is the fibre volume fraction. This means that a standard graphite-epoxy ply with nominal thickness of 0.134 mm [3] will have as many as 16 to 17 unit cells stacked in the thickness direction. It must be noted that building an entire laminate with such UCs of 8.018 microns will be computationally very expensive. A simplification of an effort to model constituent lamina materials could thus be to use one fibre per lamina in the thickness direction as represented in figure 2.8. Moreover, these UCs are scale independent. If homogeneous properties of a unidirectional lamina is to be predicted, then a choice of unit cell could comprehensibly be a cubic unit cell as shown in figures 2.13 and 2.15.

Packing of UCs

The UCs can be stacked up in different directions and in different array patterns. For example, UCs can be arranged in a square array, in hexagonal array or in rectangular array. The determination of overall properties of a lamina can be represented through the Halpin-Tsai relation mentioned in *Whitney et al* [32]. Among the few approaches mentioned for the study of such models, is the semi-empirical Halpin-Tsai relationship which takes into account the packing array of UCs. The formulation establishes a relationship between the various macro scale elastic properties of a lamina and the individual constituent properties of fibre and matrix. The following equations (2.3) and (2.4) define these relations.

$$P = \frac{P_m(1 + \xi\chi v_f)}{(1 - \chi v_f)} \tag{2.3}$$

where,

$$\chi = \frac{P_f - P_m}{P_f + \xi P_m} \tag{2.4}$$

P is the effective property of the lamina while P_f and P_m are respective properties of the fibre and matrix. The scaling parameter ξ varies while determining longitudinal and transverse properties and is used to ensure that the properties lie between the upper bound of Voigt and lower bound of Reuss (explained in section 2.4) [33]. χ is stated as reduced properties of the components. As the UCs repeat to form the entire laminate, the fibre volume fraction of the RVE is equal to the fibre volume fraction of the lamina.

The Rule of Mixtures (RoM) approach is another strength of materials based approach for determining the effective engineering properties of a lamina based on constituent material properties of fibre and matrix. For longitudinal modulus of elasticity and longitudinal Poisson's ratio, the assumption of uniform strain in fibre and matrix is made and the effective property can be given as mentioned in equation (2.5) [8].

$$P = P_f v_f + P_m(1 - v_f) \tag{2.5}$$

Transverse moduli of elasticity and longitudinal shear moduli are calculated by assuming uniform stress in fibre and matrix [8]. the form of equation for effective property is given by equation (2.6).

$$\frac{1}{P} = \frac{v_f}{P_f} + \frac{(1 - v_f)}{P_m} \tag{2.6}$$

The transverse Poisson's ratio is calculated by using the relation between transverse elastic modulus and transverse shear modulus if the fibre has transverse isotropic symmetry as shown in equation (2.16).

In context of the current study, as we are interested in dealing with free edge stresses, the UCs as shown in figure 2.8 can be stacked up along the width (transverse direction) to represent a zero-ninety layer combination of a heterogeneous cross-ply laminate. This approach enables the use of individual properties of fibre and matrix and therefore abrupt material discontinuity between layers could be mitigated. Unlike in homogeneous layer models, the interface between two layers would be represented by matrix properties common to both layers. A schematic zero-ninety layer UC is shown in figure 2.9. The heterogeneous model will not enforce abrupt change in material properties at interface and hence, may allow examination of a definite stress value at intersection of free edge and interface without exhibition of high gradient stresses as in case of homogeneous layer models.

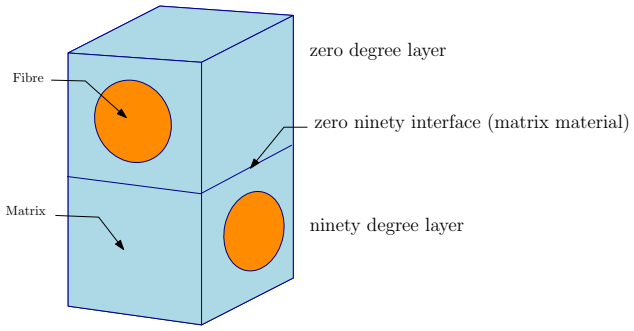

Figure 2.9: Zero-ninety layers' interface made of matrix material in a heterogeneous cross-ply UC

2.4 Appropriate boundary conditions for periodic heterogeneous media

The main idea behind heterogeneous modelling is to be able to correlate the results obtained from the heterogeneous model with that of the homogeneous material layer model. For this to happen, the two models must have the same stiffness. Apart from the application of uniform traction and uniform strain boundary conditions mentioned in subsection 2.3 for deriving effective engineering constants, the use of Periodic Boundary Condition (PBC) by which effective stiffness from a heterogeneous medium could be extracted, is described through a homogenization principle in *Suquet* [6]. The nature of heterogeneous medium plays an important role in choice of a suitable boundary condition for finding an effective stiffness. Hence, it becomes pre-requisite to understand the nature of the heterogeneous model. Since, the modelling of a heterogeneous cross-ply laminate through UC described in figure 2.9 would result in a periodic medium, the suitable boundary conditions and homogenisation procedure applicable to periodic heterogeneous media is highlighted.

Dependence of structural moduli on applied boundary conditions

R.Hill (1963) [34] describes the approach to derive the inequalities between structural moduli of a two isotropic phase mixture bonded together at arbitrary concentrations due to application of different boundary conditions. The nature of reinforcement is considered to be arbitrary which could be of fibrous, spherical or plate-like shape. However, the phases themselves are considered isotropic. The paper is aimed at determining the overall or macroscopic elastic properties which the author believes involves dependence on relative concentration of constituents as well as on their arrangement. The paper describes the volumetric average of stress and strain as the integral over a specified region divided by the volume of the region. The equations (2.7) and (2.8) describe the relation for overall stress and strain tensors in heterogeneous medium.

$$< \boldsymbol{\Sigma} >= c_1 < \boldsymbol{\Sigma}_1 > + c_2 < \boldsymbol{\Sigma}_2 > \tag{2.7}$$

$$< \boldsymbol{\varepsilon} >= c_1 < \boldsymbol{\varepsilon}_1 > + c_2 < \boldsymbol{\varepsilon}_2 > \tag{2.8}$$

where $< \boldsymbol{\Sigma} >$ and $< \boldsymbol{\varepsilon} >$ are the average stress and strain tensors for any region in micro heterogeneous state containing the phases while $< \boldsymbol{\Sigma}_1 >$ and $< \boldsymbol{\Sigma}_2 >$ are average stress tensors of corresponding phases and $< \boldsymbol{\varepsilon}_1 >$ and $< \boldsymbol{\varepsilon}_2 >$ are average strain tensors for corresponding phases. Parameters c_1 and c_2 are fractions of concentration by volume of the two phases in the mixture. Replacing the average stresses in corresponding phases with respective stiffness tensors ($\mathbf{C}_1$ and $\mathbf{C}_2$) and average of strain tensors ($\boldsymbol{\varepsilon}_1$ and $\boldsymbol{\varepsilon}_2$), equation (2.9) is obtained.

$$< \boldsymbol{\Sigma} >= c_1\mathbf{C}_1 < \boldsymbol{\varepsilon}_1 > + c_2\mathbf{C}_2 < \boldsymbol{\varepsilon}_2 > \tag{2.9}$$

Similarly, replacing the average strains with the respective compliance and stress tensors, equation (2.10) is obtained.

$$< \boldsymbol{\varepsilon} >= c_1\mathbf{S}_1 < \boldsymbol{\Sigma}_1 > + c_2\mathbf{S}_2 < \boldsymbol{\Sigma}_2 > \tag{2.10}$$

where, $\mathbf{S}_1$ and $\mathbf{S}_2$ are compliance tensors.

In equation 2.9, if the strains in the two phases i.e. $< \boldsymbol{\varepsilon}_1 >$ and $< \boldsymbol{\varepsilon}_2 >$ are equal to the overall average strain shown in equation 2.8, then we have the uniform strain condition proposed by Voigt. Likewise, if we consider the stresses in the two phases i.e. $< \boldsymbol{\Sigma}_1 >$ and $< \boldsymbol{\Sigma}_2 >$ in equation 2.10 equal to the overall average stress in equation 2.7, then we arrive at the Reuss's condition of uniform stress. However, application of Voigt's condition could result in discontinuous tractions at the interface of the two phases and application of Reuss's condition could result in discontinuous displacements at the interface of the two phases which means that the two phases would no longer remain bonded. Hence, neither assumption is completely correct.

Since the phases are isotropic, only two moduli, the bulk modulus κ and shear modulus G are sufficient to represent the phases. By imposing the sum of two concentration fractions $c_1 + c_2 = 1$, the moduli values in Voigt's condition is always found to be greater than that of Reuss's as shown in equation (2.17).

It is described that for the mixture with two isotropic phases,

$$\kappa \leqslant \kappa_v, \quad G \leqslant G_v \tag{2.11}$$

where v represents Voigt's moduli and

$$\kappa_v = c_1\kappa_1 + c_2\kappa_2, \quad G_v = c_1G_1 + c_2G_2 \tag{2.12}$$

Likewise, it is shown that

$$\kappa \geqslant \kappa_r, \quad G \geqslant G_r \tag{2.13}$$

where r represents Reuss's moduli and

$$\frac{1}{\kappa_r} = \frac{c_1}{\kappa_1} + \frac{c_2}{\kappa_2}, \quad \frac{1}{G_r} = \frac{c_1}{G_1} + \frac{c_2}{G_2} \tag{2.14}$$

Using the relations (2.15) and (2.16),

$$E = 3\kappa(1 - 2\nu) \tag{2.15}$$

$$E = 2G(1 + \nu) \tag{2.16}$$

where E is the Young's modulus and ν is the Poisson's ratio of the mixture, it follows from equations 2.11 and 2.13 along with equations 2.12 and 2.14 that

$$E_r \leqslant E \leqslant E_v \tag{2.17}$$

Hence, the work done by *R.Hill* (1963) [34] indicates that the correct modulus of multi-phase mixtures like the one discussed here needs to be dealt with boundary conditions which are different from the homogeneous strain (Voigt's limit) and homogeneous traction (Reuss's limit) conditions. This inspires the study of appropriate boundary conditions which could tackle the difficulties posed in heterogeneous media.

2.5 Homogenisation procedure

The work by *Suquet* (1987) [6] provides an approach for homogenization of periodic media with a view to calculate a homogeneous medium stiffness tensor. For this purpose, the paper adopts the use of PBC as a means to evaluate the homogenised stiffness tensor. This method has proven to evaluate the stiffness matrix between the bounds of stiffness tensors evaluated through uniform traction and uniform displacement boundary conditions.

Relation between macroscopic and microscopic quantities

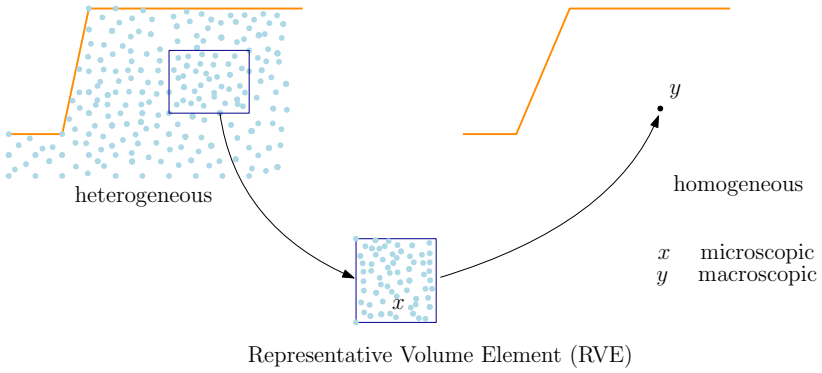

Figure 2.10: Schematic representation of microscopic and macroscopic scale composites and a RVE of heterogeneous medium [6]

Two scales have been defined in the literature by *Suquet* (1987) [6], the macroscopic scale on which the size of the heterogeneities is very small and the microscopic scale which is the scale of heterogeneities. The work mentions that to be able to derive macroscopic (or homogenised) law for the composite, statistically homogeneous specimen or RVE can be

defined in a composite. It describes that from classical arguments on oscillating functions, the macroscopic stress and strain tensors must be the averages of microscopic stress and strain tensors respectively. The oscillating functions have two parts, the mean part and a periodic part. The volumetric average of the periodic part of oscillating functions is zero and hence, the macroscopic stress and strain tensor components are an average of corresponding stress and strain tensor components over the volume V of microscopic RVE. Hence equations (2.18) and (2.19) could be written.

$$\sigma_{ij} = \frac{1}{|V|}\int_V \Sigma_{ij} dx \quad = \quad < \Sigma_{ij} > \tag{2.18}$$

$$\epsilon_{ij} = \frac{1}{|V|}\int_V \varepsilon_{ij} dx \quad = \quad < \varepsilon_{ij} > \tag{2.19}$$

where σ_{ij} represents the ij^{th} macroscopic stress tensor component and ϵ_{ij} represents the ij^{th} strain tensor components while $< \Sigma_{ij} >$ and $< \varepsilon_{ij} >$ represent the average of microscopic stress and strain tensor components respectively. The local microscopic position vector is represented by $\mathbf{x}$ whereas $\mathbf{y}$ represents the global macroscopic position vector. The displacement vector in the RVE is represented by $\mathbf{u}$.

The procedure which relates macroscopic quantities $\boldsymbol{\sigma}$ and $\boldsymbol{\epsilon}$ (and possibly their derivatives with time and other parameters) with the help of equations 2.18 and 2.19 along with equilibrium equation, micro constitutive relations and boundary conditions is termed as homogenization [6]. The inverse procedure is termed as localization which permits the determination of microscopic quantities like $\boldsymbol{\Sigma}(\mathbf{x})$ and $\boldsymbol{\varepsilon}(\mathbf{x})$ from the macroscopic ones. The following microscopic equilibrium equation is defined (when no body force or surface force is applied):

$$\mathrm{div}(\boldsymbol{\Sigma}) = 0 \tag{2.20}$$

The average $< . >$ of stress and strain tensors is defined as:

$$< \boldsymbol{\Sigma} >= \boldsymbol{\sigma}, \quad < \boldsymbol{\varepsilon}(\mathbf{u}) >= \boldsymbol{\epsilon} \tag{2.21}$$

Next, the choice of the RVE and boundary conditions are specified to solve the equilibrium equation with the help of constitutive relations. An RVE with a volume V and boundary ∂V is depicted in figure 2.11.

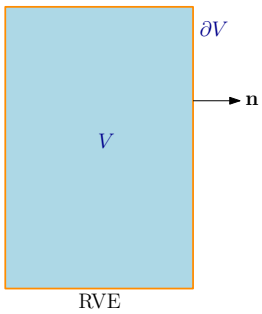

Figure 2.11: Schematic representation of RVE region and normal vector on its boundary

The periodicity conditions in a periodic microscopic medium is given as follows:

1. The microscopic traction $\boldsymbol{\Sigma}\mathbf{n}$ is anti-periodic.

2. The microscopic strain $\boldsymbol{\varepsilon}(\mathbf{u})$ is split into its average and a fluctuating term as $\boldsymbol{\varepsilon}(\mathbf{u}) = \boldsymbol{\epsilon} + \boldsymbol{\varepsilon}(\mathbf{u}^*)$, where $\boldsymbol{\epsilon}$ is the macro strain and $\mathbf{u}^*$ can be shown to be a periodic field up to a rigid body displacement that we disregard i.e $< \boldsymbol{\varepsilon}(\mathbf{u}^*) >= 0$.

This leads us to defining the following boundary conditions at the microscopic level on the boundary ∂V:

$$\text{uniform stresses on } \partial V: \quad \boldsymbol{\Sigma}\mathbf{n} = \boldsymbol{\sigma}\mathbf{n} \tag{2.22}$$

$$\text{uniform strains on } \partial V: \quad \mathbf{u} = \boldsymbol{\epsilon}\mathbf{x} \tag{2.23}$$

$$\text{and the periodicity conditions on } \quad \partial V: \quad \boldsymbol{\Sigma}\mathbf{n} \quad \text{is anti-periodic and} \tag{2.24}$$

$$\mathbf{u} = \boldsymbol{\epsilon}\mathbf{x} + \mathbf{u}^*, \ \mathbf{u}^* \text{ is periodic} \tag{2.25}$$

where, $\mathbf{u}$ and $\mathbf{n}$ represent displacement and normal vectors respectively while $\mathbf{u}^*$ is periodic part of displacement vector $\mathbf{u}$. Equations (2.22), (2.23), (2.24) and (2.25) are the set of boundary conditions for $\mathbf{u}$ and $\boldsymbol{\Sigma}$.

Further, for periodic microscopic media, application of periodicity conditions is suitable. Hence, the equilibrium equation given by equation (2.20) along with mentioned boundary conditions and constitutive relation given by equation (2.26) could be solved when $\boldsymbol{\sigma}$ or $\boldsymbol{\epsilon}$ are given for a linear elastic case.

$$\boldsymbol{\Sigma}(\mathbf{x}) = \mathbf{c}(\mathbf{x})\boldsymbol{\varepsilon}(\mathbf{u}(\mathbf{x})) = \mathbf{c}(\mathbf{x})(\boldsymbol{\epsilon} + \boldsymbol{\varepsilon}(\mathbf{u}^*(\mathbf{x}))) \tag{2.26}$$

Suquet (1987) [6] could be referred to for a solution of macroscopic stress tensor $\boldsymbol{\sigma}$ which is given by equation (2.27).

$$\boldsymbol{\sigma} =< \boldsymbol{\Sigma} >=< \mathbf{c}\boldsymbol{\varepsilon}(\mathbf{u}) >=< \mathbf{cD}\boldsymbol{\epsilon} >=< \mathbf{cD} > \boldsymbol{\epsilon} \tag{2.27}$$

where, $\mathbf{c}$ represents microscopic stiffness tensor and $\mathbf{D}$ represents the localisation tensor. For derivation of $\mathbf{D}$ *Suquet* (1987) [6] could be referred to. Equation 2.27 could be re-written as

$$\boldsymbol{\sigma} = \mathbf{C}\boldsymbol{\epsilon} \tag{2.28}$$

where, $\mathbf{C}$ is the homogeneous (macroscopic scale) stiffness tensor and is represented by $< \mathbf{cD} >$. The calculation of homogenized stiffness tensor ($\mathbf{C}$) is rather straightforward when calculated by internal energy approach as given in equation (2.33) than through calculation of localisation tensor ($\mathbf{D}$).

Equality of strain energy

The Hill's macrohomogeneity equality condition described in *Suquet* (1987) [6] gives the relation between the microscopic and macroscopic work. For a set of boundary conditions, a displacement field $\mathbf{u}$ satisfying the boundary condition is said to be admissible displacement field, while a divergence free stress filed satisfying the boundary conditions is said to be an admissible stress field. Now, if $\boldsymbol{\Sigma}$ and $\mathbf{u}$ be the admissible fields of stress and displacements, then the average of microscopic work of $\boldsymbol{\Sigma}$ in strain field $\boldsymbol{\varepsilon}(\mathbf{u})$ is equal to macroscopic work $\boldsymbol{\sigma\epsilon}$ as shown in equation (2.29).

$$< \boldsymbol{\Sigma\varepsilon}(\mathbf{u}) >= \boldsymbol{\sigma\epsilon} \tag{2.29}$$

Cristescu et al (2003) [35] point out the Hill-Mandel's lemmas which describe the following relations:

$$< \boldsymbol{\Sigma\varepsilon} >=< \boldsymbol{\Sigma} >< \boldsymbol{\varepsilon} >=< \boldsymbol{\Sigma} > \boldsymbol{\epsilon} \tag{2.30}$$

$$< \boldsymbol{\Sigma\varepsilon} >=< \boldsymbol{\Sigma} >< \boldsymbol{\varepsilon} >= \boldsymbol{\sigma} < \boldsymbol{\varepsilon} > \tag{2.31}$$

Through interpretation of equation (2.29), the internal energy density of a RVE (with volume V) can be given as in equation (2.32)

$$U = \frac{1}{2}\boldsymbol{\sigma\epsilon} \tag{2.32}$$

Taking reference from equation (2.28), equation (2.32) can be written as equation (2.33).

$$U = \frac{1}{2}\boldsymbol{\epsilon}^{\mathrm{T}}\mathbf{C}\boldsymbol{\epsilon} \tag{2.33}$$

where T represents transpose.

The procedure for calculating homogeneous stiffness tensor $\mathbf{C}$ through equation (2.33) has been shown in the next subsection.

Calculation of strain energy through FEM

We can see from equation(2.33) that for a given macroscopic strain $\boldsymbol{\epsilon}$, the stiffness tensor $\mathbf{C}$ can be calculated if the strain energy of the RVE is known. For a body subjected to elastic deformation, external forces must be equal to internal elastic forces for the body to be in equilibrium. Therefore, work will be done on the body to maintain the applied strain. Let's consider figure 2.12 for a general solid isotropic body.

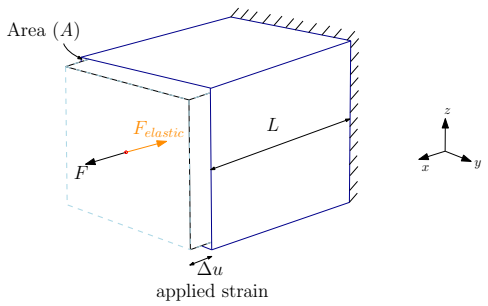

Figure 2.12: General elastic deformation of a cubic solid elastic body

Referring to figure 2.12 for a micro scale UC, in which for a general uniaxial load F in a given direction produces a displacement u in that direction. The external force would be equal to the internal elastic reaction force of the body.

$$F = F_{\text{elastic}} \tag{2.34}$$

The stress and strain produced in the direction of load application could be given as

$$\Sigma_x = \frac{F}{A} \tag{2.35}$$

$$\varepsilon_x = \frac{\Delta u}{L} \tag{2.36}$$

where, for a linear elastic case, A and L are the cross-sectional area of surface normal to x axis and length of the body in x direction respectively. Considering global equilibrium, the average of other stress components will be zero. Now, if the volume of the body is V, the strain energy is given by equation (2.37)

$$U = \frac{1}{2}\Sigma_x \varepsilon_x V \tag{2.37}$$

Replacing Σ_x and ε_x in equation (2.37) by equations (2.35) and (2.36) we get

$$U = \frac{1}{2}\frac{F}{A}\frac{\Delta u}{L}V \tag{2.38}$$

or

$$U = \frac{1}{2}F\Delta u \tag{2.39}$$

Thus, the strain energy can be represented in the form of force and displacement at nodes in a finite element model. In case of deformation of heterogeneous RVE (of volume V), nodal forces (which are internal elastic forces) and nodal displacements could be determined through FEM analysis. The work done on the RVE is equal to the strain energy generated in the RVE. Thus, equation (2.33) could be related to work done on RVE for a given macroscopic strain $\boldsymbol{\epsilon}$ as shown in equation (2.40).

$$\frac{1}{2}(\boldsymbol{\epsilon}^{\mathrm{T}}\mathbf{C}\boldsymbol{\epsilon})V = \frac{1}{2}\sum_{i=1}^{n}(F_i u_i)^{\mathrm{RVE}} \tag{2.40}$$

where, as defined earlier, $\mathbf{C}$ is the macroscopic stiffness tensor, V is the volume of RVE, F_i and u_i represent force and displacement in a direction at the i^{th} nodes in RVE FEM model along a corresponding degree of freedom, n is the number of nodes on the exterior surface of RVE.

Python scripting can be used to extract data of nodal forces and displacements on the boundary surfaces of RVE with the help of *Abaqus user manual* (2014) [36] and *Langtangen et al* (2006) [37]. The obtained data then can be used to obtain the right hand side value of equation 2.40. Using equation (2.40), we can define selective combinations of strain tensor components to solve for the constants in stiffness tensor $\mathbf{C}$ with respect to a given symmetry like orthotropic symmetry or transverse isotropy. Therefore sufficient number of combination of strain components must be taken to be able to solve for all the required constants of the stiffness tensor.

Comparison of stiffness tensors

With the help of aforementioned PBC, the following inequality of strain energies for cases of homogeneous traction, periodic displacement and homogeneous strain boundary conditions have been proposed in *Suquet* (1987) [6]:

$$\boldsymbol{\epsilon}^{\mathrm{T}}\hat{\mathbf{C}}\boldsymbol{\epsilon} \leqslant \boldsymbol{\epsilon}^{\mathrm{T}}\mathbf{C}\boldsymbol{\epsilon} \leqslant \boldsymbol{\epsilon}^{\mathrm{T}}\tilde{\mathbf{C}}\boldsymbol{\epsilon} \tag{2.41}$$

where $\boldsymbol{\epsilon}$ is the macroscopic strain, $\hat{\mathbf{C}}$, $\mathbf{C}$ and $\tilde{\mathbf{C}}$ represent the macroscopic elasticity tensors for the homogeneous traction, periodic displacement and homogeneous displacement boundary conditions respectively. From the aforementioned representation, it can be deduced that for a given macro strain, stiffness obtained by application of PBC lies in between homogeneous traction and homogeneous strain boundary conditions. Also, it is clear that homogeneous displacement boundary condition overestimates the stiffness of a periodic medium and homogeneous traction underestimates the stiffness of a periodic medium.

2.6 Application of PBC in FEM

Xia et al (2003) [7] discuss the results for a pure shear deformation mode for both PBC and homogeneous displacement boundary condition. In application of displacement difference boundary condition, plane remains plane constraint is not imposed after deformation while this constraint is imposed in the case of homogeneous displacement boundary condition. Similarly, *Xia et al* (2006) [38] have published findings after application of the two types of boundary conditions discussed above.

2.6.1 Implementation of PBC through displacement difference approach

The displacement field for periodic structure can be expressed as described *Suquet* (1987) [6] through equation (2.25). This equation shows the presence of periodic part of displacement field which can be difficult to determine. Thus, there needs to be a way by which this difficulty could be averted for application of periodic displacement field. One such approach for implementation of PBC is explained in the work of *Xia et al* (2003) [7]. The paper describes the application of unified displacement difference PBC on RVE by specifying a displacement difference approach between opposite faces of a RVE. Before specifying the approach described in the paper, the following schematic RVE is shown in figure 2.13 for a unidirectional lamina.

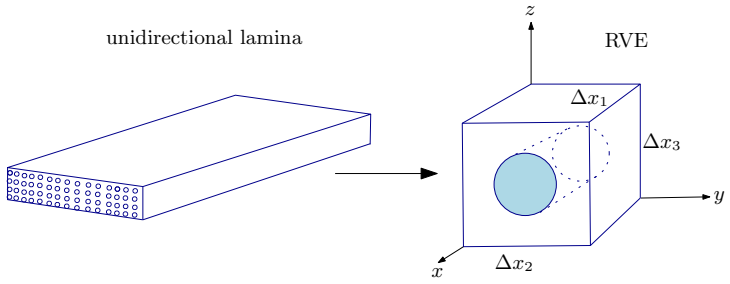

Figure 2.13: Representative Volume Element of a unidirectional lamina [7]

The relations involved through displacement difference approach for applying PBC is given as follows:

$$u_i = \epsilon_{ik} x_k + u_i^* \tag{2.42}$$

where, u_i is the displacement vector component, ϵ_{ik} is the average of microscopic strain tensor component, u_i^* is a periodic part of the displacement on boundary surfaces and x_k represents the dimension of RVE along the k^{th} axis where, $k = 1, 2, 3$ corresponding to x, y and z axes respectively. This periodic part of the displacement is generally unknown and depends on the load applied. A more suitable form of PBC for applications on parallelepiped RVEs can be derived further. For a cubic RVE, as shown in figure 2.13, the displacements on a pair of opposite boundary surfaces with their normals along x_j axis can be given as:

$$u_i^{j+} = \epsilon_{ik} x_k^{j+} + u_i^* \tag{2.43}$$
$$u_i^{j-} = \epsilon_{ik} x_k^{j-} + u_i^* \tag{2.44}$$

Index j_+ means along positive x_j direction and j_- means along negative x_j direction. Since u_i^* is the same on both the surfaces, after subtracting equation 2.44 from 2.43, we get

$$u_i^{j+} - u_i^{j-} = \epsilon_{ik} \Delta x_k^j \tag{2.45}$$

For any parallelepiped RVE, Δx_k^j is a constant. Therefore, the following unified PBC is obtained:

$$u_i^{j+} - u_i^{j-} = c_i^j \tag{2.46}$$

Where c_i^j represents the average stretch or contraction of the RVE due to 3D traction including normal and shear components.

Work done by *Xia et al* (2006) [38] further suggests that in equation 2.45, since Δx_k^j is a constant for each pair of opposite boundary surfaces, the equation can be interpreted as a displacement difference boundary condition. In context of FEA, application of displacement difference boundary condition is convenient as these displacement differences can be applied to nodes on opposite parallel faces of a RVE through nodal constraint equations. Hence equation 2.45 is a special type of displacement equation wherein instead of giving absolute values of displacement, we can assign a displacement difference between two opposite boundaries. Therefore, displacement continuity is guaranteed with the application of displacement difference boundary condition. However, as seen earlier the traction continuity is also vital and application of displacement difference boundary condition must also satisfy traction continuity at opposite faces.

Xia et al (2006) [38] describe that in displacement based FEM, the solution to equation 2.45 is unique. This can be explained by the tendency of the structure to deform in a manner that complies to the principle of minimum potential energy in displacement based FEM and hence the unique solution to equation 2.45 for a given average strain on the RVE. However, in displacement based finite element approach, the condition of traction continuity is automatically satisfied with application of equation (2.45). In context of current project, the application of PBC has to be done through a FEA package. Hence, study of the application procedure of this boundary condition is imperative.

Wu et al (2014) [39] have presented a comprehensive approach for applying PBC in Abaqus FEM package. For the application of PBC on opposite faces of a RVE, it is important that the in-plane location of nodes is the same. Thus, an algorithm is needed to pair up corresponding nodes on opposite surfaces for application of constraint equations to specify PBC.

Finite element modelling of Unit Cells and choice of material properties

Hyer (2009) [8] describes constituent material properties of a graphite fibre and epoxy matrix for heterogeneous modelling of a lamina through which a laminate of desired fibre orientation can be built. These material properties can be referred to for modelling of heterogeneous UC during execution of the project. The individual fibre and matrix properties for graphite-epoxy laminate is listed in table 4.1. The finite element modelling of the UC can be done with the help of standard 3D elements available in finite element packages like Abaqus which offer the use of elements like wedge or hexahedral elements. The meshing of UCs is an important step towards determination of results in heterogeneous analysis while dealing with periodic repetitions of cells (as described in the subsection 2.6.1). The PBCs can be applied through nodal constraint equations in Abaqus for which it becomes important that nodal location on opposite faces of the UC are symmetric (i.e they have same in-plane coordinates). With this in mind, studies have been carried out to mesh the UC symmetrically with the help of 3D elements.

Hyer(2009) [8] gives an understanding of the finite element modelling approach in square and hexagonal packed array models in a unidirectional lamina. The figure 2.14 gives a view of the discretisation pattern in quarter section of the two packing models.

(a) Finite element discretisation in square UC **(b)** Finite element discretisation in hexagonal UC

Figure 2.14: Finite element discretisation of square and hexagonal UCs [8]

Xia et al (2003) [7] illustrate the use of 3D eight-node hexahedral elements. The finite element mesh is constructed with the help of 1881 nodes and 1536 elements to model one block of unidirectional RVE. The mesh is represented in the figure 2.15. The paper mentions further that the mesh grid on the opposite faces on the RUC are the same and that the in-plane coordinates of the nodes are therefore the same. This means that the nodes on the $x = 1$ plane and $x = 0$ planes have the same (y, z) coordinates which provides convenience in application of displacement difference PBCs.

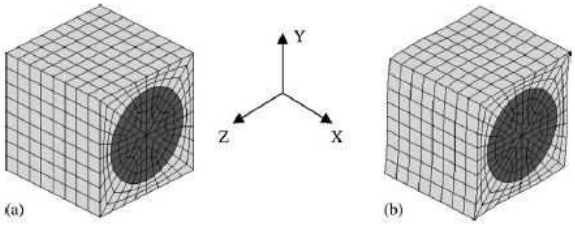

Figure 2.15: (a) Meshing of unidirectional UC using hexahedral elements. (b) Deformation state of UC upon application of periodic shear strain boundary condition [7]

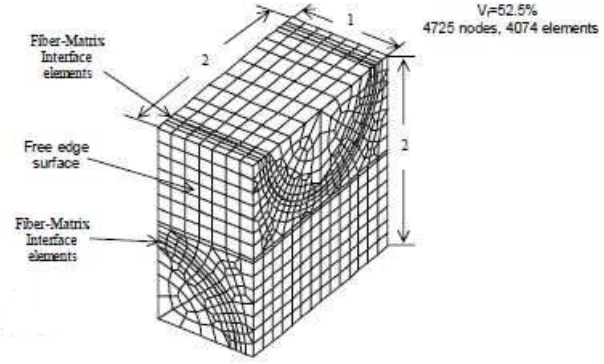

Figure 2.16: Finite element meshing of heterogeneous cross-ply laminate [5]

Ellyin et al (2002) [5] through figure 2.16 describes the meshing of a $[0/90]_{ns}$ cross-ply laminate (considering fibre and matrix sections) with 3D eight node hexahedral elements. The meshing of zero-ninety layers' interface could also be seen in the figure 2.16.

It is observable that the mesh in the zero and ninety degree parts of a zero-ninety RVE must be identical for them to get *merged* or *tied* together at the interface in FEM package like Abaqus. This is achievable with the use of 3D elements like wedge or hexahedral elements. In Abaqus, modelling with hexahedral elements gives the option of developing a structured mesh which would enable the symmetric meshing of the RVE. However, while modelling with hexahedral elements in particular, care needs to be taken to keep the element aspect ratio low in critical regions so that the elements do not get distorted upon deformation.

The literature review suggests that in general two to four elements are used to discretise the narrowest region between the fibre and side of RVE [7], [5]. Here, it is to be highlighted that with every single increase in the number of elements in the region between fibre and RVE's side, there would be a large increase in the number of elements volumetrically in the UC and subsequently in the laminate's model.

2.7 Prediction of delamination initiation due to free edge stresses

One of the objectives of this research is to study the effect of interlaminar stresses near the free edge region on delamination initiation. Since the determination of point stress values at the free edge is cumbersome due to high gradient stresses and sometimes not feasible because of the presence of singularity [12], there need to be other methods which could take the stresses near the free edge into account for prediction of delamination initiation. Hence, literatures in this section are studied to arrive at a suitable method through which the prediction of delamination initiation in homogeneous model laminates could be carried out from the perspective of free edge stresses.

Criteria for prediction of delamination initiation

C.T Herakovich (1989) [40] in his paper explores the effect of free edge stresses on delamination initiation on cross-ply, angle-ply and quasi-isotropic laminates. In context of cross-ply laminates, analyses pertaining to stress profiles based on effect of layer stacking sequence on $[90_2/0_2]_s$ and $[0_2/90_2]_s$ is presented. Local mismatch in properties between adjacent layers and stacking sequence play a part in interlaminar stresses and delamination. It has been highlighted that the free edge boundary conditions require interlaminar shear stress τ_{yz} to be zero but there can be an existence of interlaminar normal stress σ_z at the free edge. The interlaminar normal stress σ_z is considered responsible for delamination initiation. Further, it has been mentioned that because tensile interlaminar normal stress initiate delamination and compressive interlaminar normal stress suppresses delamination, sign of σ_z is important. The sign of σ_z is reported to be a function of sign of axial load and stacking sequence of the laminate. For elastic response, while changing the direction of axial load directly changes the sign of stress, changing the stacking sequence does not result in exact reversal of interlaminar normal stress.

Some of the criteria accounting for the interlaminar stresses in delamination initiation have been proposed in this subsection. One of them is a criteria for prediction of delamination onset by *O'Brien* (1982) [41]. The paper presents through-thickness and through-width distribution of interlaminar normal stress σ_z for a $[\pm 30/\pm 30/90/90]_s$ laminate from finite element analysis.

The peak interlaminar normal stresses are reported to be obtained at the interface of the $-30/90$ layers and the value has been reported to change at the free edge with refinement in mesh size. Thus, the use of failure criterion based on maximum interlaminar stress value was not possible citing the presence of singularity for linear elastic analysis. Hence, an alternative approach based on strain energy release rate was proposed. The critical stress at the detection of delamination is determined from the load level for a given specimen. The critical stress is used to determine the critical strain which in turn is used to determine the strain energy release rate at delamination initiation. This value of strain energy release rate is then used to predict the nominal strain for delamination initiation in further studies.

Brewer et al (1988) [12] propose a criterion for predicting delamination initiation which considers the interlaminar stresses and their combination near the free edge of composite laminates. An average stress based Quadratic Delamination Criterion (QDC) is introduced. In this approach, the initiation of delamination is established by noticing a drop in load and observation of delamination. The values of initiation stress measured is correlated using the strain energy release rate approach and it is found that the strain energy release rate is not able to accurately correlate data for two of the three laminate families taken into consideration. The data obtained shows that the critical strain energy release rate is dependent on ply thickness.

The QDC compares the interlaminar stresses to their related strength parameters and has been reported to show excellent correlation with delamination initiation stress data. In this paper, the average of a stress component σ_{ij} is given as:

$$< \sigma_{ij} >= \frac{1}{y_{avg}} \int_0^{y_{avg}} \sigma_{ij} dy \tag{2.47}$$

where, y is the distance along the transverse direction of homogeneous layer laminate from the free edge on an interface.

The value of y_{avg} is determined experimentally and this characteristic length from the free edge region along the interface is used as a normalization parameter for the high gradient interlaminar stresses near free edge. The value of y_{avg} as the upper limit of integral is the same as the value of y_{avg} used for averaging. But if a stress curve changes sign before the value of y_{avg} then the distance from free edge until where the curve changes sign is used as upper limit of integration. This is because the portion of the curve after the cross-over point where sign gets changed, is not considered to have a major impact in counteracting the effect of stress near the free edge. Considering $< \sigma_{xz} >$ and $< \sigma_{yz} >$ as average interlaminar shear stresses and $< \sigma_z >$ as average interlaminar normal stress, the quadratic delamination criterion is given as:

$$(\frac{< \tau_{xz} >}{Z^{s1}})^2 + (\frac{< \tau_{yz} >}{Z^{s2}})^2 + (\frac{< \sigma_z^t >}{Z^t})^2 + (\frac{< \sigma_z^c >}{Z^c})^2 = 1 \tag{2.48}$$

where
Z^t = tensile interlaminar normal strength;
Z^c = compressive interlaminar normal strength;
Z^{s1} = interlaminar shear strength for τ_{xz} stress and
Z^{s2} = interlaminar shear strength for τ_{yz} stress

The superscripts t and c indicate the tensile and compressive values of interlaminar stresses should be compared to the corresponding values of interlaminar normal strengths. Further,

the paper proposes a single averaging distance for a material. Thus, the averaging distances for different layup configurations have been averaged all together statistically to propose a single averaging distance for a particular material.

2.8 Laminates susceptible to failure by delamination initiation

This section covers the study of laminates which could be analysed for failure by delamination initiation. *Wang et al (1985)* [9] report the failure of laminates with different layup orientations when subjected to uniaxial strain. For T300/934 material, when $[0_2/90_n]_s$ laminates (where n is the number of ninety degree layers) are analysed, it is found that the free edge effect under tension is negligible and that edge delamination alone cannot occur. Specimens 25 mm wide by 225 mm long and with nominal ply thickness of 0.132 mm are tested. For $n = 1$, the paper reports that through the strain energy release rate approach, the laminate would undergo transverse cracking at a strain value of 0.0059. Similarly, for $n = 2$ at 0.0036 and for $n = 4$ at 0.00273.

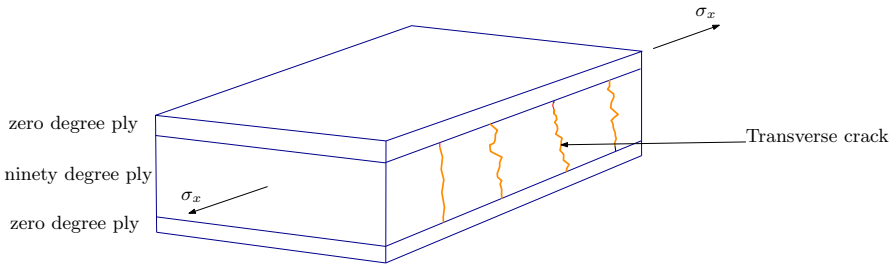

Figure 2.17: Schematic representation of transverse cracks in cross-ply laminate [9]

It is calculated through strain energy release rate approach that for $n = 2$, free edge delamination onset would happen at strain values of 0.036 and for $n = 4$ at 0.052. However, at strain values of 0.01 to 0.012, the laminate is reported to fail by fibre fracture. Hence, it is suggested that free edge delamination might never occur.

A study on laminates with $[\pm\theta/90]_s$ configuration is conducted and it is revealed that for $[\pm 25/90]_s$ laminates free edge delamination is predicted to happen at 0.6 % strain. Experimental range of delamination initiation is reported to be 0.58 % to 0.61 % for T300/934 material. The $[\pm 25/90]_s$ laminate has three different interfaces between adjacent layers, the $+25/-25$ interface, the $-25/90$ interface and the 90/90 symmetric mid-plane interface. It becomes interesting now to study the interface at which the delamination occurs.

Wang et al (1985) [9] and *Schellekens et al* (1991) [10] report the delamination to occur at the 90/90 symmetric mid-plane of the laminate when subjected to longitudinal tensile strain. A schematic delamination in the $[\pm 25/90]_s$ laminate is shown in figure 2.18.

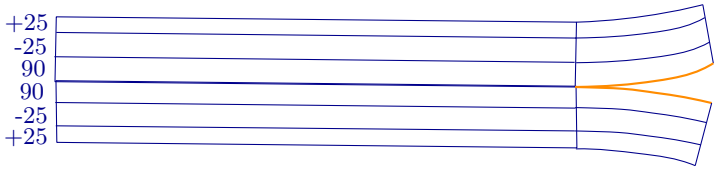

Figure 2.18: Schematic representation of delamination in $[\pm 25/90]_s$ laminates [10]

Brewer et al (1988) [12] propose an averaging distance of 0.145 mm from for T300/934 material for a combination of $[\pm 25/\bar{9}0]_s$, $[\pm 25/90]_s$ and $[\pm 25_2/90]_s$ layup specimens. Hence, it can be inferred that according to QDC, a single averaging distance can be proposed for a combination of layup configurations made of T300/934 material.

2.9 Numerical integration of stresses

Equation (2.47) requires the averaging of stresses along the width (transverse direction) of a laminate. The averaging itself involves integration of the stresses and this makes it relevant to highlight the methods of numerically integrating the stress data points. If the mesh in heterogeneous and homogeneous models are fine enough to produce continuous and smooth plot of stress points, then a suitable employment of a numerical integration method could be made conveniently. The nature of free edge stresses signals a steep rise in stresses near the free edge. The curve flattens out as we move away from the free edge. It has also been seen that the mesh needs to be finer near the free edge compared to far-off regions from the free edge. Hence the spacing of data intervals is irregular based on the requirements of finite element mesh. Given the small element size in the region of high gradient of stress, the approximation of curves to linear line segments is feasible and therefore the error in calculation of area under the curve numerically could be minimised. This calls for a rather simplified use of numerical integration schemes such as the trapezoidal method. For a continuous function f divided into n number of equally spaced intervals of size s in the domain [a,b], the trapezoidal integration $T_n(f)$ is defined by *Davis et al* [42] by equation (2.49) :

$$T_n(f) = s[\frac{f(a)}{2} + f(a+s) + f(a+2s) + \cdots + f(a+(n-1)s) + \frac{f(b)}{2}] \tag{2.49}$$

The implementation of trapezoidal integration scheme for $n+1$ evenly spaced points is provided in Matlab documentation as follows in equation (2.50):

$$\int_a^b f(x)dx = \frac{b-a}{2n}[f(x_1) + 2f(x_2) + \cdots + 2f(x_n) + f(x_{n+1})] \tag{2.50}$$

where, the spacing between each point is equal to the scalar value $\frac{b-a}{n}$. However, for our convenience, we need to find the area under the curve when the data points are not evenly spaced. An unevenly spaced data plot may appear for example as in figure 2.19. For such a distribution, the trapezoidal integration scheme is defined in Matlab documentation as follows in equation (2.51):

$$\int_a^b f(x)dx = \frac{1}{2}\sum_{n=1}^{n=N}(x_{n+1} - x_n)[f(x_n) + f(x_{n+1})] \tag{2.51}$$

where $(x_{n+1} - x_n)$ is the spacing between each constitutive pair of points. Matlab function *trapz* can be used to calculate numerical integration for discrete data sets.

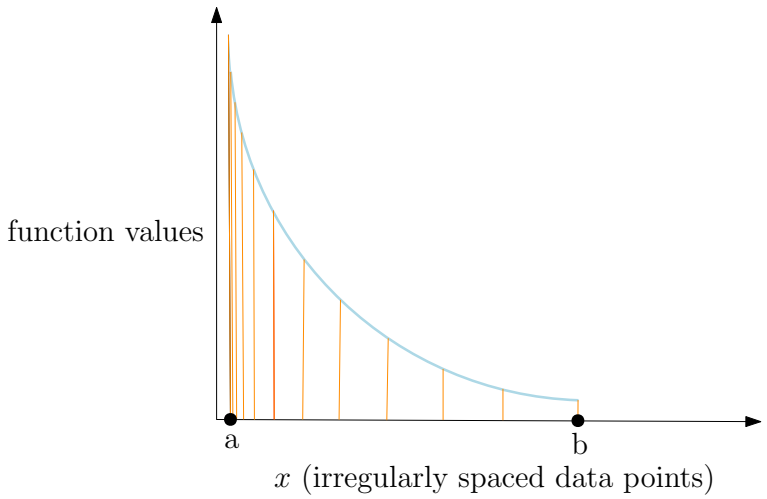

Figure 2.19: Segmented area under the plot with unevenly distributed data points

2.10 Conclusions

With the help of the studies performed in all the above sections, it is evident that among various methods studied for analysis of free edge stresses in cross-ply composite laminates, FEM is one of the most effective techniques which provides results up to a substantial level of accuracy. Moreover, the availability of commercial FEM packages like Abaqus and good computational facilities make this method viable and efficient. The large amount of literature available for comparison of results obtained from FEM also make use of FEA a comparatively better method to analyse the free edge effect in context of the present project. Particularly, it has been observed that use of 3D FEA have served as benchmark analysis until as recently as 2016. With the help of finite elements, the homogeneous material layer models of the cross-ply laminates could be efficiently modelled with considerable detail.

The modelling of heterogeneous models has been studied through FEM. Finite element modelling of heterogeneous models has been seen to be carried out effectively in the literatures studied. For effective extraction of overall properties from RVE, application of PBC has appeared to be the best approach forward. The ability of FEA package like Abaqus to facilitate the application of PBCs in the heterogeneous models, further makes FEM a preferred analysis method in context of the project. Use of hexahedral elements has found good application in heterogeneous FEM models. The possibility of generating structured mesh through hexahedral elements favours its usability, particularly while applying PBCs. Use of scripts through commercially available packages like Matlab could be made for the implementation of PBCs through Abaqus. Further, the post-processing of results from Abaqus could be carried out by scripting tools like Python, which is readily available as well. Python scripting could also facilitate the establishment of stiffness equivalence homogenisation between the homogeneous material layer model and heterogeneous model.

The last portion of the literature study deals with studying the relevant literatures available for understanding the roles of free edge stresses in initiating delamination and further understanding of the suitable criteria which could facilitate the analysis of delamination initiation. It has been found that the QDC proposed by *Brewer et al* (1988) [12] best suits the analysis of delamination initiation due to free edge effects in context of the current project. The criterion involves an interaction of interlaminar free edge stresses and has been reported to provide results correlating well with experimental findings for problem at hand. The combined results obtained from the homogeneous material layer model and heterogeneous models would facilitate the delamination initiation analysis through the QDC. Further, $[\pm 25/90]_s$ laminate configuration has been identified as a potential layup for implementation of QDC. Suitable materials for modelling of homogeneous laminae and heterogeneous models comprising of fibres and matrix properties have been identified. Hence, during the course of following chapters, the fibre and matrix properties used for heterogeneous modelling and effective engineering constants for modelling homogeneous layer laminates have been tabulated as per need.

Hence, the state of the art work reported in this chapter provide the basis for implementation of suitable modelling and analysis approaches. Some of the results cited in the literature also provide the basis for comparison of results generated during the course of the research. Work by *Lessard et al* (1996) [3] provides the basis for FEM modelling of homogeneous layer laminates. Further, a review work by *Mittelstedt et al* (2007) [1] advocates the use of FEM for analysis of free edge stresses because of the reliability of FEM for free edge analysis. Works by *Suquet* (1987) [6] and *Xia et al* (2003) [7] provide an understanding of heterogeneous modelling and analysis of laminates. QDC proposed by *Brewer et al* (1988) [12] enable the prediction of delamination initiation due to free edge stresses on a laminate susceptible to exhibiting delamination initiation.

Chapter 3

Free Edge Stresses in Homogeneous Layer Model of $[0/90]_s$ Laminate

3.1 Background

Previously in literary findings, the high gradient stresses at free edges, sometimes to an effect of a singularity, is reported to be a mathematical artefact. The essence of this project is to overcome the barrier to be able to consider free edge stresses for assessing their effect on delamination initiation. For this purpose, it is imperative to study the stresses in the vicinity of free edges and to confirm the presence of high stress gradients in the first place. Literary findings have advocated the use of FEM as a reliable method for detection and analysis of free edge stresses. In the course of this chapter, FEA of a cross-ply laminate is conducted to study the 3D stress fields near the free edge. An attempt will be made to verify the presence of expected steep gradients near free edges according to literature. Also, the compliance of analysed stress components with their expected nature would be verifiable based on laminate's equilibrium as described in subsection 1 of chapter 1. As seen in the previous chapter, the Quadratic Delamination Criterion proposed by *Brewer et al* [12] is identified as a potential criterion for studying delamination initiation. The criterion employs averaged stresses from the free edge and hence, in the course of this chapter, the interlaminar stresses due to free edge effect will be averaged along the laminate's transverse direction.

3.2 Investigation of interlaminar of stresses near free edge

Classical Laminate Theory (CLT) suggests the presence of in-plane stresses for a laminate under in-plane loading. However, it becomes interesting to study the presence of interlaminar stresses for in-plane loading, especially near the free edge. The generation of interlaminar stresses would be bolstered by the the difference in material properties at the interfacial junction between two layers. This difference is bound to be maximum at the zero-ninety layer interface in a cross-ply laminate and hence, a cross-ply laminate is a simple and obvious

candidate for the study of free edge interlaminar stresses. Therefore, it's important to frame the best procedure for modelling of cross-ply laminates and employment of suitable FEM practices which could allow a comprehensive study of the problem at hand. The following subsections are concerned towards addressing these areas.

Modelling of cross-ply laminates for studying interlaminar stresses

The idea in this section is to find out the variation in interlaminar stresses along the width of the laminate at zero-ninety degree layer interface in transverse direction. Essentially, this would capture the free edge effects produced by the edges running through the laminate's thickness as shown in figure 1.1. Keeping in mind the fundamental of Saint Venant's principle, it is expected that the dependence of stresses would no longer be present on the longitudinal coordinate after a certain distance from the point of load application. Thus, for a laminate under in-plane longitudinal extensional strain loading, the interlaminar stresses at a sufficiently far-off distance from the surface of applied loading would allow us to investigate the free edge effect in transverse direction. The transverse mid-section (shaded blue) in figure 3.1 below explains the region of interest for free edge stress analysis.

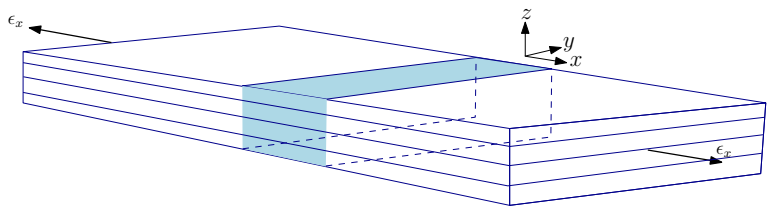

Figure 3.1: Transverse mid-section of a laminate far away from boundary loaded under extensional longitudinal strain

The analysis of free edge effect through FEM could be a computationally taxing affair because a fine mesh would be needed around the edges to capture the state of stress as closely as possible. It thus becomes logical to maximise the use of elements in the area of interest. This calls for an important judgement on *'an optimum form of model for analysis of the free edge problem'*. One of the best solutions to this questions was found through the model proposed by *Lessard et al* (1996) [3]. *Lessard et al* call it a *slice* model as shown in figure 2.3. The slice model is essentially a thin strip of laminate which represents a transverse section far-off from from the point of load application. If the independence of stresses on longitudinal coordinates is to be imposed, then minimising the length of the strip (in x direction) would allow utilisation of computational effort towards capturing of the free edge phenomenon. Thus, modelling a strip with only one element in the length direction makes for a sensible modelling approach. Thus, the shaded region in figure 3.1 could be modelled as a slice with one element in longitudinal (x) direction. The thin slice when modelled with 3D elements, facilitates application of longitudinal extensional strain conveniently.

Further, it has been proposed in the literatures that 3D finite elements have the potential of capturing free edge stresses reliably [3]. One of the elements found to have been suitable for free edge stress detection is the 3D hexahedral element [3]. It is notable that nodes in hexahedral elements do not have rotational degree of freedom (DoF). So, it is important to mesh critical regions, especially the region near free edges with small element sizes to

capture deformations in detail at the critical region. The other key approach could be the use of quadratic elements for providing increased flexibility to hexahedral elements. Thus, considering all factors, the use of 20 node hexahedral elements (C3D20R) in Abaqus is chosen as the best element for modelling the slice.

3.3 Modelling of cross-ply quarter slice

A $[0/90]_s$ cross-ply laminate has been chosen for developing the slice model. A schematic representation of the slice model is shown below in figure 3.2. The slice model, as mentioned before, represents the transverse cross-section of the laminate. However, given the symmetry of the $[0/90]_s$ laminate about the $z = 0$ and $y = 0$ planes referring figure 1.2, it would be computationally optimal to model a quarter of the laminate for analysis of free edge stresses on one of the free edges.

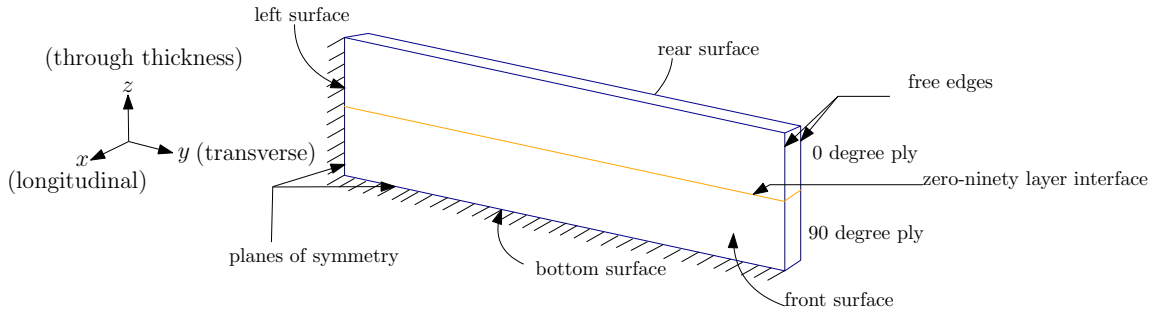

Figure 3.2: Schematic representation of symmetric quarter slice of a $[0/90]_s$ laminate

The finite element modelling of the quarter slice in figure 3.2 of the $[0/90]_s$ laminate is done in Abaqus FEA software (version 6.14). The objective of the analysis in this section is to analyse through a suitable FEM model, the 3D stress states near the free edge.

As understood from the force equilibrium analysis of a laminate under extensional loading in linear deformation regime in chapter 1, at the intersection of the free edge and interface between the zero and ninety degree layers there must be a 3D stress state. *Lessard et al* (1996) [3] have published the non-zero interlaminar stresses along the interface in the transverse (y) direction and along the free edge itself in the through thickness (z) direction. It is worthwhile to check the appropriateness of the chosen modelling scheme by comparing the obtained results with those published in *Lessard et al* (1996) [3]. To this effect, the element, material properties and loading conditions are the same as that in *Lessard et al* (1996) [3] to draw a comparative analysis between the results and hence verify the analysis.

To be able to do so, the material properties in table 3.1 (which is also the material used by *Lessard et al* (1996) [3]), is chosen for modelling.

Table 3.1: Engineering properties of high modulus graphite-epoxy lamina [2]

Properties	Value
E_x(GPa)	137
E_y (GPa)	14.5
E_z(GPa)	14.5
ν_{xy}	0.21
ν_{xz}	0.21
ν_{yz}	0.21
G_{yz}(GPa)	5.86
G_{xz}(GPa)	5.86
G_{xy} (GPa)	5.86

Further, C3D20R quadratic hexahedral element (with reduced integration) is chosen. A linear analysis is carried out with application of longitudinal extensional strain of 0.01. Since the region of intersection of the zero-ninety degree layers' interface and free edge is of prime importance, mesh density in the region has been increased to capture the stress states sufficiently. The figure 3.3 represents a generic finite element modelling approach followed for the cross-ply quarter slice. The slice is modelled with one element in longitudinal (x) direction.

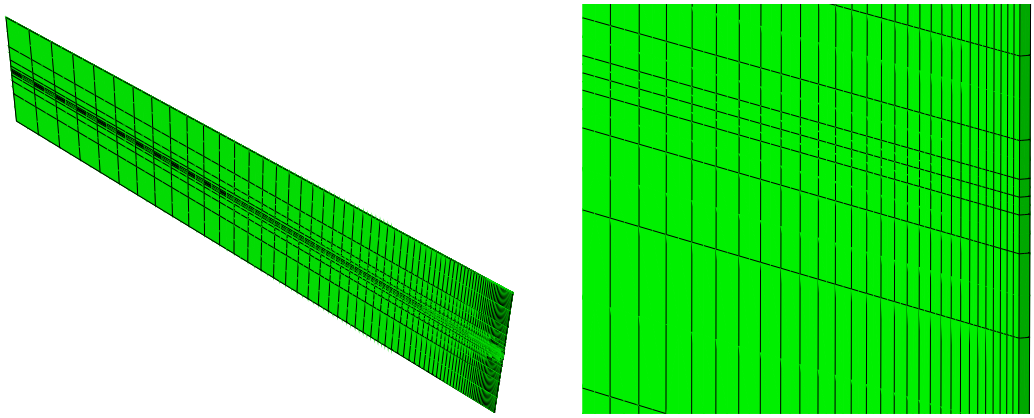

(a) FEM modelling of symmetric quarter slice of a $[0/90]_s$ laminate in Abaqus

(b) View of intersection of free edge and zero-ninety layers' interface

Figure 3.3: Finite element mesh on a quarter symmetric part of $[0/90]_s$ laminate

With reference to figure 3.2, the slice (x direction) is modelled with a length of 0.001 mm (1 micron). The size of the element at the intersection of free edge and interface (shown in figure 3.3b) is taken such that the aspect ratio of less than 2 is maintained [3]. The ply thickness (z direction) considered is 0.134 mm (standard nominal ply thickness for graphite-epoxy material laminates [3] and [12]). As an initial measure, the width of the quarter part is modelled with ten times the ply thickness in y direction.

For building the model, a script was written in Python scripting tool using Abaqus Scripting Interface with the help of Abaqus user manual [36]. This was done to be able to parametrize the model for carrying out subsequent parametric variations with ease and efficiency. As

can be seen in figure 3.3, a rectangular mesh has been produced with biasing towards the intersection of free edge and transverse interface. Since the length of the slice is taken to be 0.001 mm, the size of the element at the intersection point has been modelled as a function of the slice length. This is important to ensure the mitigation of element distortion at the critical region of analysis. The entire model is discretised using seed biasing by size and structured mesh option is used to create a symmetric and structured mesh.

To begin with the analysis, the model is built with 876 C3D20R elements to come close to the use of 856 elements by *Lessard et al* (1996) [3]. This approach allowed a comparison of results between the two models in terms of interlaminar stress results with almost same level of discretisation.

With reference to figure 3.2, the left and bottom surfaces are provided $y-$symmetry and $z-$symmetry respectively. The rear surface is constrained in $x-$direction and the front surface is provided a longitudinal extensional displacement in $x-$direction corresponding to a strain of 0.01.

Analysis results of the quarter slice model

The output results obtained from analysis of the model described above is to be discussed herein. Before analysis the two primary expectations from the results are:

1. Comparatively higher transverse deformation of zero degree layer.
2. Generation of maximum interlaminar normal stress at the point of intersection of free edge and zero-ninety layer interface.

The figures 3.4 and 3.5 illustrate the analyses carried out for determining the interlaminar stresses in the slice model. The convention followed for reporting of the results is based on the coordinate system described in figure 3.2 i.e. longitudinal direction as x, horizontal transverse direction as y and through thickness direction as z. Since the stress doesn't vary longitudinally (Saint Venant's principle), a 2D representation of stress distribution has been shown for optimum visualisation.

The interlaminar normal stress σ_z is represented in figure 3.4.

Figure 3.4: Distribution of interlaminar normal stress σ_z (MPa) for 876 elements

The above analysis suggests a concentration of stress σ_z at the intersection of free edge and zero-ninety degree layers' interface.

Similarly, the results for interlaminar shear stresses τ_{yz} and τ_{xz} are shown in figure 3.5 as follows:

(a) Interlaminar shear stress τ_{yz} (MPa) for 876 elements

(b) Interlaminar shear stress τ_{xz} (MPa) for 876 elements

Figure 3.5: Distribution of interlaminar shear stress (MPa)

The interlaminar normal stress σ_z and interlaminar shear stress τ_{yz} appear to have a non-zero distribution near the free edge. The distribution of other interlaminar shear stress component τ_{xz} appears to be zero throughout the laminate.

As expected the zero degree ply has undergone more transverse deformation than the ninety degree layer. This is in line with lower stiffness of zero degree layer in transverse direction compared to the ninety degree layer.

The following plots generated through Matlab software package cast a clearer picture of the stresses along the zero-ninety degree layers' interface in transverse direction. The ply thickness (0.134 mm) is denoted by h.

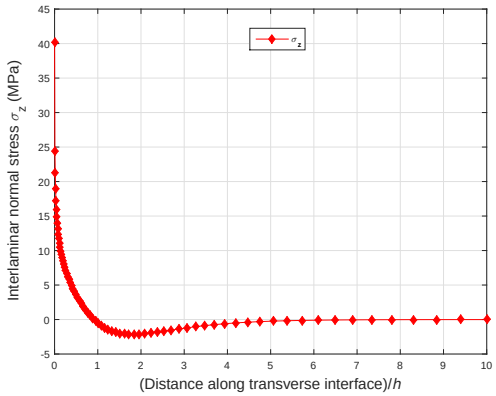

Figure 3.6: Interlaminar normal stress σ_z at zero-ninety layers' interface

Figure 3.6 represents the interlaminar normal stress at the interface of the zero and ninety degree layers. In Abaqus, the stresses are computed at the nodes through interpolation. Since the nodes at the interface are shared between the elements lying in the zero degree layer and the elements lying in the ninety degree layer, two stress data are obtained at nodes close to the free edge due to considerable difference in interpolated stresses from elements across the interface. In such a scenario, the stresses from elements across the interface are averaged at the interfacial nodes to obtain the distribution of stresses along the interface. A Matlab script

is written for the purpose of averaging the stresses. In a similar way the interlaminar shear stress components τ_{yz} and τ_{xz} have been plotted as shown in figure 3.7.

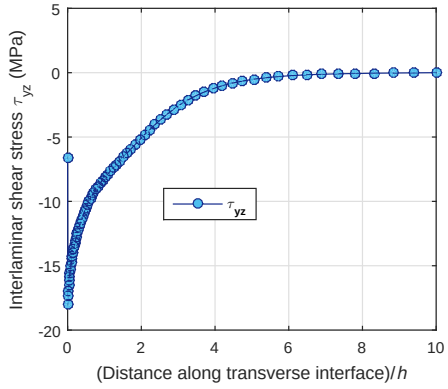

(a) Interlaminar shear stress τ_{yz} at zero-ninety layers' interface

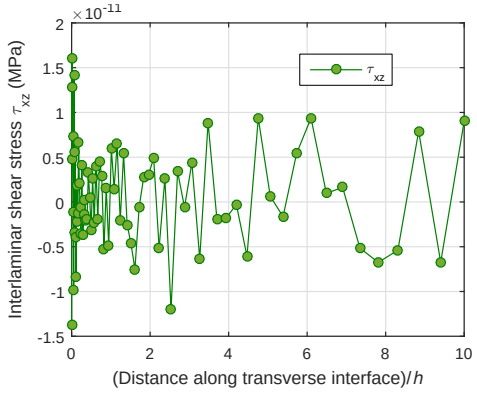

(b) Interlaminar shear stress τ_{xz} at zero-ninety layers' interface

Figure 3.7: Interlaminar shear stress distribution along laminate's transverse interface

In figures 3.6 and 3.7, the zero value of abscissa represents the free edge at interface. It can be interpreted from the figure 3.6 that the maximum value of interlaminar normal stress occurs at the free edge. The stress changes its sign after a certain a distance (cross-over point [12]) before fading out in compliance with CLT. The stress changes its sign before reducing to zero far away from the free edge. This nature of the plot is in alignment with physical equilibrium in $z-$direction along the interface (as the sum total of forces in $z-$direction must be zero on interface).

Figure 3.7a shows the behaviour of τ_{yz}. The stress component is zero far away from the free edge. The stress goes compressive in nature before rising with high gradient in the vicinity of free edge. This behaviour of approaching zero as free edge nears is in compliance to the requirement of traction free boundary at the free edge and hence appears logical. The interlaminar shear component τ_{xz} in figure 3.7b is found to be negligible (in the order of 10^{-11}) as seen in figure 3.7b. The random distribution of data in the plot can be ascertained to noise in calculation by finite element solver. The negligible occurrence of τ_{xz} has also been reported in literature [3].

Plots obtained from the analysis remain to be compared with findings in literature. For this purpose, results published for $[0/90]_s$ laminate by *Lessard et al* (1996) [3] have been used wherein the ply thickness used for analysis is also 0.134 mm. As it has been found that the interlaminar stress component τ_{xz} is negligible, comparisons have been made only for σ_z and τ_{yz}. Figure 3.8 represents the comparison along transverse (y) direction interface of interlaminar normal stress results between the current analysis and the result published in [3]. Similarly, the comparison of interlaminar normal stress along the free edge through laminate's thickness (z) direction is represented in figure 3.9. The data points from *Lessard et al (1996)* [3] have been reproduced using plot digitiser software for carrying out the comparison.

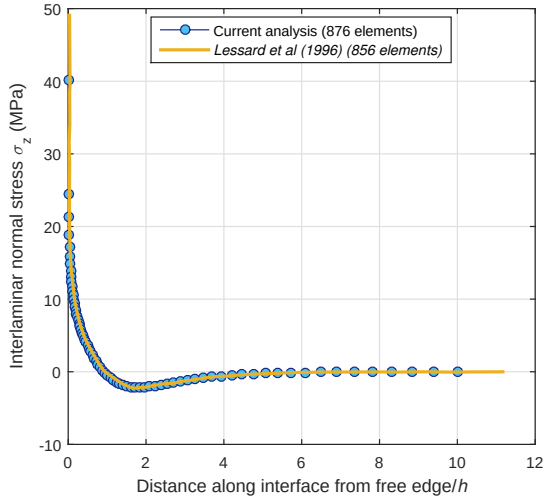

Figure 3.8: Comparison of interlaminar normal stress σ_z with *Lessard et al* (1996) [3] along interface in transverse ($y-$direction)

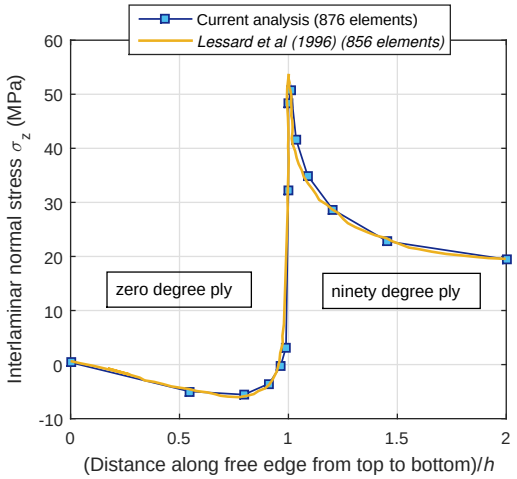

Figure 3.9: Comparison of normal stress σ_z with *Lessard et al* (1996) [3] along free edge in through thickness ($z-$direction)

It is also noticeable in figure 3.9 that the stress σ_z is at it's highest value at the interface

($h = 1$) and reduces in value on either side of the interface. Similarly, the comparisons for interlaminar shear stress component τ_{yz} is shown in figure 3.10.

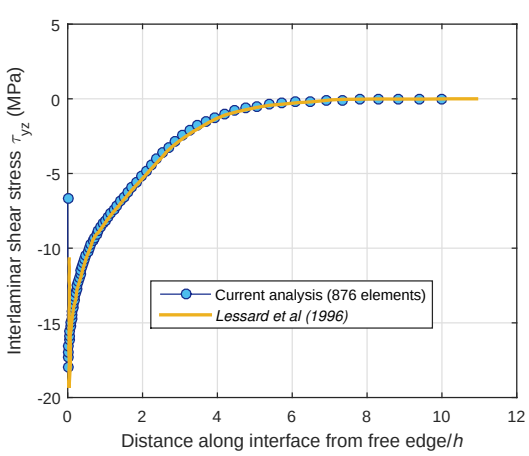

(a) Comparison of interlaminar shear stress τ_{yz} along transverse interface

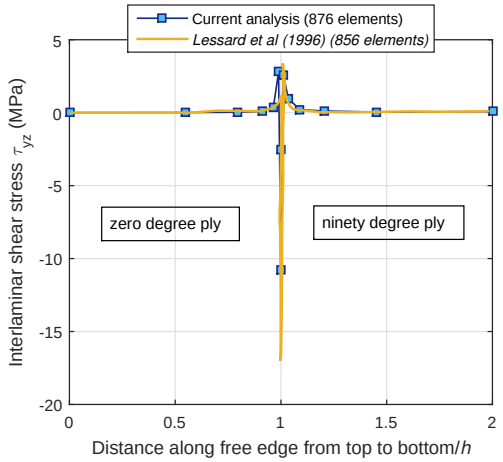

(b) Comparison of interlaminar shear stress τ_{yz} along free edge

Figure 3.10: Comparison of interlaminar shear stress τ_{yz} with *Lessard et al* (1996) [3]

The comparison of plots suggests that the obtained results correlate closely with that in literature and hence, the adopted modelling method could be relied upon for further investigation of interlaminar stresses near free edges.

3.4 Investigation of stresses at free edge

From the previous section it is obvious that the stresses σ_z and τ_{yz} rise with high gradient as the free edge approaches. However, variation of peak stress at the free edge is to be studied for a constant strain value. For this purpose, the elements across the interface in transverse ($y-$direction) are refined in size to increase the number of elements across the width. The minimum and maximum element sizes on the interface were divided by equal factors while biasing the mesh towards the region of high gradient. This approach enables cutting of the elements by a chosen factor and thereby facilitates the increase of mesh density at the critical region. The elements are subsequently divided and this approach leads to development of four successively refined meshes. Analyses were conducted for 876, 2420, 10212 and 42720 elements. For these meshes, the interlaminar stresses are studied to investigate stress values at free edge.

Table 3.2 lists the sizes of element in transverse (y) direction at the intersection of free edge and zero-ninety degree layer interface corresponding to every mesh. Along the interface, the element dimension in transverse direction is minimum at the free edge and the size increases as distance from free edge increases.

Table 3.2: Dimension of element in transverse direction at the free edge on zero-ninety degree layers' interface corresponding to different meshes

Number of elements in mesh	Element dimension at free edge in transverse direction (mm)
876	0.001
2420	$0.001/1.5 = 0.00066$
10212	$0.001/3 = 0.00033$
42720	$0.001/6 = 0.0001$

The results found are produced in figure 3.11.

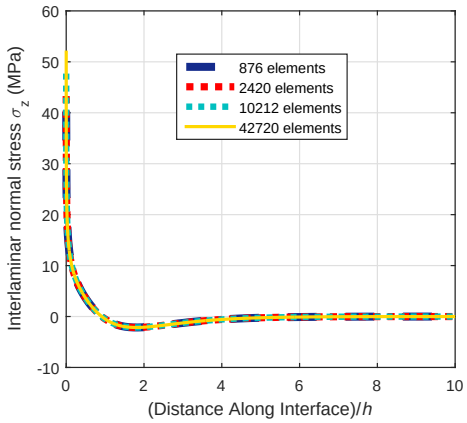

(a) Comparison of σ_z along interface in transverse direction

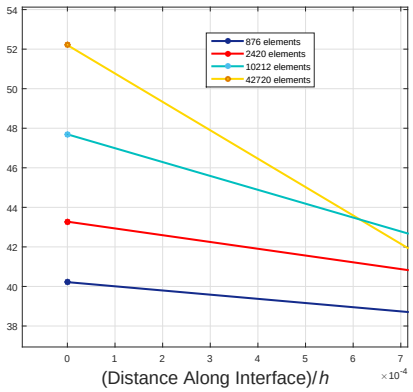

(b) View of comparison of σ_z at free edge

Figure 3.11: Comparison of σ_z for different meshes along interface in transverse direction

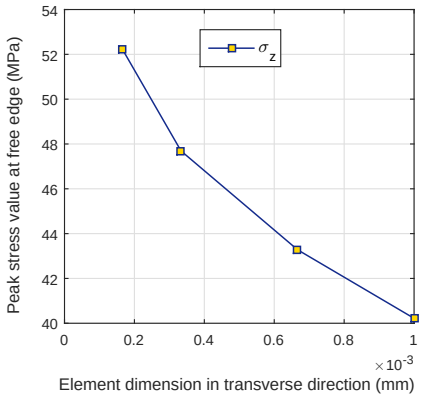

Figure 3.12: Free edge stress σ_z corresponding to element dimension in transverse direction

The view in figure 3.11b shows a rise in stress at free edge with mesh refinement. For 876 elements, the peak stress is found to be 40.22 MPa. Upon increasing the number of elements to 2420, the peak stress rises to 43.28 MPa. For 10212 elements, the free edge stress is 47.69 MPa and for 42720 elements the peak stress rises to 52.2 MPa. The variation of free edge

stress as a function of free edge element dimension in transverse direction is plotted in figure 3.12. It is clear that that with every mesh refinement the free edge stress rises by more than 5 % and even after reaching an element size as small as 0.3 microns (corresponding to 10212 elements) in transverse direction, a rise in stress is found. Hence, the analysis indicates high computational requirement in dealing with high gradient free edge σ_z stress.

Similar analysis has been carried out for τ_{yz} and has been reported in figure 3.13.

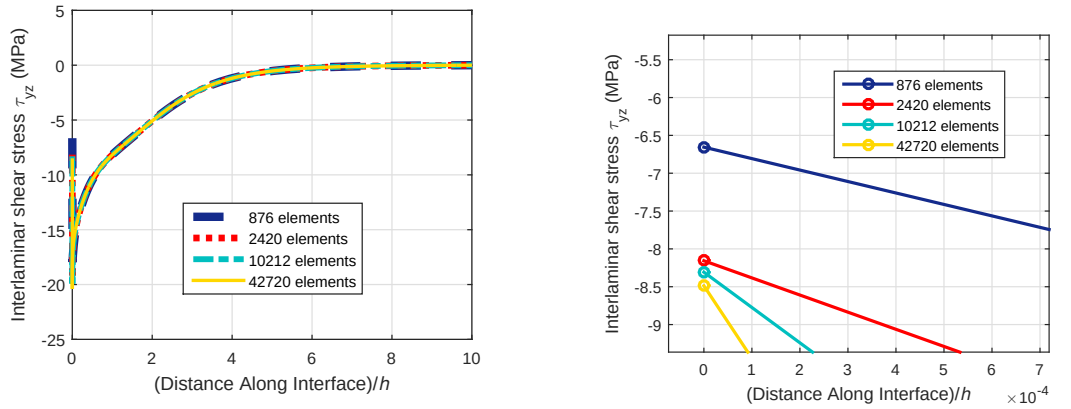

(a) Comparison of shear stress τ_{yz} for different meshes

(b) View of comparison of τ_{yz} at free edge

Figure 3.13: Comparison of τ_{yz} for different meshes along interface in transverse direction

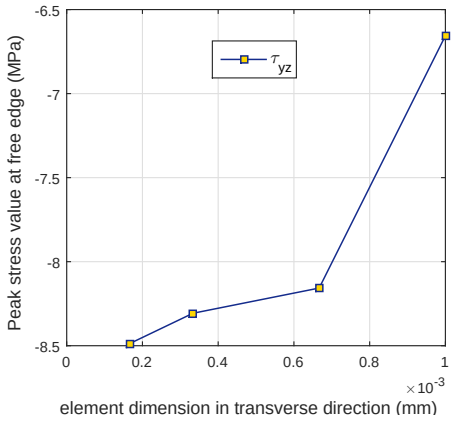

Figure 3.14: Free edge stress τ_{yz} corresponding to element dimension in transverse direction

Like in case of interlaminar stress σ_z, it is observable from figures 3.13 and 3.14 that reaching convergence of τ_{yz} at free edge of zero-ninety degree layers' interface is difficult even with element dimension of 0.3 micron (corresponding to 10212 elements) in transverse direction. This analysis also shows high computational requirement when dealing with high gradient τ_{yz} at free edge.

This brings us to a point where we understand that reaching to a point of convergence of interlaminar stresses σ_z and τ_{yz} with variation in mesh is rather difficult. However, the study

of averaged stress values at distances away from free edge would yield useful information as regards to convergence of average stress values with mesh variation. This arises the need to study the average of interlaminar stresses across the laminate's interface in transverse direction. Also, the need to utilize averaged stress values for determination of delamination initiation through QDC in later chapters necessitates the understanding and determination of averaged stresses at this point.

3.5 Average stress states and their convergence

In this section, numerical integration of interlaminar stresses has been carried out along the interface of zero and ninety degree layers. The average of a stress component along the transverse (y) direction, as shown in chapter 2, is presented again for convenience in equation (3.1).

$$< \sigma_{ij} >= \frac{1}{y_{avg}} \int_0^{y_{avg}} \sigma_{ij} dy \tag{3.1}$$

where, 0 represents the intersection of free edge and interface and y_{avg} is the averaging distance.

With reference to figure 3.15, since the stress is invariant in longitudinal (x) direction, stress values obtained at end nodes of interfacial elements in transverse (y) direction and their coordinates are of importance. Hence, in figure 3.15, stress values relevant to nodes 1 and 2 have been considered. Whereas, data at nodes 3 and 4 have been neglected. At nodes 1 and 2, average of interpolated stress values from the elements sharing nodes 1 and 2 have been considered. Likewise, for every pair of elements across the interface throughout the transverse direction, two stress values at end nodes of an element and their corresponding nodal coordinates are obtained.

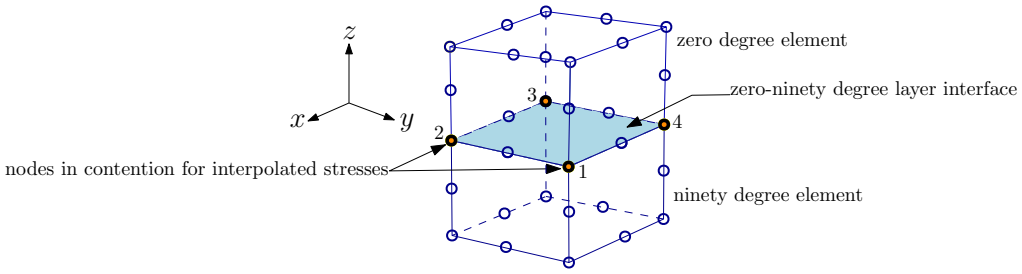

Figure 3.15: Data points on C3D20R element in Abaqus at interface

Likewise, every element along the interface will have two data points and hence, every element will correspond to a segment with two stress values. Thus, a one-dimensional averaging of stresses is carried out. Newton-Cotes quadrature makes way for a comprehensive integration of discrete data sets for uniformly spaced data points. Since two stress function points are available per segment (element width), implementation of trapezoidal integration scheme is a favourable option. However, in this case the segments are not equally spaced (as the mesh is biased), a generalised form of the trapezoidal scheme as highlighted in equation (2.51) is used for plotting of average stress values of interlaminar stresses along the transverse direction.

It was imperative to calculate the average stresses in a manner that the variation in mesh for different analyses could be taken into account. This would facilitate a comparison of average stress values corresponding to different meshes. Hence, the approach employed for calculation of average stress independent of mesh variation is described as follows:

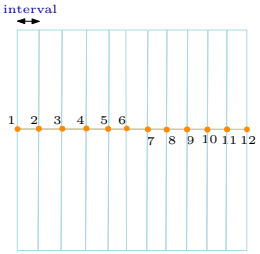

Figure 3.16: Schematic dependence of Trapezoidal integration on interval selection

In figure 3.16 every interval for trapezoidal integration is analogous to the size of elements used for discretisation in transverse direction. So, in this way every two stress point will define an interval for calculation of segmented area under stress plot along the interface in transverse direction. Subsequently, any variation in mesh is taken into account likewise. A convergence study conducted in the following subsections highlights the point discussed herein.

Average stresses along transverse interface

To study the nature of averaged values of interlaminar stresses as a function of distance from the free edge, the following plots have been obtained for mesh with 876 elements

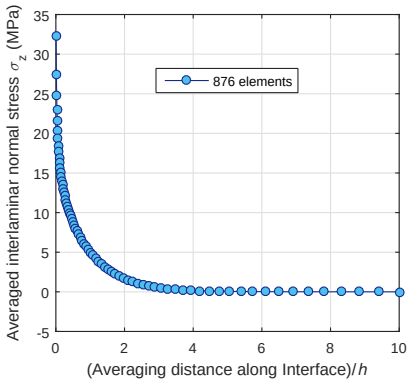

(a) Average σ_z from free edge

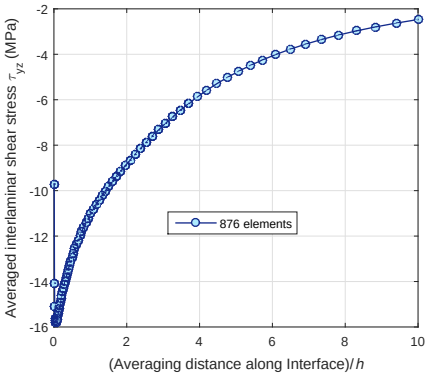

(b) Average τ_{yz} from free edge

Figure 3.17: Variation of average interlaminar stresses along zero-ninety layers' interface for 876 elements

The average values on the plot correspond to the average of all the stress points until the corresponding abscissa (distance from free edge) on the plot. Hence, the plots represent a continuous averaging of stresses until the corresponding point of examination. From figure 3.17a it is noticeable that the average value of interlaminar normal stress σ_z converges to

zero after a certain distance for a sufficiently wide laminate. Since the model represents a symmetric part, the other symmetric part is expected to follow a similar trend and therefore the overall value of average stress at half laminate width would be zero. This trend also satisfies the prediction of self-equilibrating nature of σ_z. Similarly, average value of τ_{yz} has been found to be approaching zero as the distance from free edge increases. This is expected because far away from the free edge the value of τ_{yz} itself approaches to zero after being negative near the free edge as seen in figure 3.7a. Hence, after a certain distance away from the free edge, the average of stresses must approach zero as well.

The plots in figure 3.17 are for a slice model with 876 elements. It would be interesting to examine the nature of averaged stresses with variations in mesh. The next subsection pertains to an investigation of convergence of average stresses with mesh variation along the interface.

Convergence of average stress plots

For carrying out the study under this subsection, various meshes are generated by division of element approach explained earlier. It must be noted that all this is done while the width of the laminate is constant at ten times the ply thickness ($10h$). Thus, in the present investigation, only the effect of change in mesh is studied for a fixed laminate width of $10h$. Meshes with 876, 2420, 10212 and 42720 elements have been considered for calculation of average stresses. The average value of stresses obtain through this procedure would enable determination of average stress value at a certain characteristic distance (determined in following chapters) from the free edge. Usually, the characteristic distance reported thus far in literatures is in the order of one ply thickness (h). Hence, it is vital that as we progress away from the free edge along interface of laminate in transverse direction, we obtain a converged value of average stress for a given material and laminate layup. This would make the average stress value independent of mesh variation upon use of requisite number of elements and would also enable the choice of an optimum mesh as well.

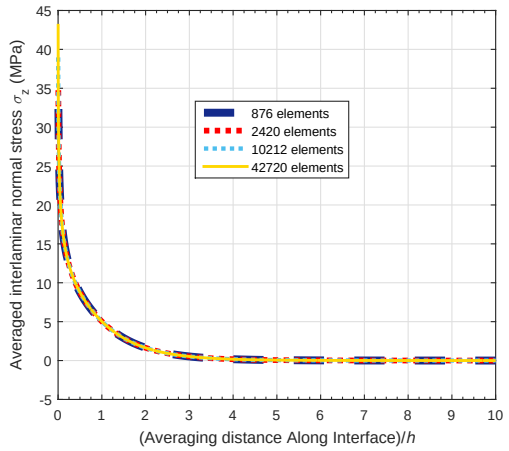

(a) Comparison of average σ_z

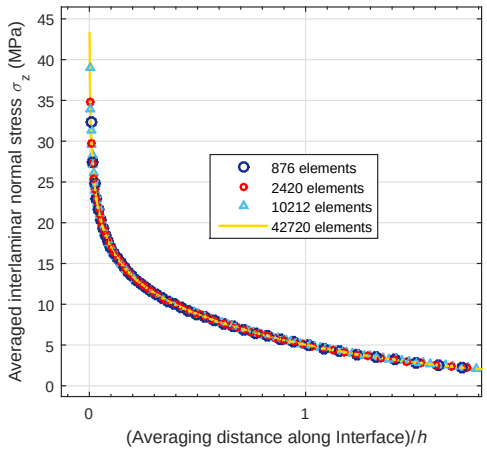

(b) Refined view of converged average σ_z around $1h$ from free edge

Figure 3.18: Variation of average interlaminar σ_z stresses along interface for different meshes

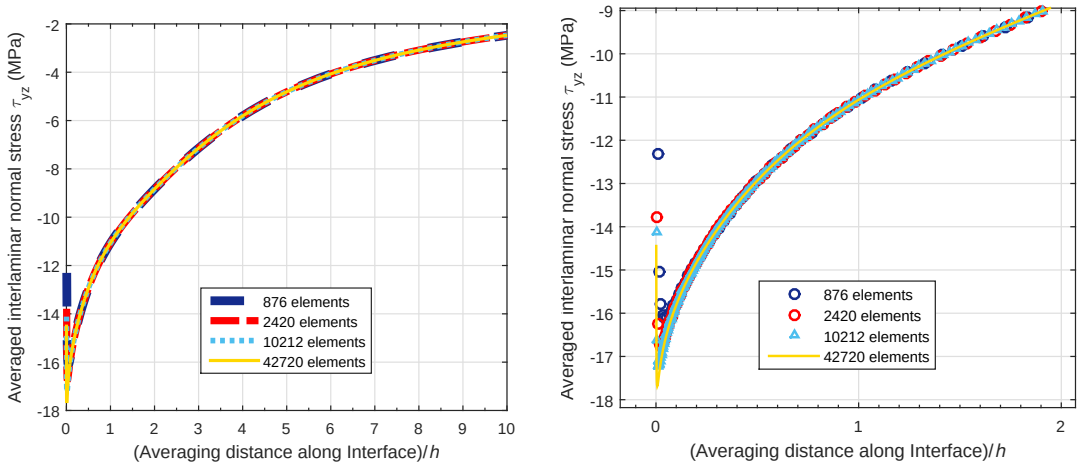

(a) Comparison of average τ_{yz}

(b) Refined view of converged average τ_{yz} around $1h$ from free edge

Figure 3.19: Variation of average interlaminar τ_{yz} stresses along interface for different meshes

The plots in figures 3.18 and 3.19 suggest clearly that as we move away from the free edge region, the average values converge completely with each other for different meshes. Moreover, at around $1h$ distance from free edge, which is a region of high interest based on previously reported averaging distance, complete convergence of average stresses is found for all meshes. Thus, it suggests that 876 elements are in fact sufficient for determination of average stresses. Any refinement beyond 876 elements indicates to provide a mesh sufficient enough for producing converged average stress value.

3.6 Determination of optimum laminate width for converged average stresses

Although the mesh with 876 elements appears good enough for studying converged average stresses, as a conservative approach, a mesh refined one step further with 2420 elements can be chosen for investigating optimum dimension of laminate's half width (since quarter symmetric part is considered for analysis). Although the width over which the average stresses have been plotted ($10h$) has proven to be wide enough for at least σ_z to approach zero completely after a certain distance from free edge, it remains to be seen what the optimum distance is from the free edge which proves wide enough for the average stress values to get distributed in a converged manner across the width at the interface. Thus, an analysis in which for a constant number of elements, the optimum width of a laminate is determined to obtain a converging trend of average stress values with variation in widths, is needed. In this manner, for an optimum width, the average stress for a given mesh would be converged and this would facilitate comparison of average stresses between different meshes. This analysis bears importance in optimising the size of the model that should be considered for analysis.

To this effect, the width of the quarter slice model was varied from three times the ply thickness ($3h$) to twenty times the ply thickness ($20h$). The parameters for maximum and

minimum element sizes are varied in the modelling script by factors such that the number of elements in the mesh remained unaltered i.e. to 2420 elements. This enables designing of the problem in such a way that the only variable left to play a part is the slice's width towards obtaining a converging profile of average stresses. The modelling approach is explained below by a simple illustration.

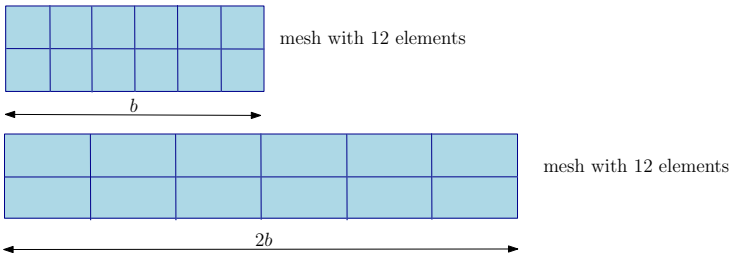

Figure 3.20: Schematic variation of width for a constant mesh

In figure 3.20, by increasing the size of every element by a factor of two, the mesh with 12 elements is kept constant for an increase in width from b to $2b$. However, in the FEM analysis conducted, the elements are biased towards the singular point and therefore the factor of variation of minimum and maximum element sizes ia chosen through trial and error. For convenience, *FINER* constraint option was switched on in Abaqus while generation of mesh. This constraint enables producing a mesh finer than mesh corresponding to stipulated element size when there is a scope. Thus, when the element division factors are close to producing the exact number of 2420 number of elements, the *FINER* constraint refines the mesh to produce 2420 elements. The results obtained for various widths are reported below.

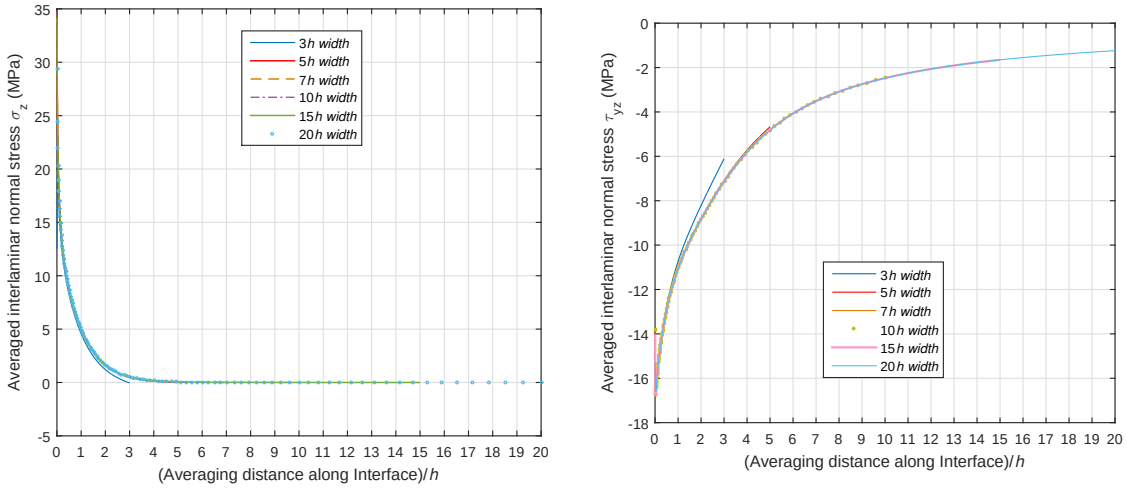

(a) Comparison of average σ_z **(b)** Comparison of average τ_{yz}

Figure 3.21: Comparison of average stress with variation in width for 2420 elements

From figure 3.21a, it is noticed that the average σ_z values diverge until a width of $5h$. From $7h$ onwards, the average value converges without variation until the examined width of $20h$. A similar trend has been observed for average τ_{yz} stress component. This suggests that

for a given mesh, the optimum width to be considered for modelling should be at least $7h$. A conservative approach would be to model the quarter part with a width equal to $10h$ as this would ensure converged average stress values for a given mesh and would also be computationally affordable.

3.7 Interlaminar stresses at ninety-ninety layers' interface of $[0/90]_s$ cross-ply laminate

So far, analyses at zero-ninety layers' interface has revealed that mesh with 876 elements is sufficient for analysing converged average stresses. Being a rectangular mesh, the element dimensions along the transverse (y) direction are the same at zero-ninety and ninety-ninety layers' interface. Hence, mesh with 876 elements can been chosen to analyse the nature of interlaminar stresses at ninety-ninety layers' interface. This study is being done to study the nature of interlaminar stresses near the free edge at ninety-ninety layers' interface.

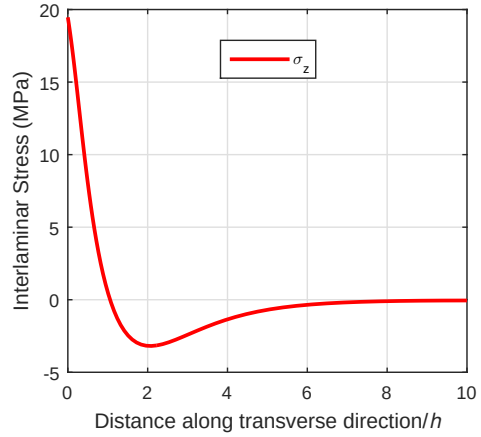

(a) σ_z at ninety-ninety layers' interface

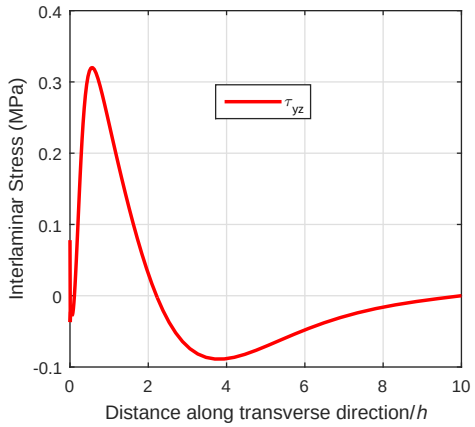

(b) τ_{yz} at ninety-ninety layers' interface

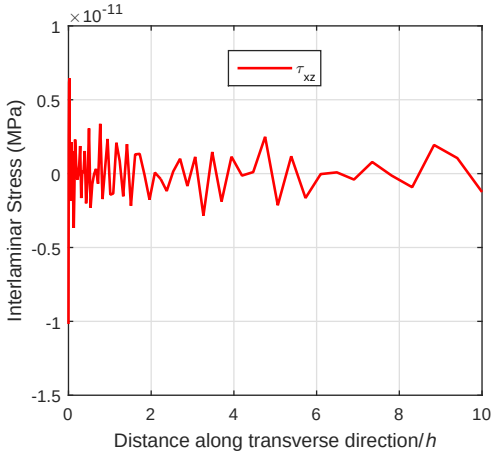

(c) τ_{xz} at ninety-ninety layers' interface

Figure 3.22: Interlaminar stresses at ninety-ninety layers' interface of $[0/90]_s$ cross-ply laminate for 876 elements

Figure 3.22 suggests a steep gradient in σ_z near free edge (0 abscissa). Compared to σ_z, other interlaminar shear stresses τ_{yz} and τ_{xz} are lower in value near the free edge. Figure 3.23 shows a comparative analysis of the three interlaminar stresses for 876 elements. Overall it can be inferred that the interlaminar shear stresses are negligible compared to the interlaminar normal stress σ_z at the ninety-ninety degree layers' interface.

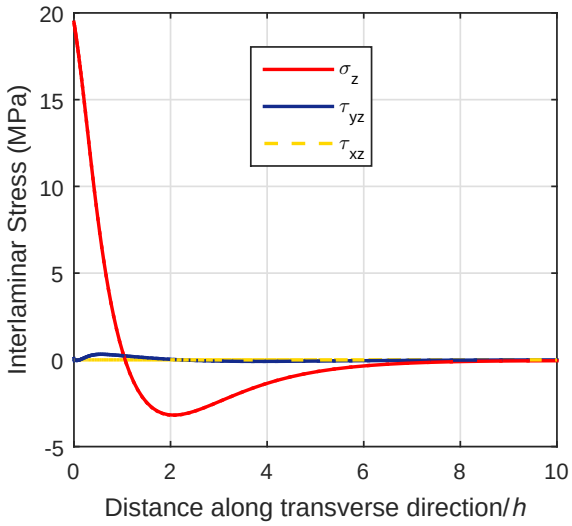

Figure 3.23: Comparative analysis of interlaminar stresses at ninety-ninety layers' interface of $[0/90]_s$ laminate for 876 elements

It is clear that also at the ninety-ninety layers' interface, high gradient interlaminar stress exists. As seen from the analyses at zero-ninety layers' interface, for high gradient free edge stress, it could be expected that the convergence study of average stresses would be computationally less taxing than convergence study of the actual stresses themselves.

Chapter 4

Free Edge Stresses in Constituent Material Model of $[0/90]_s$ laminate

4.1 Background

As seen from chapter 3, the material discontinuity at a zero-ninety layer interface can introduce very steep gradients in stresses near free edges. However, in reality such high gradient stresses sometimes which even tend to a singularity, is not possible and hence this calls for a different modelling approach to study the nature of stress profiles without sudden material discontinuities at layer interfaces. In other words, a different modelling approach needs to be adopted than the one implemented in chapter 3. To be able to see material behaviour at ply interfaces in a detailed manner, there is a need to understand the material behaviour in a manner that allows to disregard the assumption of homogeneous material layers. This is because as a matter of fact, a lamina is made of a combination of fibres and matrix and the distinguished roles of these constituent materials in a lamina could not be denied. Hence, as a development to the analyses carried out in the previous chapter, it would be interesting to investigate the nature of interlaminar stresses at interfaces of a $[0/90]_s$ cross-ply laminate through a model with heterogeneous layers. Therefore, in this chapter, layers of a $[0/90]_s$ laminate are modelled heterogeneously so as to avert the assumption of a homogeneous layer laminate and to further, carry out FEA for getting interlaminar stresses on layer interfaces. The heterogeneous model in this chapter has been modelled with symmetric boundary conditions on the longitudinal and through thickness mid-planes like in chapter 3. Longitudinal tensile strain has been simulated with the application of PBC through displacement difference approach [7] in Abaqus.

4.2 Important considerations to heterogeneous modelling

Like in the case for homogeneous material layer model, the interest in this chapter is on assessing the free edge effect across the transverse direction on interfaces of a cross-ply laminate.

For this matter, a strip of the laminate's transverse section could be analysed. However, this time around with fibres and matrix modelled separately. As seen in *Hyer et al* (2009) [8], an idealistic representation of a composite layer makes way for assuming a periodic arrangement of UCs for example in square or hexagonal arrays. A periodic repetition of these UCs builds a lamina in desired manner. Along similar lines, a cubic UC comprising of one fibre embedded in matrix could be used to model different layers of a cross-ply laminate as shown in figure 4.1. This would allow repetition of the cube in such a way that the fibres are aligned in longitudinal (x) direction to represent a zero degree layer and likewise when they are aligned in transverse (y) direction, they could represent ninety degree layer. In doing so, when the zero and ninety degree layers are put together, the interface between layers would comprise of only matrix material. This paves way for an important observation based on equilibrium descriptions in chapter 1. Since the material discontinuity is being nullified at the interfaces, although the occurrence of interlaminar stresses is expected, the convergence of stress at the free edge is to be keenly investigated. Primarily because there is no abrupt material discontinuity at the interfaces. The effect of free edge is expected to fade out as it did for the homogeneous material layer case as the distance from free edge increases (in transverse direction in present case). Nevertheless, the variations due to local changes in material properties within UCs are expected.

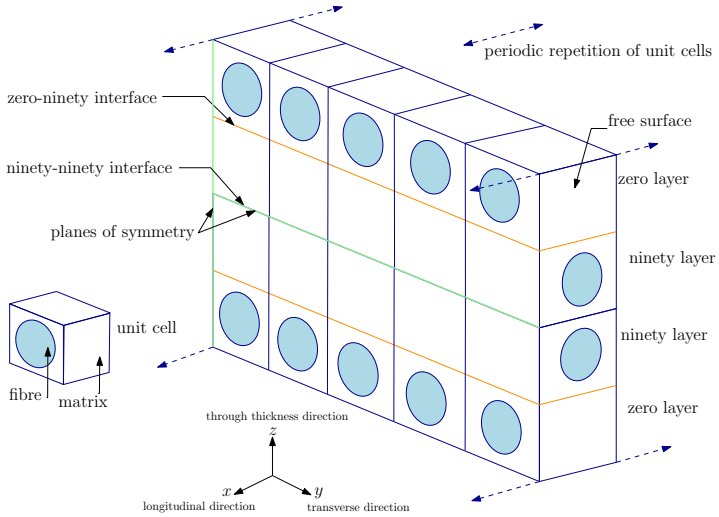

Figure 4.1: Schematic representation of a heterogeneous slice of a $[0/90]_s$ laminate

Like in homogeneous material layer case, the analysis of free edge effect (or effect on free surface of UCs) can be carried out through FEM. But before moving to the heterogeneous modelling of the laminate, some key aspects are to be highlighted. In context of the current research, a heterogeneous analysis is being carried out by modelling every layer with one unit cell in the thickness (z) direction. This means that every layer is being modelled with one fibre in thickness direction. Although, in general, a set of fibres are stacked through the thickness of a layer, the work in this research has been limited to analysing laminate response with just one unit cell through a layer's thickness. This is because a full scale three-dimensional micromechanical modelling of the laminate would have proven to be computationally too expensive considering the objectives of the project and such a micromechanical modelling is not intended during this thesis project. The adequacy of a single UC through thickness to

represent a layer is considered sufficient in allowing the modelling of the laminate in such a manner that the primary objective of avoiding material discontinuity at dissimilar layer interfaces is achieved. Such a modelling approach involving one fibre in UC through layer thickness of cross-ply laminates have been adopted in, for example, works of *Ellyin et al* (2002) [5] and *Chen et al* (2001) [43].

The strip of laminate represented in figure 4.1 is conceptualised to analyse the free edge effect in transverse direction. Hence, the strip is supposed to repeat periodically in longitudinal direction for simulation of the laminate.

4.3 Finite element modelling of heterogeneous cross-ply laminate

The free edge effect analysis on heterogeneous model is being carried out using FEA to be able to draw comparisons with results obtained from homogeneous layer models. This is based on the results obtained from homogeneous layer modelling on free edge stresses using FEM in chapter 3 and reliable applicability of FEM for free edge effect analysis [1]. In this section, an effort has been made towards finite element modelling of a heterogeneous $[0/90]_s$ cross-ply laminate using constituent fibre and matrix properties for a graphite-epoxy fibre-matrix material combination.

Table 4.1: Fibre and matrix properties for combinations of graphite fibre and epoxy matrix [8]

Properties	Graphite fibre	Epoxy matrix
E_{xf} (GPa)	233.0	-
E_{yf} (GPa)	23.10	-
E_{zf} (GPa)	23.10	-
ν_{xyf}	0.2	-
ν_{xzf}	0.2	-
ν_{yzf}	0.4	-
G_{xyf} (GPa)	8.96	-
G_{xzf} (GPa)	8.96	-
G_{yzf} (GPa)	8.27	-
E_m (GPa)	-	4.62
ν_m	-	0.36

The properties of fibre and matrix used herein are graphite-epoxy material combination *Hyer* (2009) [8]. The properties are listed in table 4.1 where, f and m represent the fibre and matrix properties respectively while x, y and z represent the longitudinal, transverse and through thickness directions respectively. The fibres are assumed to be transversely isotropic while the matrix is assumed to be isotropic in nature.

Finite element modelling in Abaqus

A three-dimensional finite element model has been scripted through Abaqus Scripting Interface with the help of Abaqus user manual [36] for carrying out simulations reported in this

chapter. This is done for convenient parametrisation of the model's dimensions and mesh citing the possibilities of parametric variations for carrying out simulations through the course of this chapter. For building the finite element model, it has been emphasised that the cubic UC is built symmetrically in first place. A symmetric mesh on the UC has advantages in terms of merging (or tying) of nodes between instances, uniformity in FEA of field variables and most importantly, in application of PBC as shown in section 4.4.

To begin with, modelling of cubic UC has been done. To be able to build the cubic UC, one-eighth of a cube has been modelled with fibre and matrix solid sections defined by nine engineering constants and two engineering constants respectively as described in table 4.1. Linear and rotational patterns have been instanced subsequently to model the entire cube as shown in figure 4.2.

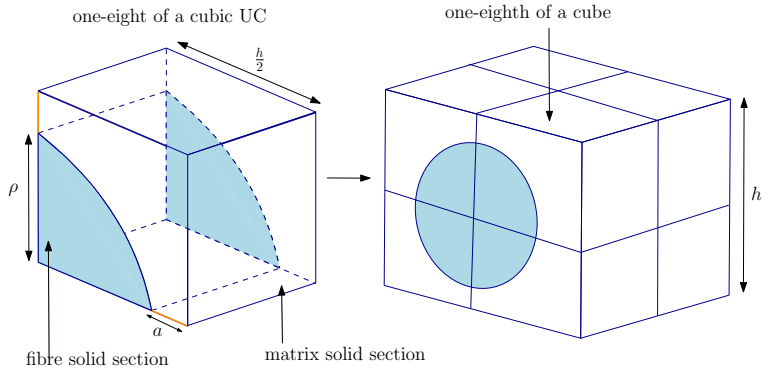

Figure 4.2: Schematic representation of symmetric instancing of one-eighth cubic UC part

The region denoted by a (in orange) in figure 4.2 is used as a basis for parametrising the element size throughout the laminate. The intention is to build the model as a function of fibre volume fraction v_f. Hence the distance a is formulated as a function of v_f for a given UC cubic side h as shown in equation 4.3 with ρ as fibre radius.

$$\rho = h\sqrt{\frac{v_f}{\pi}} \tag{4.1}$$

$$a = \frac{h}{2} - \rho \tag{4.2}$$

$$\text{or,} \quad a = \frac{h}{2}(1 - 2\sqrt{\frac{v_f}{\pi}}) \tag{4.3}$$

Hence, for example, if the region a is to be discretised by 2 elements, then the size of the element chosen for discretisation of the laminate is chosen to be $a/2$. The reason behind choosing a as the most critical location for discretisation is that a is the narrowest region between fibre and side of the UC and hence sufficient number of elements must be present in this location to avoid erratic deformation of model. A finite element mesh of one cubic UC with v_f 0.6 using three elements in the region a is shown in figure 4.3.

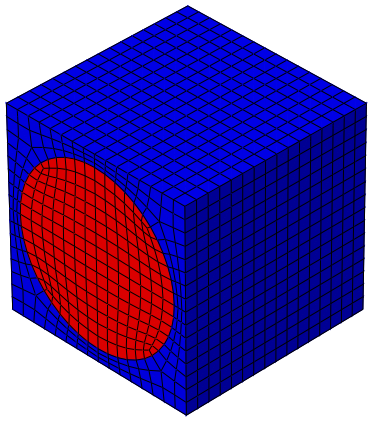

Figure 4.3: Finite element mesh of cubic UC using C3D8 elements

During the course of this chapter three-dimensional hexahedral C3D8 elements available in Abaqus have been used for mesh generation with reference to *Xia et al* (2003) [7] and *Ellyin et al* (2002) [5]. Further, structured mesh has been generated throughout the model as such a modelling practice forms a symmetric mesh which is favourable for application of PBC.

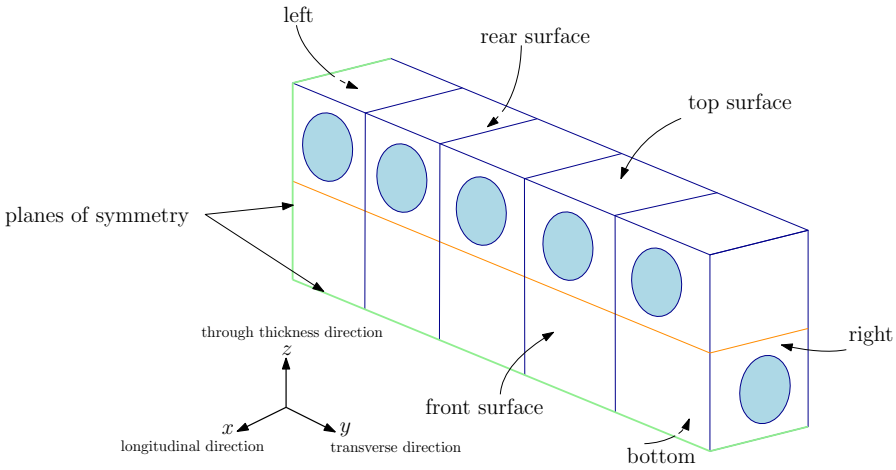

Figure 4.4: Schematic of a heterogeneous symmetric quarter slice of a $[0/90]_s$ laminate

As a $[0/90]_s$ cross-ply laminate has two symmetry planes, along the length ($y-$symmetry) and thickness ($z-$symmetry) (shown in green in figure 4.1), a quarter section of the laminate is modelled as in chapter 3. Hence, in the course of this chapter, simulation of a zero-ninety layer combination of $[0/90]_s$ laminate of a suitable width has been carried out. To start with as a trial, the reference for a suitable width is taken based on findings of converged average stresses for different widths with same mesh from homogeneous layer model in section 3.6 and the heterogeneous strip is modelled with a width equal to $10h$ ($h = 0.134$ mm). For this purpose, a combination of unit cells, one with fibre aligned in longitudinal direction and the other with fibre aligned in transverse direction (by rotation of UC about vertical through-thickness direction axis) together represent a combination of zero-ninety fibres. This block of zero-ninety fibres embedded in matrix has been repeated transversely to build the zero-ninety layers' quarter section as depicted schematically in figure 4.4. The length of the slice

has been taken to be equal to one ply thickness. The ply thickness as in chapter 3 is 0.134 mm and hence the sides of the UC cube is 0.134 mm ($h = 0.134$ mm). In this chapter, the heterogeneous model analysed is modelled with a v_f of 0.6 and three elements in the critical region a. The choice of three elements is considered optimum for discretisation of a based on example discretisation in literatures for example in [5], [7] and [11]. Since, every increase in number of elements in region a further would eventually lead to increase in large number of elements volumetrically, discretisation with three elements is considered computationally optimum for generating sufficiently converged results. The completely meshed quarter part of $[0/90]_s$ heterogeneous model is shown in figure 4.5. Ten of the single zero-ninety layer blocks have been instanced along the transverse direction through a linear pattern to develop a quarter part of width $10h$. All nodes from adjoining instances are merged together with a tolerance of one-tenth of the critical region size a using *Merge* instance option in Abaqus. This tolerance value enabled creation of merged nodes without any occurrence of distortion.

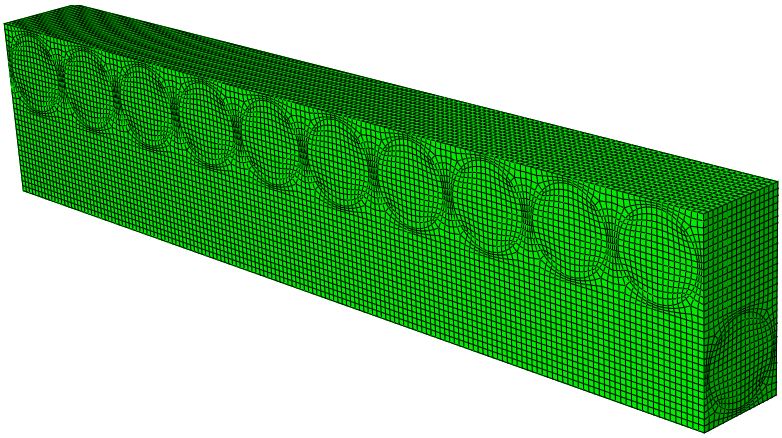

Figure 4.5: Finite element mesh of quarter heterogeneous $[0/90]_s$ laminate using C3D8 elements

As a result of the meshing strategy, every single cubic UC is modelled with 6546 nodes and 5632 elements. Consequently, the entire quarter part with width $10h$ consists of 122098 nodes and 112640 elements. For applying material properties, all elements belonging to the set of fibres (both zero and ninety degree layers) and matrix are separated in two sets. To bifurcate the fibre elements belonging to zero and ninety degree layers, element connectivity data has been extracted through a Python script. Identification of elements of zero and ninety degree fibres is done through *ismember* function in Matlab and the fibre properties are assigned correspondingly to simulate fibre properties in zero and ninety degree layers while using the same global coordinate system. Since the matrix is isotropic, properties have been assigned to matrix elements throughout the model uniformly. The model thus formed is ready for simulation through application of appropriate boundary conditions.

4.4 PBC for simulation of tensile strain

The heterogeneous model shown in figure 4.5 represents a periodically repeating structure in the longitudinal direction. Further, the model consists of sections defined with properties of fibre and matrix separately. Thus, on front and rear boundaries, if a homogeneous

traction boundary condition is applied, then the fibre and matrix will undergo unequal deformation which means that at the interface of fibre and matrix, there would be a displacement discontinuity. On the other hand, if homogeneous displacement is applied, then it would result in traction discontinuity at the fibre-matrix interface. Either of the two scenarios i.e. homogeneous traction or homogeneous displacement boundary condition are therefore unacceptable for the heterogeneous model. Hence, apart from mitigating the discontinuity of traction and displacement at fibre-matrix interface, there is also a need to satisfy traction and displacement continuity at the longitudinally opposite ends of the quarter model to be able to simulate a periodically repeating structure in longitudinal direction. Given all the aforementioned requirements, the choice of PBC has been made to subject the model to a longitudinally extensional strain of 0.01 with a motive to analyse free edge stresses. This section further deals with procedures adopted for execution of PBC.

Application of PBC for FEA in Abaqus

Wu et al (2014) [39] have proposed a rather comprehensive approach to application of PBC in Abaqus. As shown in subsection 2.6.1, *Xia et al* (2003) [7] propose the concept of displacement difference boundary condition as a means to eliminate the periodic part of periodic displacement boundary condition given by equation (2.42). This equation is repeated here for convenience.

$$u_i = \epsilon_{ik} x_k + u_i^* \tag{4.4}$$

The displacement difference condition is represented through equation (2.45) as shown here again:

$$u_i^{j+} - u_i^{j-} = \epsilon_{ik} \Delta x_k^j \tag{4.5}$$

Hence, it is clear that for a Δx_k^j of 0.134 mm (longitudinal dimension of quarter heterogeneous model) and a strain of 0.01, equation (4.5) would give a displacement difference of 0.00134 mm across the front and rear boundaries in longitudinal direction of quarter heterogeneous model shown in figure 4.5. Effectively, we have arrived at a point where we can specify a constant displacement difference across longitudinal boundaries based on global average strain of choice (0.01 in this case) to simulate tensile strain through PBC in the concerned heterogeneous model. Hereafter, it remains a matter of merely applying a displacement constraint between nodes on longitudinally opposite faces of heterogeneous model. Application of displacement constraint on two nodes allows the FEM solver to represent nodal displacement of one node in relation to the other node of the pair while solving the global equilibrium equations. The displacement difference can be conveniently applied by including nodal constraint equations in Abaqus input file.

The nodal constraint equations in Abaqus input file are constraint equations defined for every pair of nodes on the opposite boundaries of a finite element model. The displacement difference between two oppositely located nodes is applied to a dummy node along a desired direction (DoF). The direction of displacement is specified through coefficients tagged along with nodes. Since the nodes in constraint equation are represented through a node-set, the coefficients are tagged to node sets. An example constraint equation for simulating PBC is described through equation (4.6) with reference to two nodes represented through node sets

1 and 2 in the constraint equation (as Abaqus allows nodal representation through node sets in equation). An illustration is shown in figure 4.6.

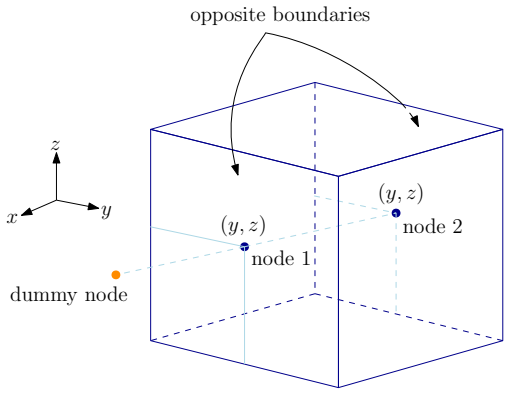

Figure 4.6: Schematic representation of nodes on two oppositely located boundaries

$$\text{Set-node 1 - Set-node 2} = \text{Set-dummy node} \tag{4.6}$$

For applying PBC through displacement difference as in equation (4.6), the node pair on opposite boundaries must have the same (y, z) coordinates with reference to figure 4.6.

In the current chapter, PBC has been applied on model represented in figure 4.5. The left, bottom, front and rear surfaces of the model are indicated schematically in figure 4.4. The quarter symmetric model in figure 4.5 has symmetry planes on the left and bottom surfaces. A tensile strain of 0.01 is to be simulated in the longitudinal direction. For this purpose, firstly, the nodal coordinates have been extracted through input file generated after modelling of part. Thereafter, every node on the front and rear surfaces are paired up based on an algorithm that from all possible combinations, a node on one surface is paired with that node on the opposite surface which is located at the minimum distance from it [39]. In this way, nodes located right opposite to each other were paired for applying PBC.

An important consideration made while specifying constraint equations along different DoFs to node pairs on model shown in figure 4.5 is to avoid over-constraining of DoFs. Since the left and bottom surfaces are already provided symmetry boundary conditions, care has been taken to not specify transverse (y) direction DoF on left surface nodes and no DoF has been specified in through thickness (z) direction on bottom surface nodes. Also, to the node lying at the intersection of left and bottom surface nodes, DoF has only been specified along longitudinal direction through PBC. To all other nodes which are neither located on left surface nor on the bottom surface, constraint equations along all three DoFs are assigned. Overall, all node pairs on front and rear surfaces have been assigned a constant displacement difference in longitudinal direction while displacement difference in transverse and through thickness direction of all these node pairs has been specified to be zero (hence, they move together in transverse and through-thickness directions). Lastly, one node at the centre of rear bottom edge has been conveniently fixed by constraining its DoFs for avoiding rigid body motion.

4.5 FEA results through application of PBC

Before analysing the stresses through application of PBC, it is prudent to check the necessary conditions of traction and displacement continuity on opposite boundary surfaces to be able to confirm the periodicity of the model in longitudinal direction. For this matter, the longitudinal nodal forces on opposite boundaries (on which PBC is applied) must be equal and opposite. On the other hand, for displacement to be continuous on opposite boundaries, the difference in displacement must be equal between every node pair on which PBC is applied (across front and rear surfaces). This difference in displacement must be equal to the displacement provided (corresponding to strain to be simulated) to the dummy node involving the node pairs.

Equal and opposite nodal forces on opposite boundaries

For the model to behave as a periodically repeating entity in longitudinal direction, it is notable that when one of these strips is stacked behind the other, then the forces in direction of applied PBC must cancel each other out. This suggests that the nodal forces, represented by *NFORC* field output, must be equal and opposite on opposite boundaries in corresponding directions of applied PBC.

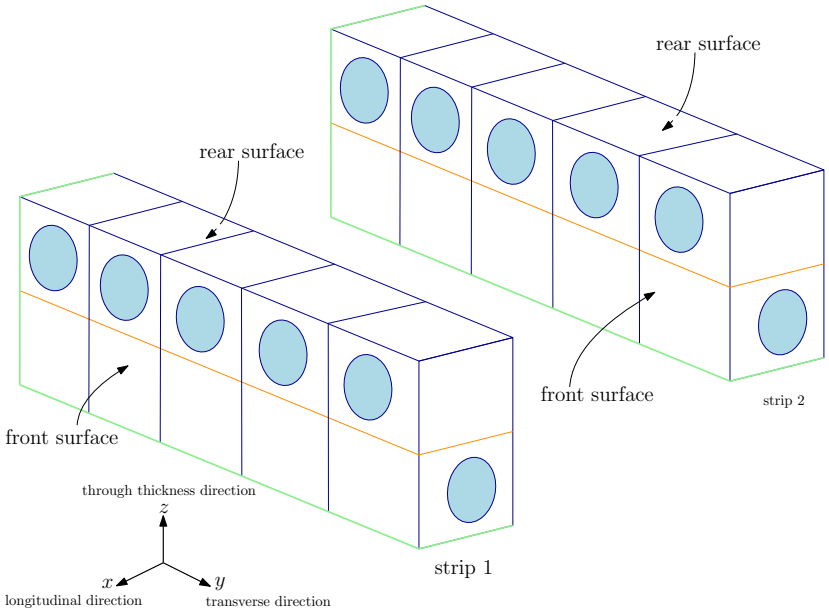

Figure 4.7: Periodic stacking of heterogeneous strips in longitudinal direction

In figure 4.7, if the front surface of strip 2 is to be stacked with the rear surface of strip 1 (longitudinal stacking), then the longitudinal nodal forces on the two surfaces must cancel out. Hence, for every strip, the longitudinal nodal forces on front and rear surfaces must be equal in magnitude but opposite in direction when PBC is applied in longitudinal direction.

Upon analysis, as a primary measure, the distribution of nodal forces has been checked on the boundary pair subjected to PBC. According to expectation, an equal and opposite distribution of nodal forces on opposite boundaries has been observed as shown in figures 4.8a and 4.8b

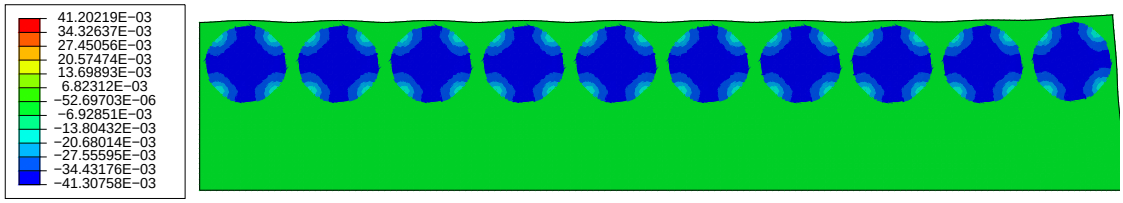

(a) Longitudinal direction nodal force on front face

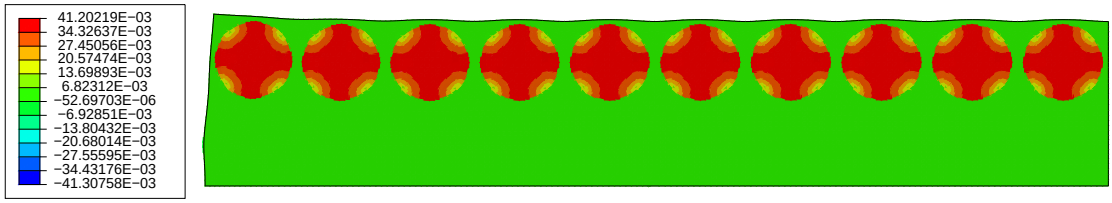

(b) Longitudinal direction nodal force on rear face

Figure 4.8: Equal and opposite nodal forces in longitudinal direction on front and rear boundaries

A Python script has been written to extract the nodal force data from opposite boundary surfaces. For the model analysed, the following plot in figure 4.9a represents nodal forces on opposite boundary surfaces. Since the nodes on front and rear boundary surfaces are not present in a rectangular grid (refer figure 4.5), the node pairs on opposite surfaces (with same in-plane coordinates) are represented linearly. This means that all nodes are represented on a line and every point on a line represents a pair of node on which PBC is applied. Thus, in figure 4.9a, every point in abscissa represents a node pair on which PBC is applied and the ordinates represent average of longitudinal nodal forces (as a node might be shared between different elements on a surface) on opposite boundary surfaces for that corresponding node pair. Since there are in total 6273 node pairs, the abscissa has 6273 points.

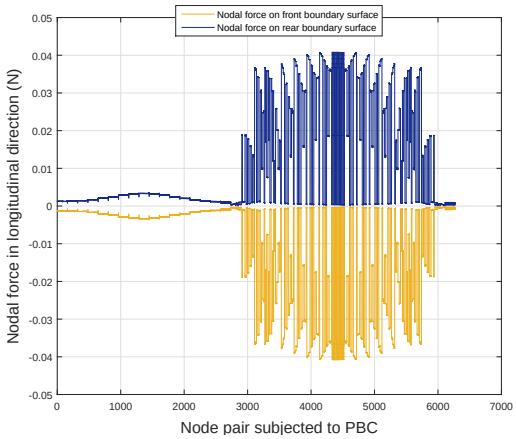

(a) Equal and opposite nodal forces on node pairs subjected to PBC in longitudinal direction

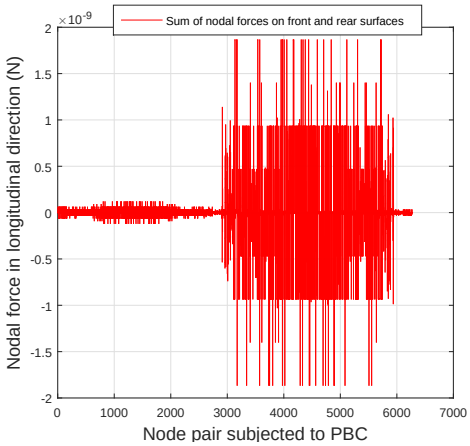

(b) Sum of nodal forces on opposite node pairs of front and rear surfaces

Figure 4.9: Equal and opposite nodal forces on node pairs of front and rear surfaces

It is verifiable from the pot in figure 4.9a that the forces on every node pair appear to be distributed in an equal and opposite manner. However, the summation of of forces on every

node pair would cast a clearer picture by verifying if they cancel each other out or not. The forces in figure 4.9a are in the order of 10^{-2}. When the sum of forces on every node pair is plotted in figure 4.9b, it becomes clear that the sum approaches zero as the values of sums are in the order of 10^{-9}. For verifying displacement continuity, the displacements of node pairs on front and rear surfaces are plotted in figure 4.10 which shows that the difference in displacement between opposite placed nodes is constant.

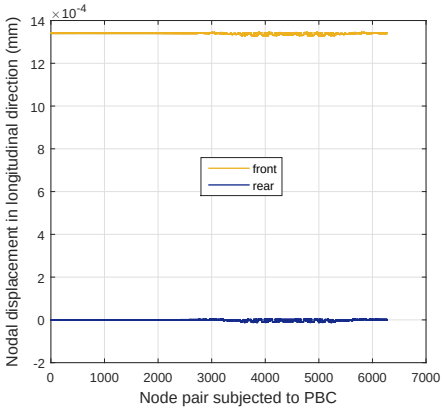

Figure 4.10: Constant displacement difference between oppositely placed nodes on front and rear surfaces

Interlaminar stress analysis at the zero-ninety layer interface surface

The idea behind heterogeneous modelling has been to understand how the interlaminar stress profiles differ from the ones obtained in homogeneous layer model case. In this subsection, stress analysis is done on zero-ninety degree layer interface. This subsection therefore deals with the results obtained for interlaminar stress components at the interface surface between the zero and ninety degree layers. The surface at interface shares nodes that belong to matrix present at both zero and ninety degree layers. To be able to extract values of relevant stress components, a Python script is written which extracts data by the means of interface surface node set from Abaqus output database. The script extracts interpolated stress values at the nodes of every element shared at interface surface. Hence, if a node is shared by eight hexahedral elements at interface, then eight stress values have been obtained through the script for that node. The stress value at common nodes are averaged through a Matlab script to finally obtain averaged values for relevant stress components at every node throughout the interface surface.

Surface plots have been generated to study the nature of the plots on the interface surface. For this purpose, a grid corresponding to the mesh in the finite element model is modelled in Matlab and the corresponding stress values are represented at grid points to arrive at the plot. In doing so, a 161 node by 17 node rectangular grid has been generated. This study would allow examination of variation of stresses along the transverse and longitudinal directions on the interface. Hence, linear FEA is carried out for a tensile strain of 0.01.

The following figures represent 3D surface plots and also their corresponding two-dimensional (2D) projections. While the 3D plots provide clear visualisation of transverse variations

in stress values, the 2D plot provides a top view on the interface to visualise longitudinal variation in values clearly.

Figures 4.11 and 4.12 represents the variation of interlaminar normal stress σ_z on the zero-ninety layers' interface surface. The side facing the colour bar represents the free edge (surface). The location transversely opposite to free edge represents symmetry plane running longitudinally through the laminate.

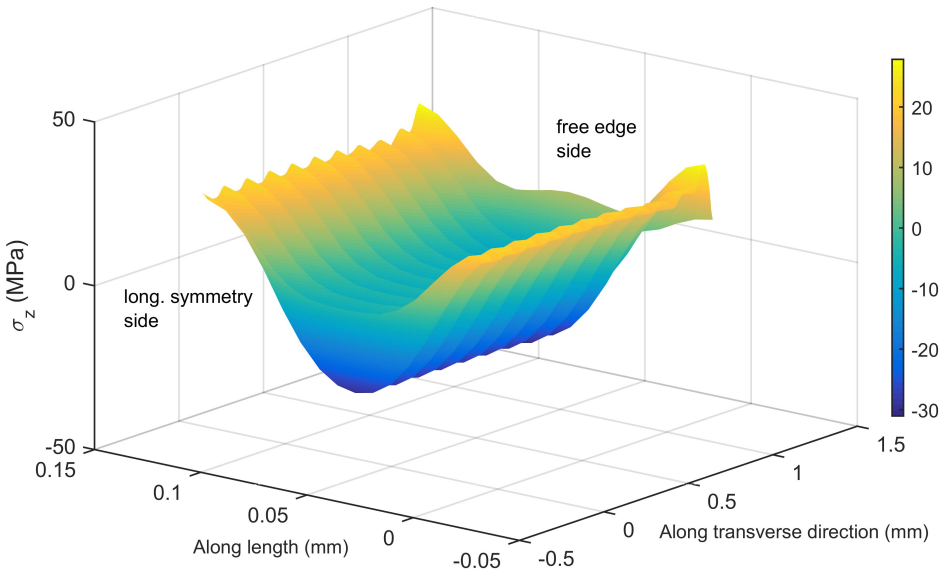

Figure 4.11: Distribution of interlaminar normal stress σ_z at zero-ninety interface surface

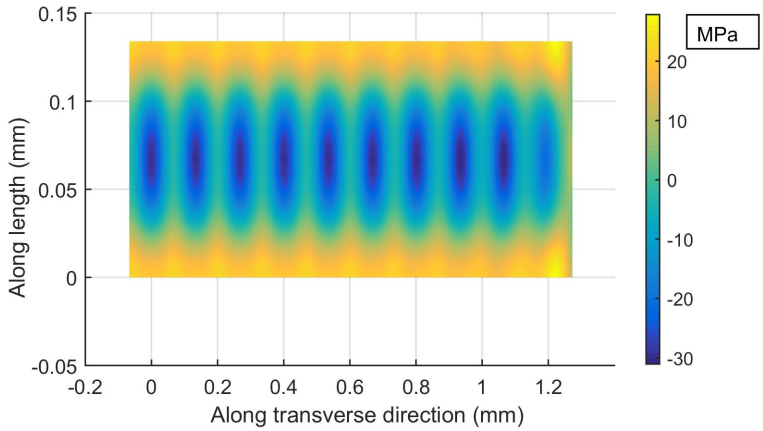

Figure 4.12: 2D projection of interlaminar normal stress σ_z at zero-ninety interface surface

It is noticeable in figure 4.11 that as the free edge approaches, the magnitude of σ_z rises before falling to a lower value at the free edge. Further, the stress is observed to be oscillating in proximity of fibre locations. Interestingly, both figures 4.11 and 4.12 show that the magnitude

of σ_z reaches equal value at the opposite boundaries. This signifies that the stress values are the same at opposite boundary surfaces.

Plots for τ_{yz} are shown in the similar manner in figures 4.13 and 4.14.

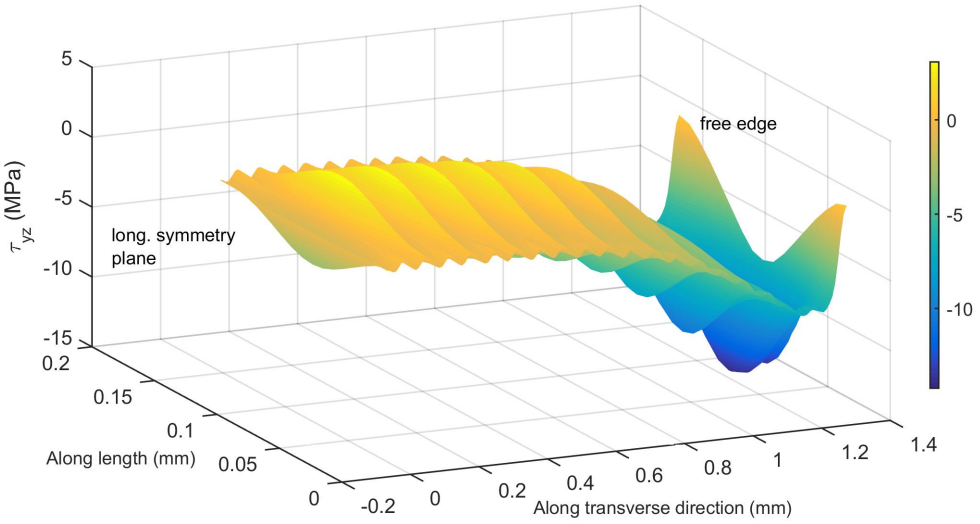

Figure 4.13: Distribution of interlaminar shear stress τ_{yz} at zero-ninety interface surface

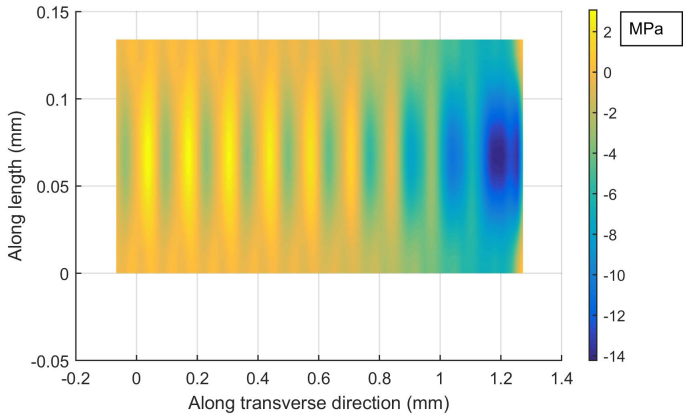

Figure 4.14: 2D projection of interlaminar shear stress τ_{yz} at zero-ninety interface surface

Like in case of σ_z, τ_{yz} shows a high gradient as the free edge region is approached. Further, oscillations are observed for τ_{yz} too according to figure 4.13. Also, like σ_z, the stresses are found to be equal on opposite boundaries which are subjected to displacement difference boundary conditions.

Finally, the results for stress component τ_{xz} are shown in figures 4.15 and 4.16.

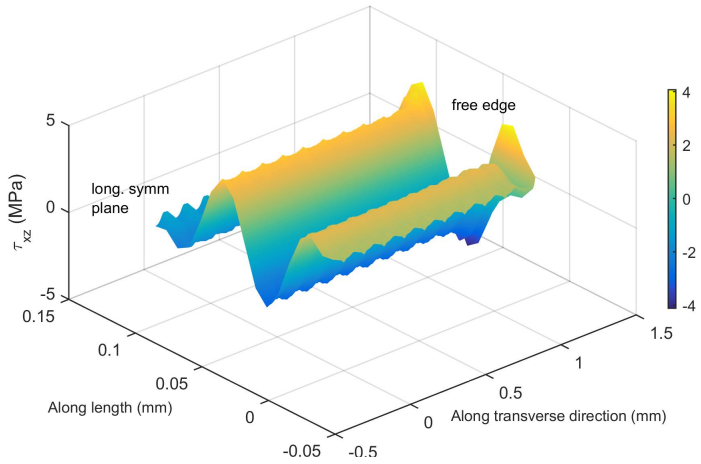

Figure 4.15: Distribution of interlaminar shear stress τ_{xz} at zero-ninety interface surface

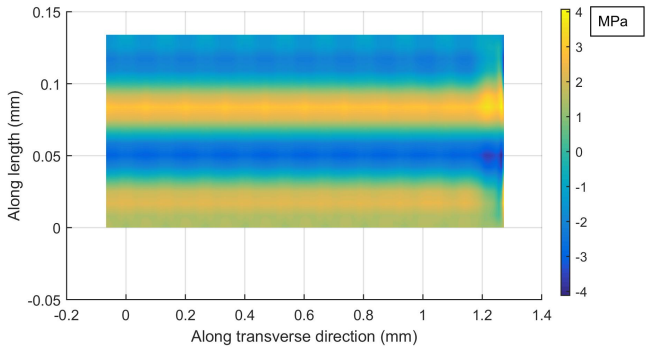

Figure 4.16: 2D projection of interlaminar shear stress τ_{xz} at zero-ninety interface surface

The stress distribution of τ_{xz} has been found to be in a manner that suggests that stress values vary in the longitudinal direction about a mean zero. It been seen in previous analyses involving homogeneous layer models, shear stress component τ_{xz} is found to be negligible. It remains to be seen what the longitudinal average of τ_{xz} comes out to be. Also, the comparison of longitudinal average of τ_{xz} with longitudinal averages of σ_z and τ_{yz} would reveal if the trend matches the one found for the homogeneous layer model (figure 3.7b).

The distribution of interlaminar stress components in heterogeneous model has a distribution in longitudinal as well as in transverse direction. To be able to analyse the stress components in the transverse direction, as it has been done for the homogeneous layer results in chapter 3, there is a need to find the longitudinal average of the stresses so that their transverse behaviour could be analysed. Work on this aspect has been conducted in the following subsection 4.5.

Longitudinal averaging of stress plots on interface surface

To compare the interlaminar stresses obtained from heterogeneous model with those obtained from homogeneous model, the stresses are averaged in longitudinal direction. Since the finite

element mesh comprises of 17 rows and 161 columns, average of 17 stress values obtained for each of the 161 columns are plotted in transverse direction.

The longitudinally averaged plots are comparable with plots obtained at the corresponding interface of homogeneous layer model shown in figures 3.6 and 3.7. In this subsection the longitudinally averaged plots are represented individually as well as combinedly for studying their comparative nature.

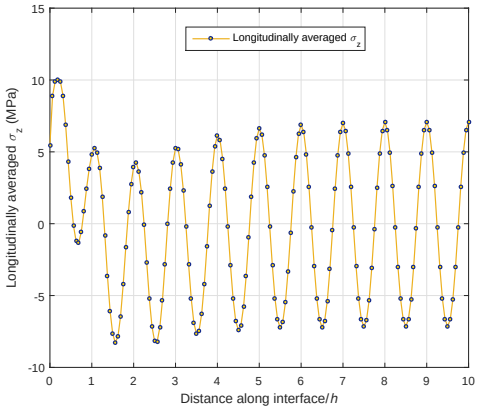

Figure 4.17: Longitudinally averaged σ_z at zero-ninety layers' interface

Figure 4.17 represents longitudinally averaged σ_z plotted in transverse direction. The plot shows signs of oscillation about zero ordinate far-off from the free edge (represented by zero value of abscissa). However, higher gradients are noticed as the free edge is approached. At the free edge, the plot converges to a finite value of 5.467 MPa. Since, longitudinally averaged σ_z is comparable to the normal stress plot of σ_z in figure 3.6 for homogeneous layer model, it is worthwhile to examine the comparison of σ_z from homogeneous and heterogeneous models to compare the steepness of gradient near free edge. Figure 4.18 shows the comparison of free edge region gradient by plotting the stresses on the same scale.

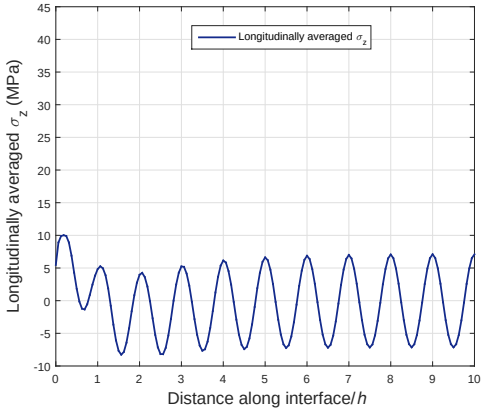

(a) Longitudinally averaged σ_z along transverse direction in heterogeneous model

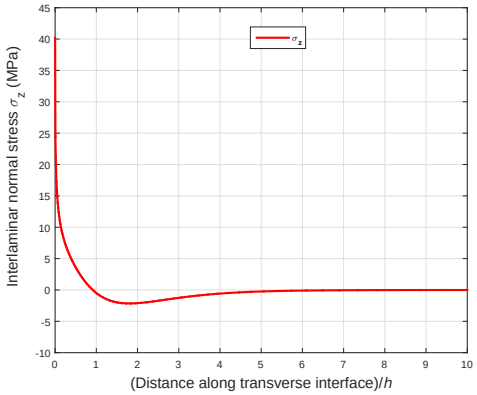

(b) σ_z along transverse direction in homogeneous model

Figure 4.18: Comparison of σ_z gradients between homogeneous and heterogeneous models at zero-ninety layers' interface

A comparison of σ_z plots in figures 4.18a and 4.18b from heterogeneous and homogeneous models respectively reveals that there is indeed a comparatively steeper gradient near the free edge in homogeneous model which can be attributed to the modelling of the layers with homogeneous material. Plot of τ_{yz} after longitudinal averaging in heterogeneous model is represented in figure 4.19. A comparison of free edge gradient between heterogeneous and homogeneous models for τ_{yz} is depicted in figures 4.20a and 4.20b.

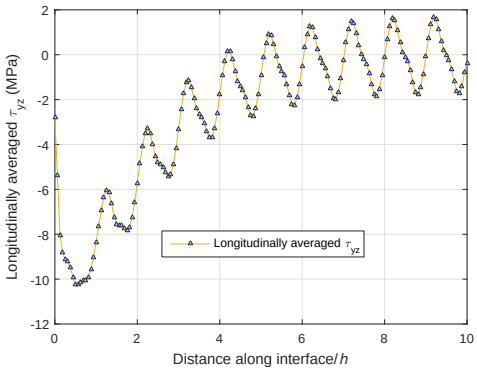

Figure 4.19: Longitudinally averaged τ_{yz}

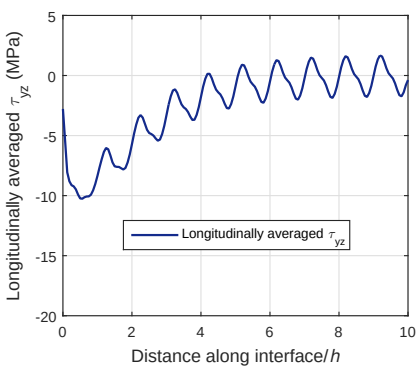

(a) Longitudinally averaged τ_{yz} along transverse direction in heterogeneous model

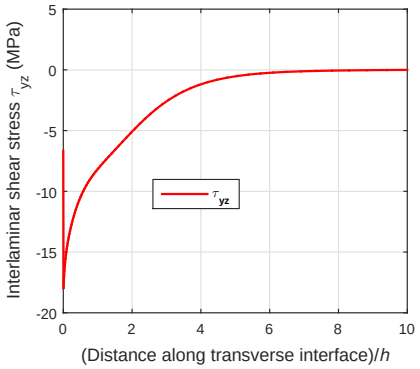

(b) τ_{yz} along transverse direction in homogeneous model

Figure 4.20: Comparison of τ_{yz} gradient between homogeneous and heterogeneous models at zero-ninety layers' interface

The comparisons of stress gradients near free edge between homogeneous and heterogeneous models (although with different stiffness) reveals that there clearly exists a steep gradient near free edge in homogeneous material layer models for σ_z and τ_{yz}. This behaviour can be attributed to the modelling of the layers with homogeneous materials. The steep stress profiles pose difficulties in convergence studies at free edges. Finer meshes are needed for their analysis and hence might get computationally taxing. The convergence of average stresses in transverse direction appears to be comparatively convenient as seen in subsection 3.5.

Figure 4.21 represents longitudinally averaged τ_{xz} on the zero-ninety interface surface. Since the magnitude of longitudinally averaged τ_{xz} is comparatively negligible to those of longitudinally averaged σ_z and τ_{yz}, the comparison of free edge region gradient analysis for τ_{xz} has

not been carried out (figure 4.22).

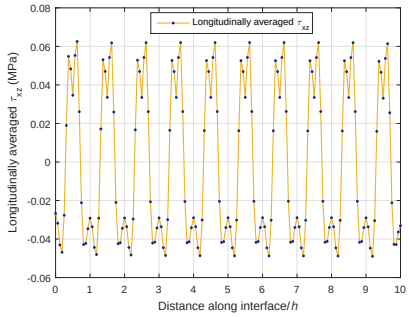

Figure 4.21: Longitudinally averaged τ_{xz} at zero-ninety layers' interface

It is worthwhile to examine the longitudinally averaged interlaminar stresses combinedly to assess their comparative nature. Figure 4.22 is a collective representation of the three stress components. It has already been seen in case of homogeneous material layer $[0/90]_s$ laminate that τ_{xz} is negligible compared to other two interlaminar stress components at the interface. Hence, the comparative analysis of the three interlaminar stress components for heterogeneous model provides a concurrent information with homogeneous layer model analysis shown in figures 3.6 and 3.7.

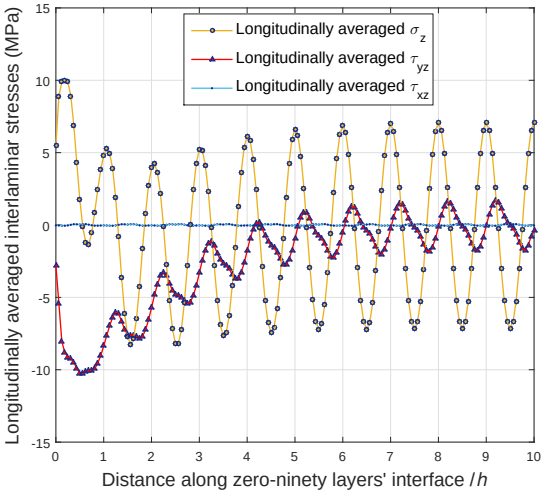

Figure 4.22: Longitudinally averaged interlaminar stresses along zero-ninety layers' interface

Transverse average of interlaminar stresses along zero-ninety layers' interface

Figure 4.23 below shows the state of transversely averaged interlaminar stresses along the zero-ninety degree layers' interface. The figure shows that the transverse average of σ_z converges to zero for a width of $10h$. The overall pattern of distribution of average stress in transverse direction is analogous to the distribution of average stresses in transverse direction for homogeneous layer model at zero-ninety interface as shown in figures 3.18a and 3.19a except near the free edge.

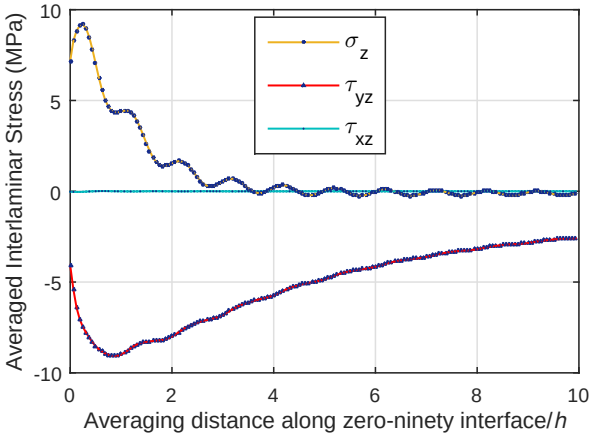

Figure 4.23: Transversely averaged interlaminar stresses along zero-ninety layers' interface

4.6 Interlaminar stress analysis at ninety-ninety degree layers' interface

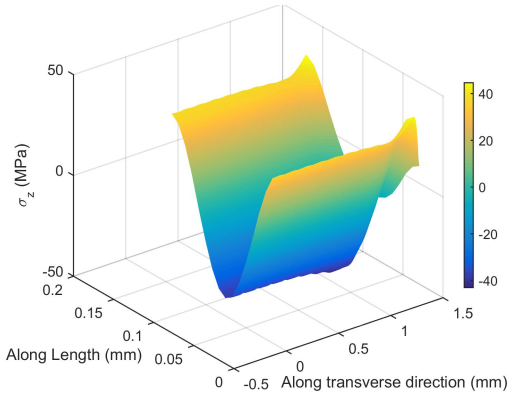

(a) Distribution of σ_z

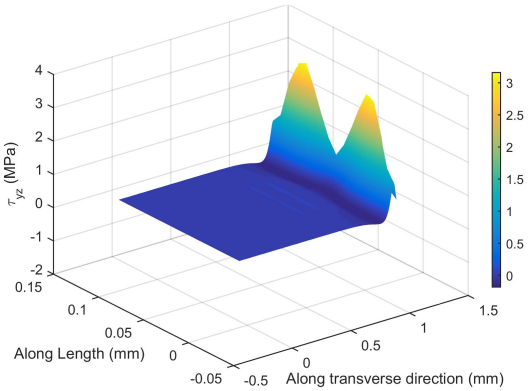

(b) Distribution of τ_{yz}

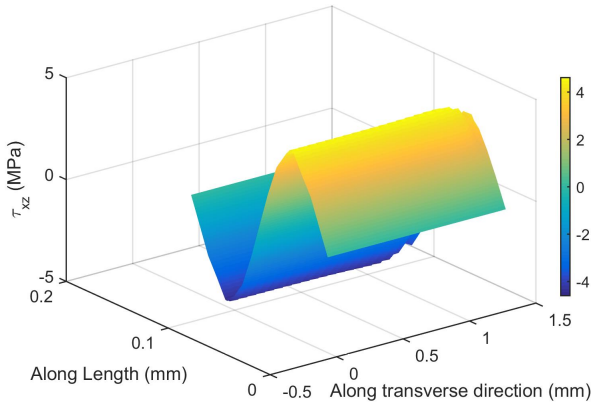

(c) Distribution of τ_{xz}

Figure 4.24: Distribution of interlaminar stresses on ninety-ninety degree layers' interface

The results on the ninety-ninety degree layers' interface surface is presented in this section. Figures 4.24a, 4.24b and 4.24c show the surface plots for σ_z, τ_{yz} and τ_{xz} respectively. Analogous to their distribution at zero-ninety layers' interface it is observed that there is a rise in σ_z near the free edge. Likewise, τ_{yz} shows higher gradient near free edge. The distribution of τ_{xz} appears analogous to one at zero-ninety layers' interface in a sense that there is equal and opposite distribution longitudinally and thus, the average of τ_{xz} longitudinally appears to be negligible.

The longitudinally averaged plots of the three interlaminar stresses is shown in figure 4.25.

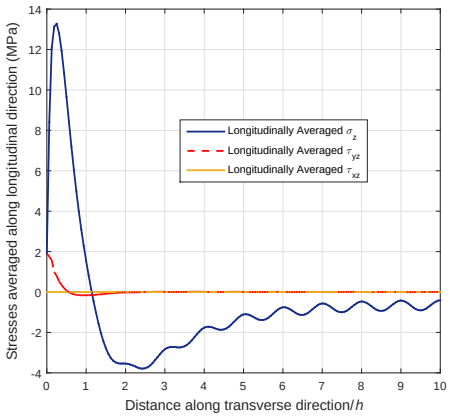

Figure 4.25: Longitudinally averaged interlaminar stresses at ninety-ninety layers' interface

It is notable from figure 4.25 that compared to longitudinally averaged values of σ_z and τ_{yz}, the longitudinally averaged value of τ_{xz} is negligible like in the case of zero-ninety layers' interface.

Further, at ninety-ninety layers' interface, the gradient of interlaminar stresses obtained at bottom surface of homogeneous layer model in section 3.7 can be compared on the same scale with longitudinally averaged σ_z and τ_{yz} of heterogeneous model like at zero-ninety layers' interface.

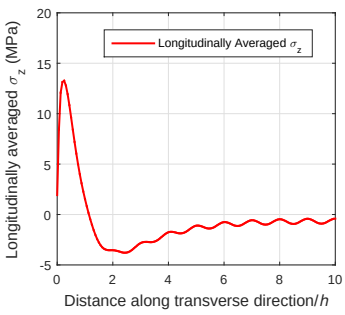

(a) Longitudinally averaged σ_z in heterogeneous model

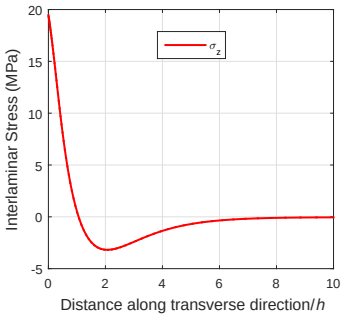

(b) σ_z in homogeneous model

Figure 4.26: Comparison of σ_z at ninety-ninety layers' interface between homogeneous and heterogeneous models

Figure 4.26 shows a comparison of equivalent σ_z stress distributed along the transverse direction in heterogeneous and homogeneous models. It can be observed that the modelling of layers with homogeneous material causes σ_z to peak higher in a steep manner at the free edge.

The comparison of τ_{yz} in a similar manner is shown in figure 4.27. It is observed that right at the free edge the stress has a very high gradient in homogeneous model plot in figure 4.27b. However, such a gradient is not observed at the free edge in heterogeneous model in figure 4.27a.

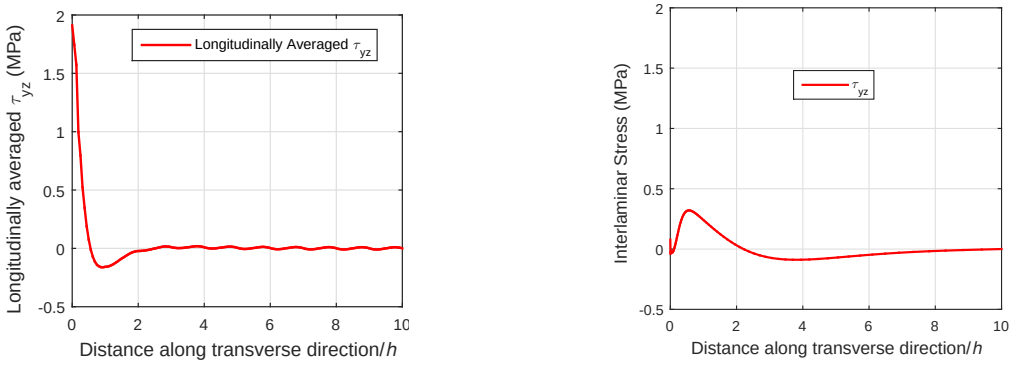

(a) Longitudinally averaged τ_{yz} in heterogeneous model

(b) τ_{yz} in homogeneous model

Figure 4.27: Comparison of τ_{yz} at ninety-ninety layers' interface between homogeneous and heterogeneous models

The gradient of τ_{yz} stress at the free edge of the two models can be seen more clearly in figure 4.28. Right at the free edge of homogeneous model in figure 4.28b, the gradient of τ_{yz} is seen to increase comparatively more than that of figure 4.28a.

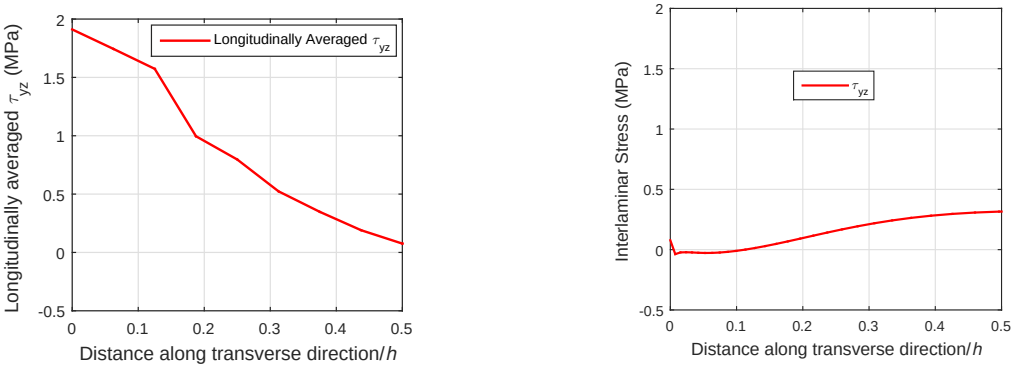

(a) Free edge gradient of longitudinally averaged τ_{yz} in heterogeneous model

(b) Free edge gradient of τ_{yz} in homogeneous model

Figure 4.28: Comparison of τ_{yz} at ninety-ninety layers' interface between homogeneous and heterogeneous models

Chapter 5

Homogenisation of Unit Cell through Periodic Boundary Conditions

5.1 Background

The high interlaminar stresses near free edge can play a role in initiating delamination. While using homogeneous layer models for prediction of delamination initiation, the high gradient require finer meshes and hence higher computational expense for arriving at a converged value at free edge. However, such gradients have not been observed in case of heterogeneous model. The high gradient stresses in homogeneous models hence act as a hurdle in determining stress value which could be incorporated in a suitable failure criterion for predicting delamination initiation. As described in chapter 2, one such criterion used for prediction of delamination initiation is the QDC proposed by *Brewer et al* (1988) [12]. This criterion focuses on determining an averaging distance (in transverse direction) from the free edge until which free edge stresses with high gradient could be averaged. This averaging of stresses enables determination of definite stress values in vicinity of free edge which can then be brought to use in the proposed QDC in equation (2.48). The stress profiles obtained from heterogeneous model can thus act as a basis for determining the averaging distance by correlation of stresses between homogeneous and heterogeneous layer models.

For correlating the stresses between homogeneous and heterogeneous models there is a need to extract homogenised engineering properties from the fibre and matrix properties of heterogeneous model. The modelling of homogeneous layer laminate with homogenised properties would enable comparison of two models with same stiffness and hence a valid correlation could be arrived upon. As highlighted in chapter 2, homogenisation through application of PBC has been considered the best option for extraction of homogenised engineering constants for a periodic heterogeneous model such as the one at hand.

5.2 Homogenisation of heterogeneous unit cell

As seen in the previous section, there is a need to find a homogenised layer model corresponding to the heterogeneous layer model. The model with homogenised properties could then be used for analysing high gradient free edge stresses. Before delving into the procedure itself, it's worthwhile highlighting the end goal of homogenisation in context of this chapter. As of now a $[0/90]_s$ cross-ply model has been built with a certain set of fibre and matrix properties listed in table 4.1. The homogenisation is being carried out to establish a procedure to eventually construct a $[0/90]_s$ cross-ply model with homogeneous material having effective engineering constants corresponding to a set of properties for fibre and matrix. Therefore, if on a unit cell of a unidirectional lamina (figure 2.13) homogenized is carried out, then the effective engineering constants of a zero degree homogeneous layer could be obtained. Subsequently, the ninety degree layer's properties could be obtained from those of zero degree layer. Hence, the choice of cubic unit cell shown in figure 5.1 has been made to carry out the homogenisation procedure.

Homogenisation procedure of UC

This section deals with homogenisation through PBC of a graphite-epoxy heterogeneous UC shown in figure 5.1 on the basis of homogenisation approach detailed in section 2.5. The homogenisation of cubic UC with one cylindrical fibre embedded in matrix as shown in figure 5.1 can be a RVE of the heterogeneous medium which could enable the derivation of effective properties of lamina and hence, the modelling of homogeneous layer cross-ply model equivalent in stiffness to the heterogeneous cross-ply model used in chapter 4 (figure 4.5).

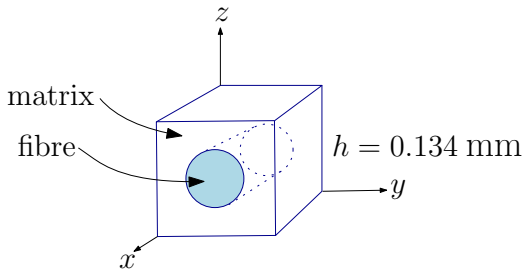

Figure 5.1: UC to be homogenised for derivation of effective properties of lamina

The governing equation followed for derivation of homogenised stiffness tensor $\mathbf{C}$ through heterogeneous UC is given by equation (2.40). The equation is reproduced here again as equation (5.1) for convenient referencing.

$$\frac{1}{2}(\boldsymbol{\epsilon}^{\mathrm{T}}\mathbf{C}\boldsymbol{\epsilon})V = \frac{1}{2}\sum_{i=1}^{n}(F_i u_i)^{\mathrm{UC}} \tag{5.1}$$

Now, the intention is to determine engineering properties in all three directions x, y and z. The fibre used for modelling the UC is considered to be transversely isotropic. Given the isotropic nature of matrix, the UC could be considered to be having a transverse isotropic symmetry. The material properties of fibre and matrix are reproduced in table 5.1.

Table 5.1: Fibre and matrix properties for combinations of graphite fibre and epoxy matrix [8]

Properties	Graphite fibre	Epoxy matrix
E_{xf} (GPa)	233.0	-
E_{yf} (GPa)	23.10	-
E_{zf} (GPa)	23.10	-
ν_{xyf}	0.2	-
ν_{xzf}	0.2	-
ν_{yzf}	0.4	-
G_{xyf} (GPa)	8.96	-
G_{xzf} (GPa)	8.96	-
G_{yzf} (GPa)	8.27	-
E_m (GPa)	-	4.62
ν_m	-	0.36

where f and m represent fibre and matrix properties respectively.

The homogeneous stiffness tensor to be considered for derivation of stiffness tensor components is shown in equation (5.2)

$$\mathbf{C} = \begin{bmatrix} C_{11} & C_{12} & C_{13} & 0 & 0 & 0 \\ C_{12} & C_{22} & C_{23} & 0 & 0 & 0 \\ C_{13} & C_{23} & C_{33} & 0 & 0 & 0 \\ 0 & 0 & 0 & C_{44} & 0 & 0 \\ 0 & 0 & 0 & 0 & C_{55} & 0 \\ 0 & 0 & 0 & 0 & 0 & C_{66} \end{bmatrix} \tag{5.2}$$

Equation (5.2) suggests that to be able to derive the stiffness matrix $\mathbf{C}$, the following nine constants, namely, C_{11}, C_{12}, C_{13}, C_{22}, C_{23}, C_{33}, C_{44}, C_{55}, C_{66} must be evaluated. Referring back to equation (5.1), the left-hand side of the equation can be expanded as follows:

$$\frac{1}{2}(\boldsymbol{\epsilon}^{\mathrm{T}}\mathbf{C}\boldsymbol{\epsilon})V = \frac{1}{2}\begin{bmatrix} \epsilon_x & \epsilon_y & \epsilon_z & \gamma_{yz} & \gamma_{xz} & \gamma_{xy} \end{bmatrix} \begin{bmatrix} C_{11} & C_{12} & C_{13} & 0 & 0 & 0 \\ C_{12} & C_{22} & C_{23} & 0 & 0 & 0 \\ C_{13} & C_{23} & C_{33} & 0 & 0 & 0 \\ 0 & 0 & 0 & C_{44} & 0 & 0 \\ 0 & 0 & 0 & 0 & C_{55} & 0 \\ 0 & 0 & 0 & 0 & 0 & C_{66} \end{bmatrix} \begin{bmatrix} \epsilon_x \\ \epsilon_y \\ \epsilon_z \\ \gamma_{yz} \\ \gamma_{xz} \\ \gamma_{xy} \end{bmatrix} V \tag{5.3}$$

In equation (5.1), ϵ_x, ϵ_y and ϵ_z represent macroscopic (homogeneous) normal strain components in longitudinal (x), transverse (y) and through thickness (z) directions respectively, while γ_{yz}, γ_{xz}, γ_{xy} represent macroscopic (homogeneous) engineering shear strain components in respective directions with reference to figure 5.1. It is notable that these macroscopic strain components are the same as the corresponding average microscopic strain components (or strain components provided in the heterogeneous UC). Thus, to simulate a macroscopic

strain, the same amount of corresponding strain could be simulated in the heterogeneous UC. V represents the volume of UC. It is given by h^3 where h is the dimension of the side of UC (also equal to ply thickness of 0.134 mm in this case). If u, v and w represent deformation of the UC in x, y and z directions respectively, then the strain components can be represented as follows:

$$\epsilon_x = \frac{\partial u}{\partial x} \tag{5.4}$$

$$\epsilon_y = \frac{\partial v}{\partial y} \tag{5.5}$$

$$\epsilon_z = \frac{\partial w}{\partial z} \tag{5.6}$$

$$\gamma_{yz} = \frac{\partial w}{\partial y} + \frac{\partial v}{\partial z} \tag{5.7}$$

$$\gamma_{xz} = \frac{\partial w}{\partial x} + \frac{\partial u}{\partial z} \tag{5.8}$$

$$\gamma_{xy} = \frac{\partial v}{\partial x} + \frac{\partial u}{\partial y} \tag{5.9}$$

Through equation (5.3) it can be deduced that to be able to derive the nine stiffness tensor components, nine linear equations need to be solved. Thus, suitable combination of strain components need to be chosen to solve for respective stiffness constants. The following table 5.2 provides the list of strain combinations that need to be applied to solve for various stiffness tensor components. During the execution of homogenisation procedure the strain component applied for derivation of every constant has been 0.01. Hence, using a value of 0.01 for every strain component, the table 5.2 can be presented:

Table 5.2: Combination of strains for determining various stiffness tensor components

For determining the constant	ϵ_x	ϵ_y	ϵ_z	γ_{yz}	γ_{xz}	γ_{xy}
C_{11}	0.01	0	0	0	0	0
C_{22}	0	0.01	0	0	0	0
C_{33}	0		0.01	0	0	0
C_{12}	0.01	0.01	0	0	0	0
C_{13}	0.01	0	0.01	0	0	0
C_{23}	0	0.01	0.01	0	0	0
C_{44}	0	0	0	0.01	0	0
C_{55}	0	0	0	0	0.01	0
C_{66}	0	0	0	0	0	0.01

Equation (5.3) with the help of equation (5.1) can be re-written as equation (5.10).

$$\begin{bmatrix} \epsilon_x & \epsilon_y & \epsilon_z & \gamma_{yz} & \gamma_{xz} & \gamma_{xy} \end{bmatrix} \begin{bmatrix} C_{11} & C_{12} & C_{13} & 0 & 0 & 0 \\ C_{12} & C_{22} & C_{23} & 0 & 0 & 0 \\ C_{13} & C_{23} & C_{33} & 0 & 0 & 0 \\ 0 & 0 & 0 & C_{44} & 0 & 0 \\ 0 & 0 & 0 & 0 & C_{55} & 0 \\ 0 & 0 & 0 & 0 & 0 & C_{66} \end{bmatrix} \begin{bmatrix} \epsilon_x \\ \epsilon_y \\ \epsilon_z \\ \gamma_{yz} \\ \gamma_{xz} \\ \gamma_{xy} \end{bmatrix} = \frac{1}{V} \sum_{i=1}^{n} (F_{\mathrm{i}} u_{\mathrm{i}})^{\mathrm{UC}} \tag{5.10}$$

Complete strain tensor (consisting of strain components in different combinations) in table 5.2 can be applied row wise one by one in equation (5.10). Applying the strain tensor in different combinations of components would lead to the generation of a coefficient matrix corresponding to each of the nine variables (C_{11}, C_{12}, C_{13}, C_{22}, C_{23}, C_{33}, C_{44}, C_{55}, C_{66}). Applying every strain tensor component of 0.01 in equation (5.10) would lead to the following coefficient matrix in equation (5.11):

$$\text{Coefficient matrix} = \begin{bmatrix} 0.0001 & 0 & 0 & 0 & 0 & 0 & 0 & 0 & 0 \\ 0 & 0 & 0 & 0.0001 & 0 & 0 & 0 & 0 & 0 \\ 0 & 0 & 0 & 0 & 0 & 0.0001 & 0 & 0 & 0 \\ 0.0001 & 0.0002 & 0 & 0.0001 & 0 & 0 & 0 & 0 & 0 \\ 0.0001 & 0 & 0.0002 & 0 & 0 & 0.0001 & 0 & 0 & 0 \\ 0 & 0 & 0 & 0.0001 & 0.0002 & 0.0001 & 0 & 0 & 0 \\ 0 & 0 & 0 & 0 & 0 & 0 & 0.0001 & 0 & 0 \\ 0 & 0 & 0 & 0 & 0 & 0 & 0 & 0.0001 & 0 \\ 0 & 0 & 0 & 0 & 0 & 0 & 0 & 0 & 0.0001 \end{bmatrix} \tag{5.11}$$

The coefficient matrix in equation (5.11) along with the right hand side value of equation (5.10) for each of the nine strain tensors (with different combinations of strain components) in table 5.2 would allow the solving of a system of linear equations for the nine variables at hand. The following form of equation has been used in context of this problem to solve for the nine stiffness tensor constants.

$$\begin{bmatrix} C_{11} \\ C_{12} \\ C_{13} \\ C_{22} \\ C_{23} \\ C_{33} \\ C_{44} \\ C_{55} \\ C_{66} \end{bmatrix} = \begin{bmatrix} 0.0001 & 0 & 0 & 0 & 0 & 0 & 0 & 0 & 0 \\ 0 & 0 & 0 & 0.0001 & 0 & 0 & 0 & 0 & 0 \\ 0 & 0 & 0 & 0 & 0 & 0.0001 & 0 & 0 & 0 \\ 0.0001 & 0.0002 & 0 & 0.0001 & 0 & 0 & 0 & 0 & 0 \\ 0.0001 & 0 & 0.0002 & 0 & 0 & 0.0001 & 0 & 0 & 0 \\ 0 & 0 & 0 & 0.0001 & 0.0002 & 0.0001 & 0 & 0 & 0 \\ 0 & 0 & 0 & 0 & 0 & 0 & 0.0001 & 0 & 0 \\ 0 & 0 & 0 & 0 & 0 & 0 & 0 & 0.0001 & 0 \\ 0 & 0 & 0 & 0 & 0 & 0 & 0 & 0 & 0.0001 \end{bmatrix} \begin{bmatrix} W_{11} \\ W_{22} \\ W_{33} \\ W_{12} \\ W_{13} \\ W_{23} \\ W_{44} \\ W_{55} \\ W_{66} \end{bmatrix} \tag{5.12}$$

where W_{11}, W_{22}, W_{33}, W_{12}, W_{13}, W_{23}, W_{44}, W_{55} and W_{66} are right hand side values of equation (5.10) when the strain tensor is applied as mentioned in table 5.2 row wise from top to bottom.

At this stage, the skeleton for calculation of stiffness tensor components is ready. The parameters needed are the right hand side values of equation (5.10) corresponding to the nine strain tensors in table 5.2. These parameters involve calculation of internal energy of the UC when subjected to various strain combinations through PBC. This involves calculation of nodal forces and displacements at nodes. The next subsection deals with the approach used during the course of the work to evaluate internal energy of the heterogeneous UC.

Use of PBC through FEA to solve for components of stiffness tensor C

The work done on a UC due to applied strain would be equal to the internal energy generated within the UC. Upon discretisation of the UC through finite elements, work done on a UC could be calculated based on the information of forces and displacements on nodes on external surfaces of UC. When a UC gets subjected to deformation due to applied strain, then the nodes on external surfaces may possess a net nodal force due internal elastic reaction forces that get generated in elements under deformation to maintain equilibrium. If there are n nodes on the external surface of a UC, then the force and displacement data on the nodes could lead to deriving the relation for the total internal energy generated within the UC. Let's consider figure 5.2.

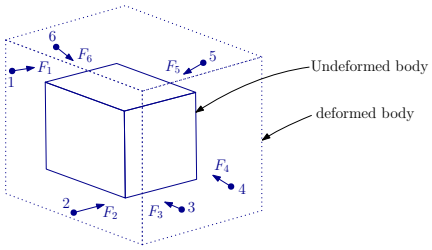

Figure 5.2: Schematic representation of elastic nodal forces and nodal displacements

For an elementary displacement du_i at an arbitrary node i, the elementary work dW_i done due to elastic force F_i could be given by:

$$dW_i = F_i du_i \tag{5.13}$$

For a nodal displacement of u_i, the total work done by force F_i at node i is given by W_i.

$$W_i = \int_0^{u_i} F_i du_i \tag{5.14}$$

For an elastic body, the internal reaction force at a point i i.e. F_i can be given by $K_i u_i$, where K_i is stiffness of material at node i. Substituting F_i with $K_i u_i$ in equation (5.14), we get

$$W_i = \int_0^{u_i} K_i u_i du_i \tag{5.15}$$

$$\therefore W_i = K_i \frac{u_i^2}{2} \tag{5.16}$$

$$\text{or, } W_i = \frac{1}{2} F_i u_i \tag{5.17}$$

The total work on the whole body would thus be a summation of all such works at nodes. Hence, the right-hand side of equation (5.1) is obtained as the total internal energy of the UC in FEA.

Hence, all that is needed now is force and displacement data at every node on the external boundaries of a UC through which the right-hand side values of equation (5.10) could be obtained for a given strain tensor. This would enable the calculation of stiffness tensor components for a given volume of UC through equation (5.12).

Deformations of UC through PBC for determination of stiffness tensor

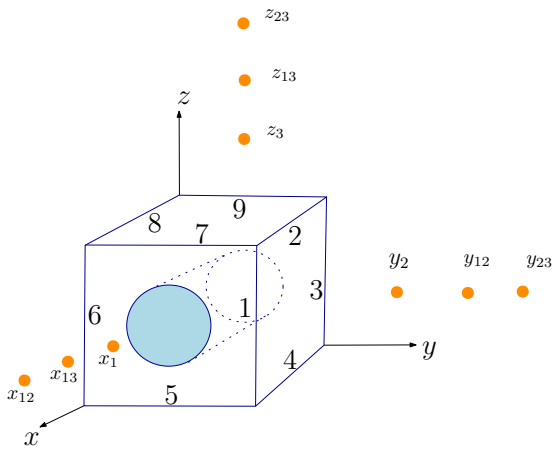

Figure 5.3: Application of PBC to simulate different strain combinations on UC

The PBCs are applied on the UC according to the nine combination of strain tensors listed in table 5.2 (row wise). Thus, nine unique deformation states are obtained for the UC. These deformation states include unidirectional normal strain deformation, bidirectional normal strain deformation or a shear strain deformation state. The internal energy of UC can be calculated corresponding to every deformation state. Hence, for a given volume of UC, the nine values of W_{11}, W_{22}, W_{33}, W_{12}, W_{13}, W_{23}, W_{44}, W_{55} and W_{66} could be calculated through the means of equation (5.10). Plugging these values of W_{11}, W_{22}, W_{33}, W_{12}, W_{13}, W_{23}, W_{44}, W_{55} and W_{66} in equation (5.12) would enable calculation of all the nine required constants of stiffness tensor.

Now, the deformations are to be provided through PBCs. In Abaqus, the PBC is applied through the means of dummy nodes as explained in subsection 4.4 (equation (4.6)). In a 3D model like that of the UC in consideration, application of PBC so as to constrain all DoFs of all the nodes can be cumbersome. More so because of common edges between different faces.

It is to be ensured that DoFs of nodes on such edges are not over constrained to be able to run successful simulations.

In total, six sets of constraint equations are simulated for every deformation state. Each of these sets of equations are defined for node pairs on opposite boundaries which participate in representing the respective strain components of a particular row in table 5.2. For simulating a strain component, the dummy node associated with that strain component is provided suitable displacement in the load step in Abaqus. Thus, if the dummy node is provided a zero displacement then the strain component corresponding to that dummy node is zero and the displacement difference between corresponding node pair is also zero.

To simulate ϵ_x, dummy node x_1 (in orange) in figure 5.3 is provided displacement in x direction. Similarly, for ϵ_y, dummy node y_2 is provided the displacement in y direction and for ϵ_z, dummy node z_3 is provided displacement in z direction. For simulating ϵ_x and ϵ_y together (like in row 4 of table 5.2), both dummy nodes x_1 and y_2 are provided displacements in x and y directions respectively. Likewise, for combinations of ϵ_x and ϵ_z and for ϵ_y and ϵ_z. For providing shear strain γ_{yz}, dummy node y_{23} is provided displacement in z direction and z_{23} is provided displacement in y direction. Likewise for shear strains γ_{xz} similar approach is followed using dummy nodes x_{13} and z_{13} and for γ_{xy} the same approach is followed with dummy nodes x_{12} and y_{12}.

As an example, if only ϵ_x of 0.01 is to be applied according to row 1 of table 5.2, then the dummy node represented by x_1 must be given a displacement of $0.01 \times 0.134 = 0.00134$ mm in x direction. At the same time, all other dummy nodes represented (in orange) by x_{13}, x_{12}, y_2, y_{12}, y_{23}, z_3, z_{13} and z_{23} are provided zero displacement so as to maintain zero strain for all other strain components. For providing the shear strain γ_{yz} of 0.01, $\frac{\partial w}{\partial y} + \frac{\partial v}{\partial z}$ (equation (5.7)) must be 0.01. Thus, the parts $\frac{\partial w}{\partial y}$ and $\frac{\partial v}{\partial z}$ could both be 0.005 to get γ_{yz} of 0.01. This means that the dummy node y_{23} must be provided a displacement of 0.005×0.134 (as length of side in y direction is 0.134 mm) and dummy node z_{23} must be provided a displacement of 0.005×0.134 (as length of side in z direction is also 0.134 mm). For providing displacements to dummy nodes while simulating shear strains, equation (2.45) could also be referred to. Similarly different strain components could be simulated for different rows of table 5.2 to get all the nine deformation states of the UC.

All the DoFs of all nodes on exterior surface of the UC must be governed by constraint equations for corresponding combination of strains according to a particular row in table 5.2. In the current work, the approach followed for applying PBC which mitigates over constraining of DoFs of nodes at common edges is by suppressing the definition of constraint equations along a particular DoF for one strain component if that DoF of concerned edge is already defined by constraint equation corresponding to another strain.

For example, if the UC is to be deformed according to strain combinations of row 1 in table 5.2, then it can be seen that only strain component ϵ_x is to be provided a non-zero value. Constraint equations corresponding to other strains will also exist but with zero displacement to their dummy nodes. So, the constraint equations for all nodes on front and rear boundary surfaces for ϵ_x will govern their x direction DoFs with the help of dummy node x_1. This means that for example, the constraint equation for shear strain γ_{xy} will not define the x direction DoF of nodes on edge 1 (shown in figure 5.3) through dummy node y_{12}. Likewise, the constraint equation for shear strain γ_{xz} will not define the x direction DoF of nodes on

edge 7 through dummy node z_{13}. in this way, over constraining of nodes on common edges has been avoided.

For running the analyses in Abaqus, all the DoFs of one node at centre of rear bottom surface has been constrained to avoid rigid body motion. C3D8 elements have been chosen for building the model as has been described in chapter 4. Periodic distribution of nodal forces is expected on opposite boundary surfaces corresponding to every deformation state. Through the deformations presented from figure 5.5 to 5.13, the periodic distributions of nodal forces are verified. For nomenclature of various surfaces of the UC and identification of coordinate axes, figure 5.4 is to be referred.

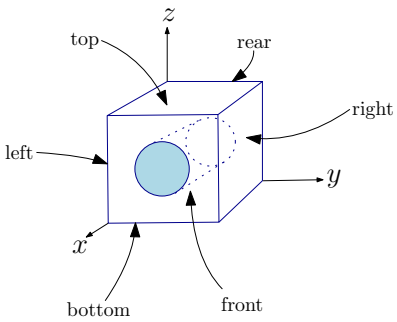

Figure 5.4: Nomenclature of surfaces of UC

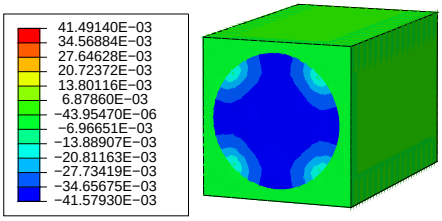

(a) Nodal force distribution in x direction on front surface

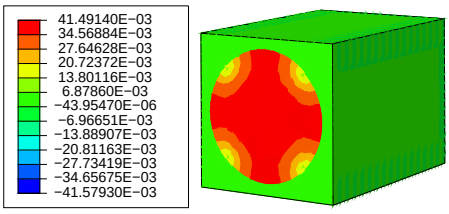

(b) Nodal force distribution in x direction on rear surface

Figure 5.5: Equal and opposite nodal force distribution for extensional ϵ_x strain

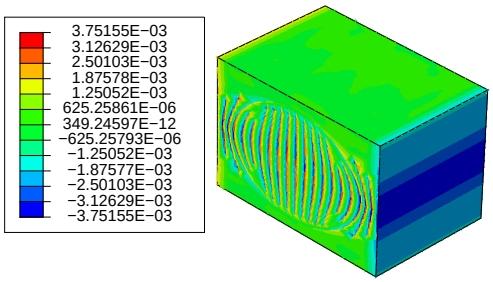

(a) Nodal force distribution in y direction on right surface

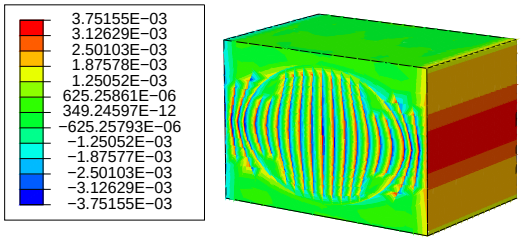

(b) Nodal force distribution in y direction on left surface

Figure 5.6: Equal and opposite nodal force distribution for extensional ϵ_y strain

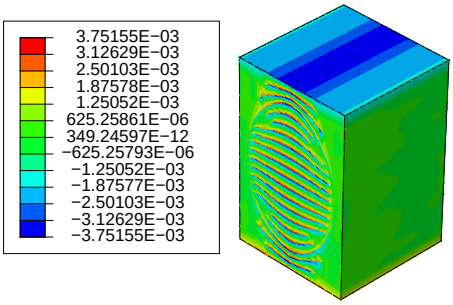

(a) Nodal force distribution in z direction on top surface

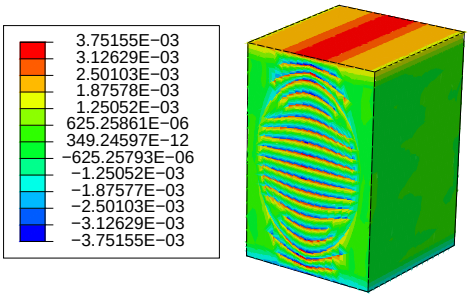

(b) Nodal force distribution in z direction on bottom surface

Figure 5.7: Equal and opposite nodal force distribution for extensional ϵ_z strain

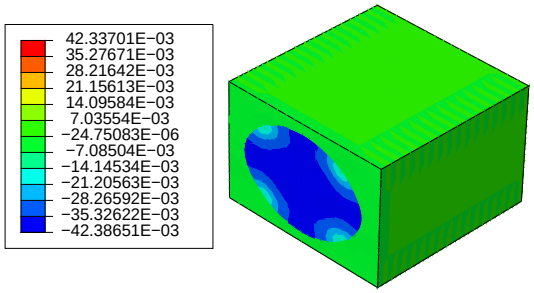

(a) Nodal force distribution in x direction on front surface

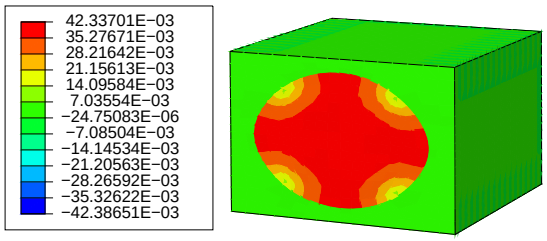

(b) Nodal force distribution in x direction on rear surface

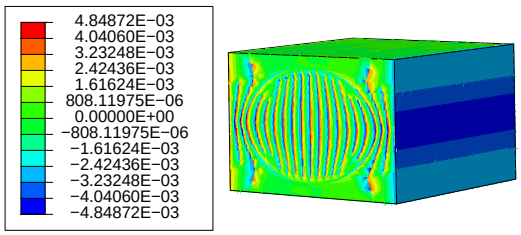

(c) Nodal force distribution in y direction on right surface

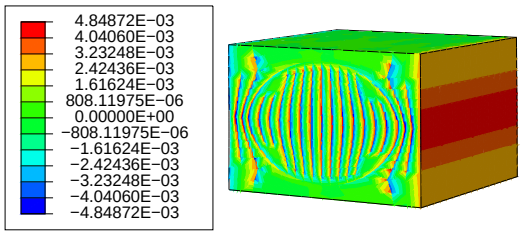

(d) Nodal force distribution in y direction on left surface

Figure 5.8: Equal and opposite nodal force distribution for combined extensional ϵ_x and ϵ_y strains

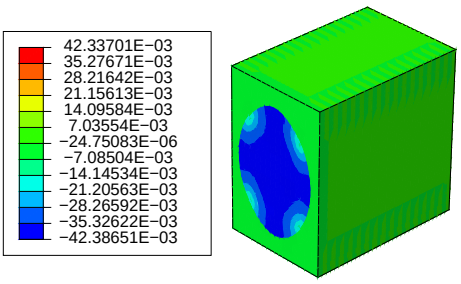

(a) Nodal force distribution in x direction on front surface

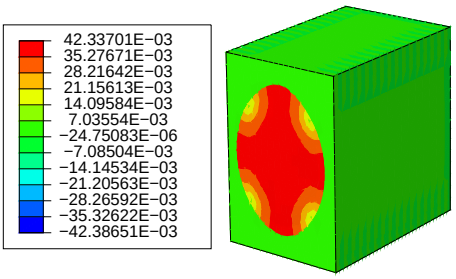

(b) Nodal force distribution in x direction on rear surface

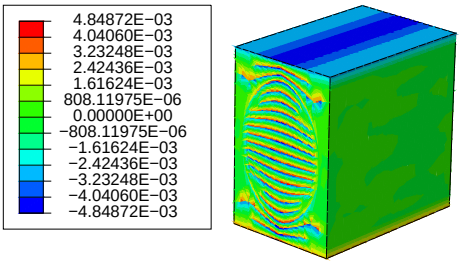

(c) Nodal force distribution in z direction on top surface

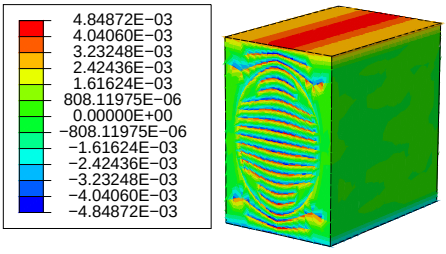

(d) Nodal force distribution in z direction on bottom surface

Figure 5.9: Equal and opposite nodal force distribution for combined extensional ϵ_x and ϵ_z strains

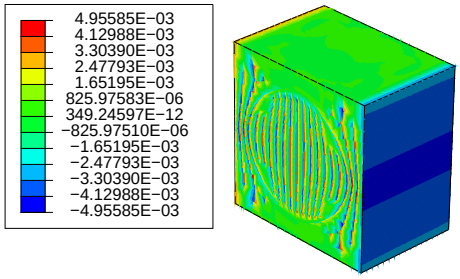

(a) Nodal force distribution in y direction on right surface

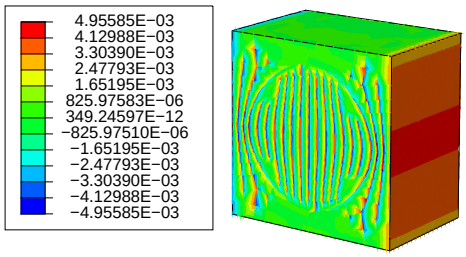

(b) Nodal force distribution in y direction on left surface

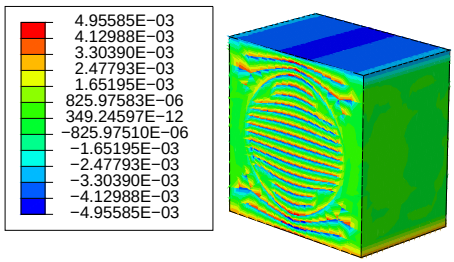

(c) Nodal force distribution in z direction on top surface

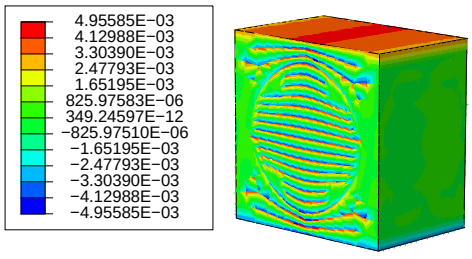

(d) Nodal force distribution in z direction on bottom surface

Figure 5.10: Equal and opposite nodal force distribution for combined extensional ϵ_y and ϵ_z strains

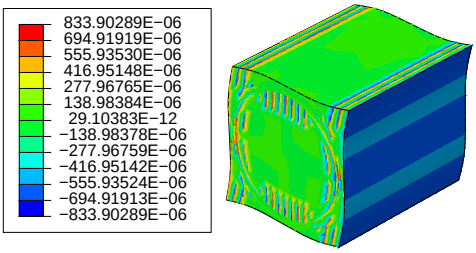

(a) Nodal force distribution in z direction on right surface

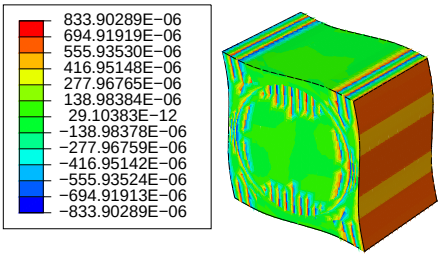

(b) Nodal force distribution in z direction on left surface

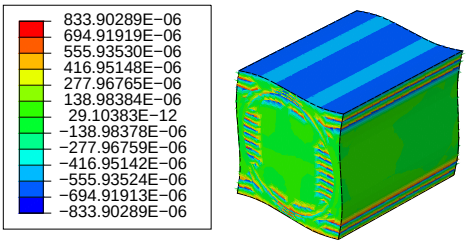

(c) Nodal force distribution in y direction on top surface

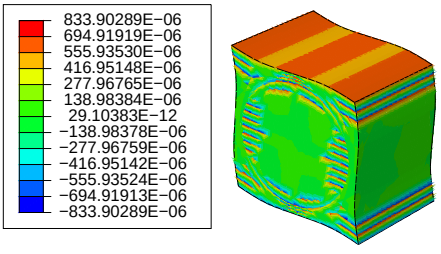

(d) Nodal force distribution in y direction on bottom surface

Figure 5.11: Equal and opposite nodal force distribution for γ_{yz}

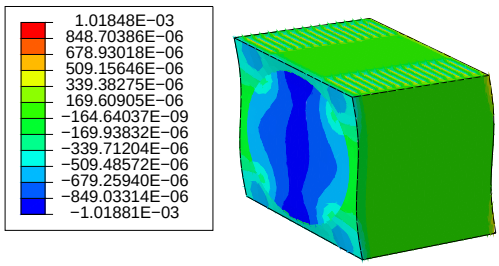

(a) Nodal force distribution in z direction on front surface

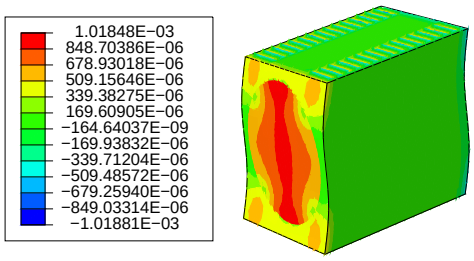

(b) Nodal force distribution in z direction on rear surface

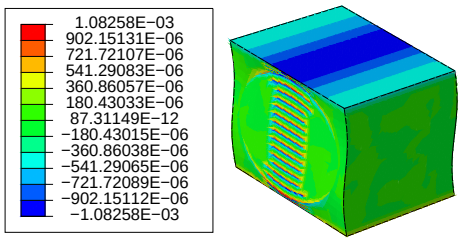

(c) Nodal force distribution in x direction on top surface

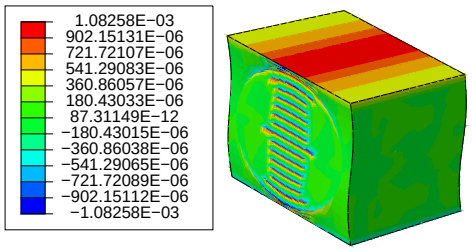

(d) Nodal force distribution in x direction on bottom surface

Figure 5.12: Equal and opposite nodal force distribution for γ_{xz}

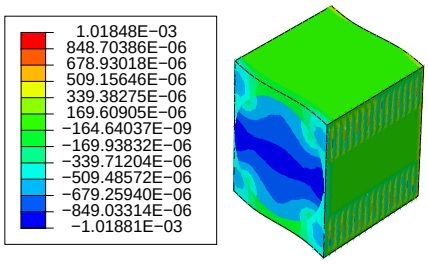

(a) Nodal force distribution in y direction on front surface

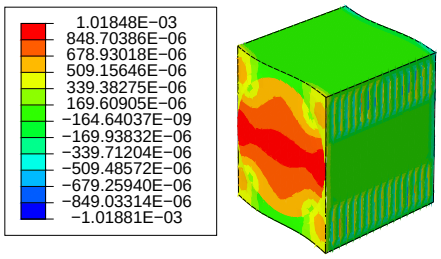

(b) Nodal force distribution in y direction on rear surface

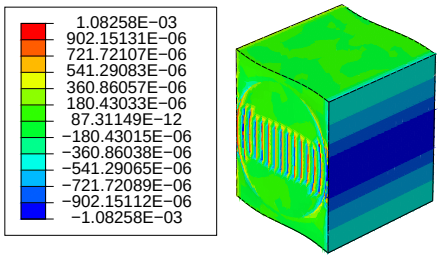

(c) Nodal force distribution in x direction on right surface

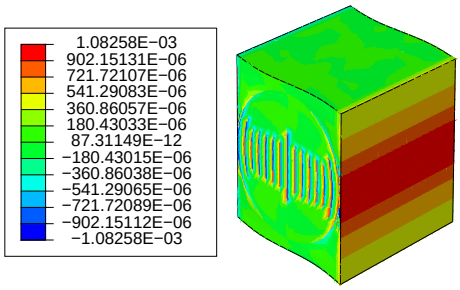

(d) Nodal force distribution in x direction on left surface

Figure 5.13: Equal and opposite nodal force distribution for γ_{xy}

It appears in all deformation states that opposite surfaces exhibit an equal and opposite distribution of nodal forces in the direction of applied PBC as expected. However, plots of nodal forces on opposite boundary surfaces would give a clearer picture. Plots of nodal forces and nodal displacements on the opposite surfaces of the UC corresponding to ϵ_x, ϵ_y, ϵ_z, γ_{yz}, γ_{xz} and γ_{xy} are reported. Plots for combined ϵ_x and ϵ_y, combined ϵ_x and ϵ_z and combined ϵ_y and ϵ_z are not represented because confirmation of veracity of ϵ_x, ϵ_y and ϵ_z strains themselves confirm the veracity of their combinations. All node pairs corresponding to opposite surfaces are represented by points linearly on abscissa.

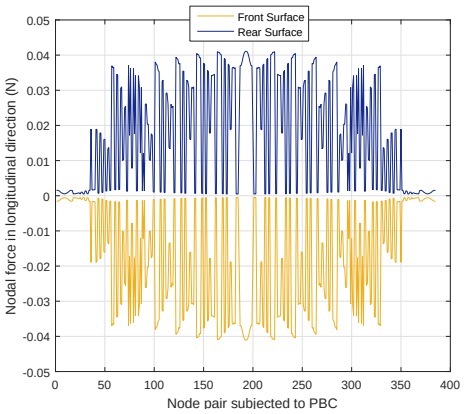

(a) Nodal force distribution in x direction on front and rear surfaces

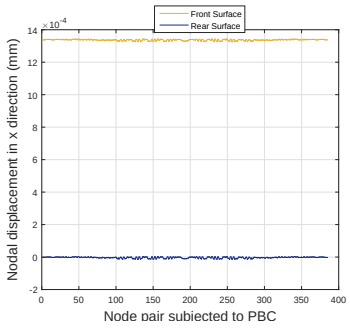

(b) Nodal displacement distribution in x direction on front and rear surfaces

Figure 5.14: Representation of nodal forces and displacements on front and rear surfaces for ϵ_x

It is importantly highlighted that to avoid rigid body motion, the centre node on rear bottom surface is fixed. It is observed that the forces are equal and opposite on node pairs on opposite boundary surfaces (front-rear). The summation of nodal forces on front and rear surfaces is expected to be zero or negligible as seen in figure 4.9b. Plots for the summation of forces on opposite boundaries for deformation states could be verified by referring to plots in appendix A.2 wherein plots for similar deformations states in UC are presented for T300/934 material. The difference in displacement between two nodes of a pair is always constant (corresponding to the strain applied in x direction of 0.01, the displacement difference is $0.01 \times 0.134 = 0.00134$ mm). In figure 5.14b, although the displacements on nodes of rear surface are negligible, a corresponding variation is observed on opposite nodes on front surface so as to keep the

displacement difference constant between front and rear surfaces. Hence both traction and displacement continuities are satisfied on opposite boundary surfaces. Similarly, nodal force and displacement distribution for all other strains are observed to satisfy required conditions. Plots for ϵ_y and ϵ_z are shown in figures 5.15 and 5.16.

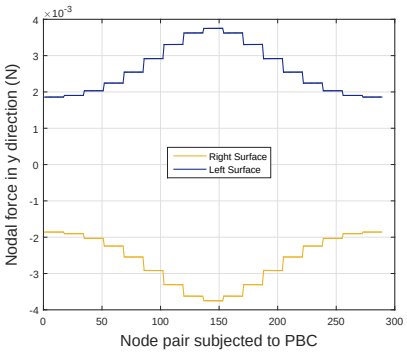

(a) Nodal force distribution in y direction on right and left surfaces

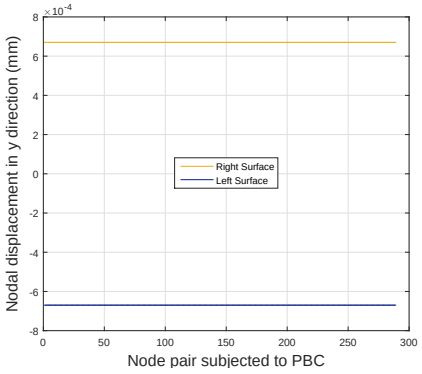

(b) Nodal displacement distribution in y direction on right and left surfaces

Figure 5.15: Representation of nodal forces and displacements on right and left surfaces for ϵ_y

Fixing the node at centre of rear bottom surface makes the right and left surfaces to displace symmetrically about the fixed node in all three directions. Hence, unlike in figure 5.14, the distribution of displacement on opposite nodes in figure 5.15 is symmetric about zero because the right and left surfaces move in opposite directions when ϵ_y is applied. Moreover, the presence of fibre on the front and rear surfaces leads to a different force distribution on front and rear surfaces as shown in figure 5.14a than on right and left surfaces in figure 5.15a. For example, in figure 5.14a, as we move from left to right on abscissa, we move from bottom to top of front and rear surfaces of UC in figure 5.5a. Since nodal forces on fibre of front and rear surfaces come to play in figure 5.14a, the nodal forces distribution differs to that of left and right surfaces in figure 5.15a which doesn't have fibre presence.

The nodal forces on front and rear surfaces in figure 5.14a exhibit higher values

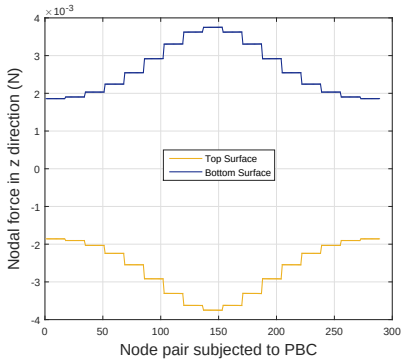

(a) Nodal force distribution in z direction on top and bottom surfaces

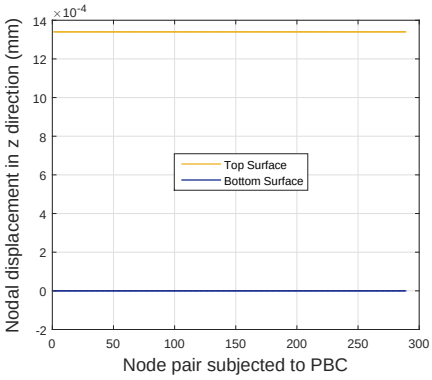

(b) Nodal displacement distribution in z direction on top and bottom surfaces

Figure 5.16: Nodal forces and displacements on top and bottom surfaces for ϵ_z

Plots for ϵ_z deformation state is shown in figure 5.16. The plots can be explained along similar arguments proposed for ϵ_x and ϵ_y

Figures 5.17, 5.18 and 5.19 show the nodal force and displacement distributions for engineering shear strains γ_{yz}, γ_{xz} and γ_{xy} respectively. Like in case of normal strains, the nodal force and displacement distributions have been found to be in compliance with PBC requirements.

For applying shear strain γ_{yz} PBC in z direction on right and left surfaces and PBC in y direction on top and bottom surfaces have been provided. Hence, distribution of nodal forces in z direction has been shown on right and left surfaces while distribution of nodal force in y direction has been shown on top and bottom surfaces. Similarly, plots for other shear strains have been shown.

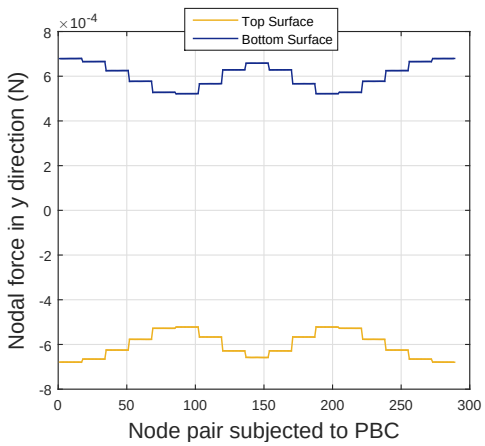

(a) Nodal force distribution in y direction on top and bottom surfaces

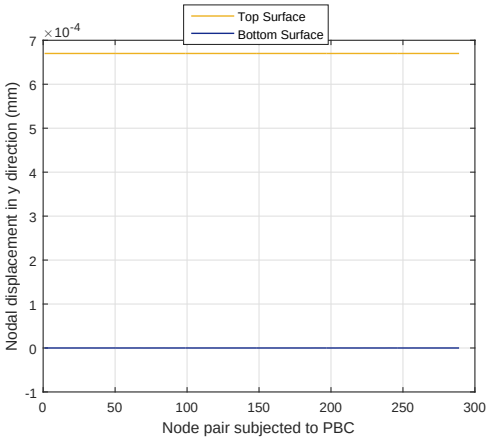

(b) Nodal displacement distribution in y direction on top and bottom surfaces

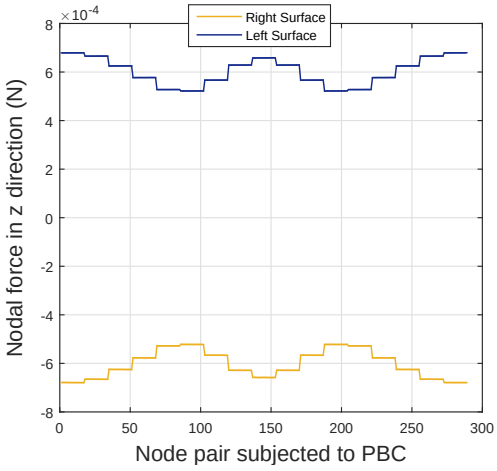

(c) Nodal force distribution in z direction on right and left surfaces

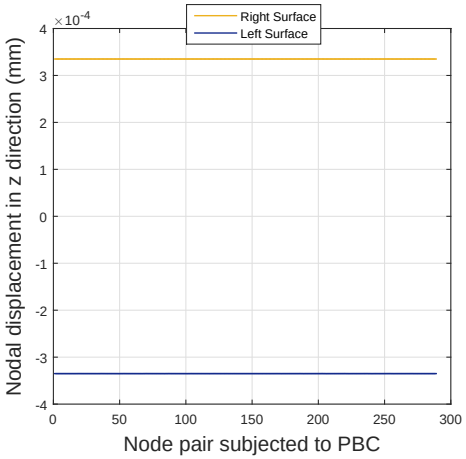

(d) Nodal displacement distribution in z direction on right and left surfaces

Figure 5.17: Nodal force and displacement distributions for γ_{yz}

According to expectations, the nodal force distribution on top and bottom surfaces have been found to be equal and opposite in y direction. The same has been observed for forces

on right and left surfaces in z direction. As far as displacements are concerned, a constant displacement difference is observed in z direction between right and left surfaces. The same has been observed for top and bottom surfaces in y direction. As expected, the displacement in z direction of right and left surfaces are symmetric about zero displacement line. In case of shear strain γ_{yz}, the combined displacements of top-bottom and right-left surface combinations produces a strain of 0.01. This means that both surface pairs show a displacement difference corresponding to a strain of 0.005 i.e 0.00067 mm. This displacement difference of 0.00067 mm can be seen in figures 5.17b and 5.17d. Similar trends have been observed for other shear strain components as shown further.

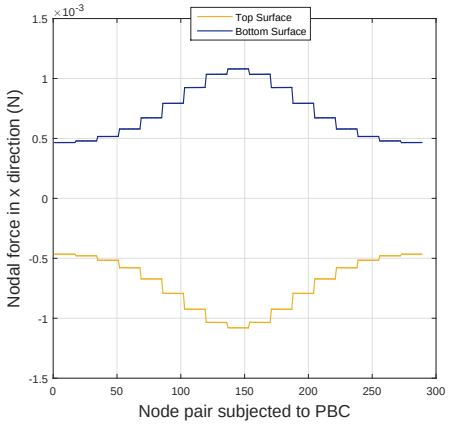

(a) Nodal force distribution in x direction on top and bottom surfaces

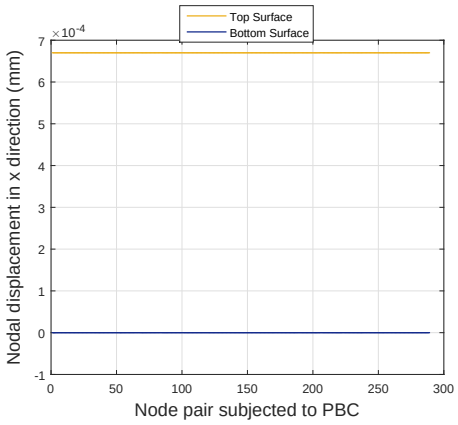

(b) Nodal displacement distribution in x direction on top and bottom surfaces

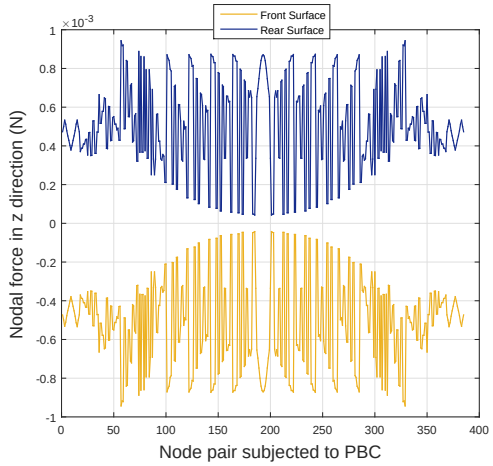

(c) Nodal force distribution in z direction on front and rear surfaces

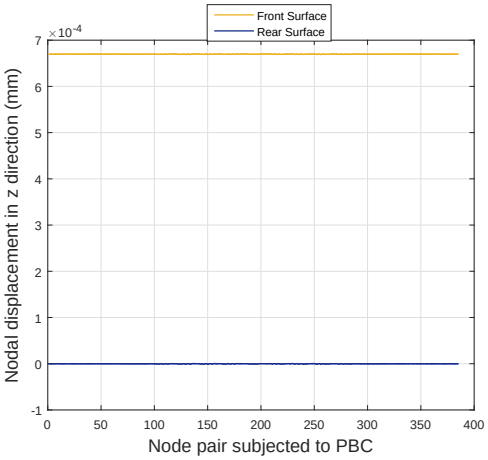

(d) Nodal displacement distribution in z direction on front and rear surfaces

Figure 5.18: Nodal force and displacement distributions for γ_{xz}

The shear strain components γ_{xz} and γ_{xy} involve the front-rear surface combination. This surface combination involves fibre material and hence the distribution of nodal forces on these two surfaces is different from the ones observed on right-left and top-bottom surface combinations as mentioned before.

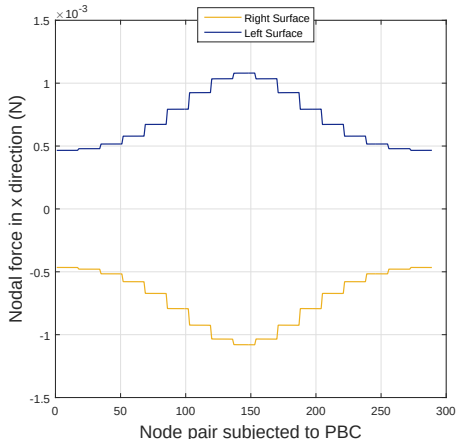

(a) Nodal force distribution in x direction on right and left surfaces

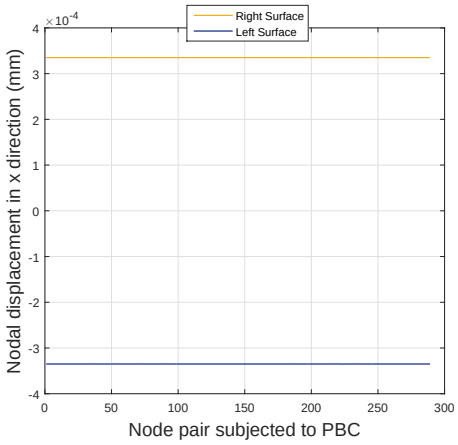

(b) Nodal displacement distribution in x direction on right and left surfaces

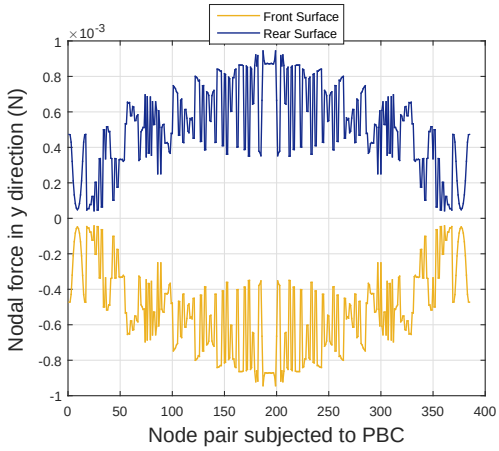

(c) Nodal force distribution in y direction on front and rear surfaces

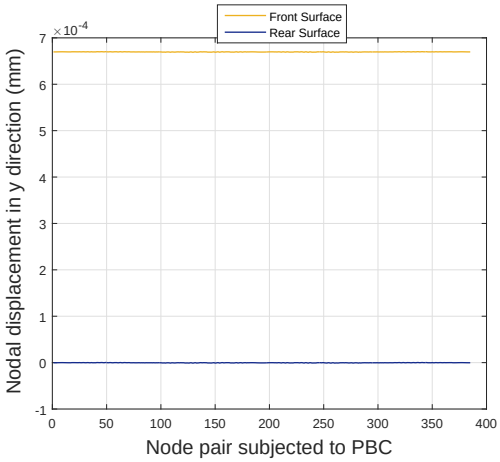

(d) Nodal displacement distribution in y direction on front and rear surfaces

Figure 5.19: Nodal force and displacement distributions for γ_{xy}

The plots in figures 5.18 and 5.19 are derived from figures 5.12 and 5.13 respectively. On the front and rear surfaces in figures 5.12 and 5.13 a different force distribution is observed compared to force distributions on right-left and top-bottom surface combinations in figure 5.11. This difference in force distribution is reflected in plots shown in figures 5.18 and 5.19 compared to force distribution plots in figure 5.17.

Solving for stiffness tensor components

Now that the correctness of nodal forces and displacements for various deformation states is verified, the use of nodal forces and displacements data can be made correctly. This allows to plug in the values of W_{11}, W_{22}, W_{33}, W_{12}, W_{13}, W_{23}, W_{44}, W_{55} and W_{66} through right hand side of equation (5.10) in equation (5.12). To obtain the right hand side value of equation (5.10), Python scripts are written (appendix B.2) to extract the nodal forces through field

output *NFORC1, NFORC2* and *NFORC3* and nodal displacements U_1, U_2 and U_3 in Abaqus after simulating nine deformations of UC according to nine combination of strains shown by rows of table 5.2 (all possible strains in table 5.2 have been presented from figure 5.5 to figure 5.13). After simulating a deformation according to a particular row of table 5.2, the force and displacement data in the three directions (x, y and z) on all six external surfaces of the UC are extracted. Forces in a particular direction at a node from every element sharing that node are summed together. At every node, the product of force and displacement in a particular direction is obtained. This product is obtained for all three directions. Since at a node, the elastic force is in opposite direction to deformation, a negative sign is combined with each of the three products of force and displacement corresponding to the three directions at a node. On a surface, the sum total of this product is obtained for all nodes in each direction. The addition of summed up products in every direction is obtained for all nodes on the surface. This procedure is followed for all surfaces. Finally, the addition of sums obtained from all surfaces along with value of volume of UC are used to calculate right hand side value of equation (5.10) through a Matlab script.

Table 5.3: Calculated values of right hand side of equation (5.10)

Parameter	Value
W_{11} (MPa)	14.4932
W_{22} (MPa)	1.6853
W_{33} (MPa)	1.6853
W_{12} (MPa)	17.4287
W_{13} (MPa)	17.4287
W_{23} (MPa)	4.8602
W_{44} (MPa)	0.3864
W_{55} (MPa)	0.4452
W_{66} (MPa)	0.4452

Table 5.3 lists the nine values of W_{11}, W_{22}, W_{33}, W_{12}, W_{13}, W_{23}, W_{44}, W_{55} and W_{66} obtained through the procedure mentioned. Substituting the values listed in table 5.3 in equation (5.12) gives the values of stiffness tensor components as shown in table 5.4.

Table 5.4: Calculated values of stiffness tensor components

Stiffness tensor component	Value
C_{11} (MPa)	144932
C_{12} (MPa)	6251
C_{13} (MPa)	6251
C_{22} (MPa)	16853
C_{23} (MPa)	7448
C_{33} (MPa)	16853
C_{44} (MPa)	3864
C_{55} (MPa)	4452
C_{66} (MPa)	4452

The compliance tensor has been obtained by finding the inverse of the obtained stiffness matrix. Upon back calculating the constants of compliance tensor, the engineering constants obtained upon homogenisation of the UC are listed in table 5.5.

Table 5.5: Homogenised engineering constants for graphite epoxy material

Homogenised engineering constant	Value
E_x (GPa)	141.715
E_y (GPa)	13.476
E_z (GPa)	13.476
ν_{xy}	0.257
ν_{xz}	0.257
ν_{yz}	0.432
G_{yz} (GPa)	3.8635
G_{xz} (GPa)	4.452
G_{xy} (GPa)	4.452

Hence, the homogeneous equivalent properties of macroscopic lamina made of graphite-epoxy material (fibre and matrix properties are mentioned in table 5.1) are obtained and the derived constants are listed in table 5.5. In this way for a given combination of fibre and matrix combination, homogenised engineering constants can be obtained for building homogeneous layer models. The correlation of stresses can then be carried out between homogeneous and heterogeneous model results at zero-ninety or ninety-ninety layers' interface. Subsequently, the averaging distance can be calculated through the correlation at either of the interfaces.

5.3 Applicability of averaging distance on different layups for a given material

In this chapter, the homogenisation approach would enable building a homogeneous layer $[0/90]_s$ cross-ply laminate. Hence, the heterogeneous and homogeneous models (with same stiffness) can be used to carry out correlation of stresses and eventually arrive at the averaging distance (as shown in chapter 6). *Brewer et al* (1988) [12] have reported one averaging distance for composites with different layups made of the same material. Hence the averaging distance is reported as a statistical average for different composite layups analysed for a given material. The reporting of one averaging distance for different layups forms the basis for the use of averaging distance on different layups made of the same material. This encourages the use of averaging distance obtained at corresponding interfaces of different layups as long as the material does not change. From this perspective, the verification of applicability of averaging distance is carried out by determining the averaging distance through correlation between homogeneous and heterogeneous $[0/90]_s$ cross-ply laminates and applying the determined averaging distance at an interface of another laminate susceptible to exhibiting delamination initiation. *Wang et al* (1985) [9] have reported the susceptibility of $[\pm 25/90]_s$ laminates to exhibit delamination initiation at the ninety-ninety layers' interface (symmetric mid-plane). Moreover, Brewer et al (1988) [12] have reported experimentally determined av-

eraging distance for use in QDC for $[\pm 25/90]_s$ laminates. Hence, it becomes interesting to first determine the averaging distance through correlation of stresses between homogeneous and heterogeneous $[0/90]_s$ cross-ply models and then verify the applicability of averaging distance through proposed correlation on $[\pm 25/90]_s$ laminate through QDC.

Chapter 6 deals with proposal of an approach for correlation of stresses between homogeneous and heterogeneous layer models and use of the approach for determining averaging distance to predict delamination initiation in $[\pm 25/90]_s$ laminate to verify the proposed approach.

Chapter 6

Implementation and Verification of Averaging Distance

6.1 Background

If the use of Quadratic delamination Criterion (QDC) is to be made to predict delamination initiation at an interface of two layers, then the averaging distance is required for that interface to be able to determine average stress values for use in the QDC. As reported in *Brewer et al* (1988) [12], the determined averaging distance could be used for different layups made of the same material. Hence, if the averaging distance is determined at an interface between two layers in a $[0/90]_s$ cross-ply laminate, then the same averaging distance can be used at a similar interface of another layup for averaging the stresses as long as the material does not change.

Use of this basis is made to determine averaging distance for application on an interface of a laminate which is susceptible to exhibiting delamination initiation. It has been reported that the ninety-ninety layers' interface of a $[\pm 25/90]_s$ laminate exhibits delamination initiation [9], [10]. This interface of $[\pm 25/90]_s$ laminate provides a good basis to predict delamination initiation using QDC. For the use of QDC at this interface, the average interlaminar stress values need to be determined for which the averaging distance is needed. As the averaging distance can be used invariably for a combination of layups (provided the material is unchanged), a $[0/90]_s$ cross-ply laminate can be used to determine the averaging distance at its ninety-ninety layers' interface. The determined averaging distance can then be used at the ninety-ninety layers' interface of $[\pm 25/90]_s$ laminate for predicting delamination initiation through QDC.

6.2 Approach for correlation

In the course of this chapter an approach has been proposed which uses a correlation between interlaminar stresses obtained from homogeneous and heterogeneous layer models to deter-

mine the averaging distance from the free edge at an interface. This involves homogenisation through PBC for a given fibre-matrix material to derive effective homogenised properties for homogeneous layer so that a correlation could be carried out between homogeneous and heterogeneous models of equivalent stiffness.

In this section, the method by which a correlation is arrived at is described. For this purpose, first a schematic overview of a high gradient free edge region stress is presented to show its averaging in transverse direction in figure 6.1.

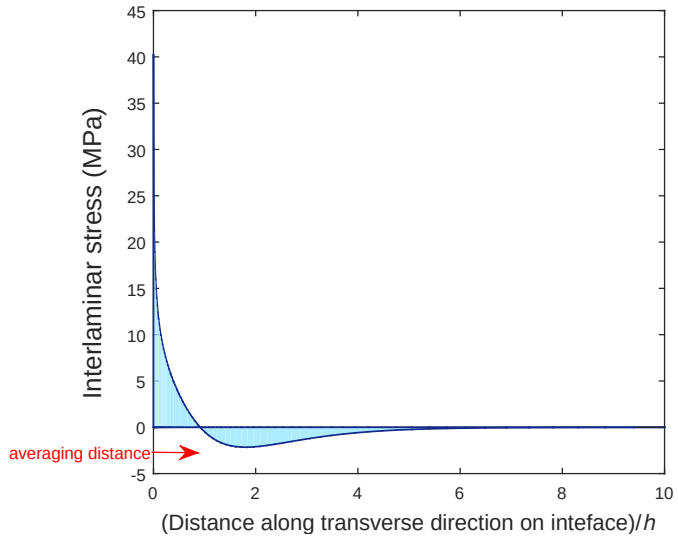

Figure 6.1: Schematic representation of area under curve of interlaminar stress at an interface in transverse direction

The average of a stress tensor component $< \sigma_{ij} >$ is given by the approach mentioned in section 3.5. The normalisation parameter y in equation 3.1 is the distance from free edge which normalises the area under the stress plot (shown in blue in figure 6.1) to arrive at the average. Thus, the average of the stress component up to an averaging distance could be calculated through equation 3.1. The averaged plots in a homogeneous layer model have been shown in 3.17. Every point on the plot in figure 3.17 represents stresses averaged until the corresponding abscissa (distance from free edge). The question now is: what should be the averaging distance at which the average value must be calculated for use in QDC?

As seen earlier chapters, interlaminar stresses might experience a rise in gradient near the free edge. However, existence of very high gradients, sometimes to an effect of a singularity is a mathematical artefact and not a reality. The core essence of the effort towards determining the averaging distance is to find the average stress value which could be used for prediction of delamination initiation through QDC. Thus, the potential of stress components to initiate delamination is considered the primary guide for determining the averaging distance.

As seen earlier, it is the interlaminar stresses in homogeneous layer models which exhibit high gradients near free edges. However, that is not found to be the case with stresses in heterogeneous layer models. This means that the heterogeneous layer models (with equivalent stiffness to homogeneous layer models) could be used to determine definite stress values in the free edge vicinity. If the interlaminar stresses in heterogeneous models in free edge vicinity

could be assessed in terms of their effect on initiating delamination, then a definite value of stress is achievable which could be used with QDC. The correlation of that definite average stress value in heterogeneous layer model with corresponding average stress distribution in homogeneous layer model would enable mapping of the average stress value in homogeneous model's average stress distribution and would eventually lead to determination of averaging distance corresponding to the average stress value in homogeneous layer model.

The choice of interlaminar stress component for arriving at the correlation depends on the effect of a stress component towards its contribution in delamination initiation. If the QDC (equation (2.48)) is seen then for a given distance from free edge in transverse direction, $< \sigma_z >$ and $< \tau_{yz} >$ could be compared in the criterion in terms of their contributions. As an example, the interlaminar normal strength is reported to be 50 MPa whereas, the interlaminar shear strength is 112 MPa for T300/934 material [12]. At a given averaging distance from the free edge, the square of ratio of $< \sigma_{ij} >$ to corresponding strength can be calculated to assess the stress component which plays a dominant part in initiating delamination. Thus, for instance, even if the transverse direction average values of σ_z and τ_{yz} are comparably equal, the square of ratio of average σ_z to interlaminar normal strength $((\frac{<\sigma_z>}{50})^2)$ would be higher than the square of ratio of average τ_{yz} to interlaminar shear strength $((\frac{<\tau_{yz}>}{112})^2)$ by a factor of more than five. Such a comparison of contribution of a stress component towards index of delamination initiation criterion paves the roadmap for selection of a stress component or a combination of stress components for obtaining the averaging distance through correlation.

For example, the distribution of an interlaminar stress in heterogeneous model is shown in figure 6.2 . It is observed that the peak stress of around 10 MPa is found in vicinity of free edge.

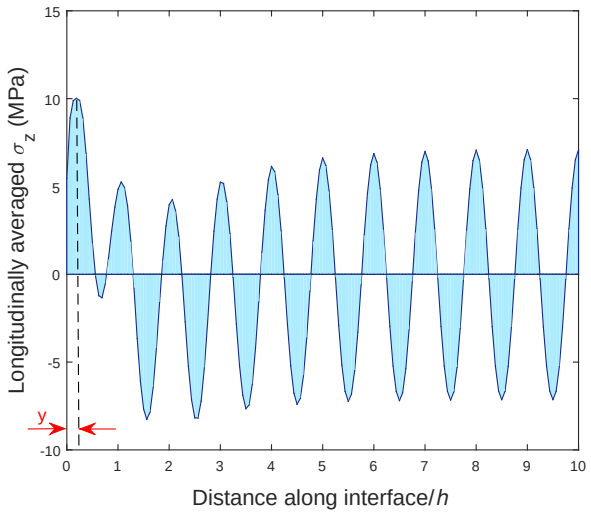

Figure 6.2: Longitudinally averaged interlaminar stress in heterogeneous model at an interface

The peak stress is obtained at a distance let's say y from the free edge. The average of stress values in transverse direction until a distance y from free edge to the point where peak stress is found in heterogeneous model would represent a collective average of stress in free edge vicinity where the maximum effect of free edge is felt. When this *transversely averaged stress value* in heterogeneous layer model is correlated with *transversely averaged*

corresponding stress value in homogeneous layer model, then the averaging distance from free edge in homogeneous layer model could be obtained.

Thus, the approach for correlation for arriving at the averaging distance involves the following two steps:

1. Determination of average stress in heterogeneous layer model (in transverse direction) until the point where peak stress is found and

2. Matching the average stress value from heterogeneous layer model with average stress distribution plot (in transverse direction) of homogeneous layer model.

It is to be highlighted that for correlation of average stress values, both the models, heterogeneous and homogeneous, must have equivalent stiffness. For this purpose, calculation of effective homogenized stiffness from a heterogeneous model of given volume fraction is essential. This is detailed in the next section.

Delamination initiation in $[\pm 25/90]_s$ laminate is reported at the ninety-ninety layers' interface [10], [9]. Therefore in this chapter, the interlaminar stresses at the ninety-ninety layers' interface of $[\pm 25/90]_s$ laminate are investigated. For analysing delamination initiation through QDC, average stress plots are needed at the ninety-ninety layers' interface of the $[\pm 25/90]_s$ laminate. For this purpose, converged average stress plots for homogeneous layer $[\pm 25/90]_s$ laminate is obtained which would enable plugging of average stress values into the QDC.

Further, for getting the average stress values for use in QDC, the average stress values at a characteristic averaging distance from free edge is needed. Drawing inference from *Brewer et al* [12] regarding proposal of one averaging distance for multiple laminates made of the same material, the averaging distance is determined at the ninety-ninety degree layers' interface of $[0/90]_s$ cross-ply laminate through the approach proposed earlier in this section. The correlation is carried out at the ninety-ninety degree layers' interface of $[0/90]_s$ cross-ply laminate because of the convenience in carrying out the correlation of average stresses (in transverse direction) between the periodically repeating heterogeneous model and homogeneous layer model (modelled upon homogenisation of properties through PBC) of $[0/90]_s$ cross-ply laminate. Simulating a periodically repeating heterogeneous $[\pm 25/90]_s$ laminate was not as viable as simulating the periodically repeating heterogeneous $[0/90]_s$ cross-ply laminate considering the orientation of fibres in $+25$, -25 and 90 degrees in $[\pm 25/90]_s$ laminate whose periodic repetition longitudinally is a matter of concern. Comparatively, the periodic repetition of transverse section strips of $[0/90]_s$ cross-ply laminate allows a convenient simulation of longitudinal extensional strain through PBC. Hence, considering the limited time frame for the current thesis, the averaging distance is determined through $[0/90]_s$ cross-ply laminate of T300/934 material while the application is made on the $[\pm 25/90]_s$ laminate of T300/934 material on the basis of reported single averaging distance for different laminates made of same material [12].

Experimentally determined averaging distance has been reported by *Brewer et al* (1988) [12] for $[\pm 25/90]_s$ laminate using T300/934 graphite-epoxy material. Hence, the averaging distance in this chapter has been obtained for T300/934 material to compare determined value against reported value. For this purpose, a periodic homogenisation of heterogeneous

UC has been carried out in a manner described in chapter 5. A homogeneous $[0/90]_s$ cross-ply laminate is built and correlation of average stresses between homogeneous and heterogeneous $[0/90]_s$ laminate models of T300/934 material is carried out to obtain the averaging distance at ninety-ninety interface of $[0/90]_s$ laminate.

Finally, the obtained averaging distance is used with QDC at strain values reported to initiate delamination in $[\pm 25/90]_s$ laminate experimentally. It has been verified whether the determined averaging distance predicts delamination initiation through QDC at experimentally reported values of strain leading to delamination initiation with variation in strain across the strain range.

As a general remark, it is to be highlighted that for a given material, the averaging distance at an interface is invariant of strain as long as a linear analysis is conducted. This is because with variation in strain, the stresses in homogeneous and heterogeneous models (with equal stiffness) would be scaled in a manner that their relative distribution with respect to each other would remain unchanged and hence, the averaging distance obtained after correlation would also remain unchanged as well.

6.3 Free Edge stresses in homogeneous $[\pm 25/90]_s$ laminate

For the purpose of carrying out interlaminar free edge stress analysis in a homogeneous layer $[\pm 25/90]_s$ laminate, FEA of the laminate is conducted with a view to determine results at the ninety-ninety layers' interface. A linear analysis has been conducted in Abaqus with a longitudinal extensional loading corresponding to a strain of 0.61 %. The strain of 0.61 % has been chosen because the reported range of experimentally determined strain at which free edge delamination initiation is reported is 0.58 % to 0.61 % [9]. As a conservative approach, the upper limit of the strain range has been chosen as this strain value is most likely to predict delamination through, the to be determined averaging distance.

A specimen similar to the reported specimen for experimental testing has been modelled. With this in consideration, the length of the laminate modelled is 225 mm, while the width is 25 mm. The material used is T300/934 for which the reported nominal ply thickness is 0.132 mm [9].

The overall objective is to capture high gradient free edge interlaminar stresses at a location far away from the boundary on which extensional loading is applied as mentioned in chapter 3. For this purpose, the laminate is built using 3D hexahedral C3D8R elements. It is notable that only one symmetry plane exists in the laminate. Since, the material definition in +25 and −25 degree layers does not allow symmetry in transverse direction, entire width of the upper part of $[\pm 25/90]_s$ is modelled, unlike the case of $[0/90]_s$ laminate in which two symmetry planes ($y-$symmetry and $z-$symmetry) exist. Composite layup section is used to model the three layers of the $z-$symmetric part of the $[\pm 25/90]_s$ laminate. Figure 6.3 represents an illustration of the symmetric part.

The large size of the model has compelled the use of comparatively large number of elements for this analysis. Keeping this in perspective, the region far away from location of applied extensional displacement has been discretised finely. The region of interest for this analysis is shown in figure 6.4. Further, since the interface between ninety-ninety degree layers is expected to be analysed for studying free edge delamination, the mesh has been biased

accordingly to capture high stress gradients in the free edge region of ninety-ninety degree layers' interface.

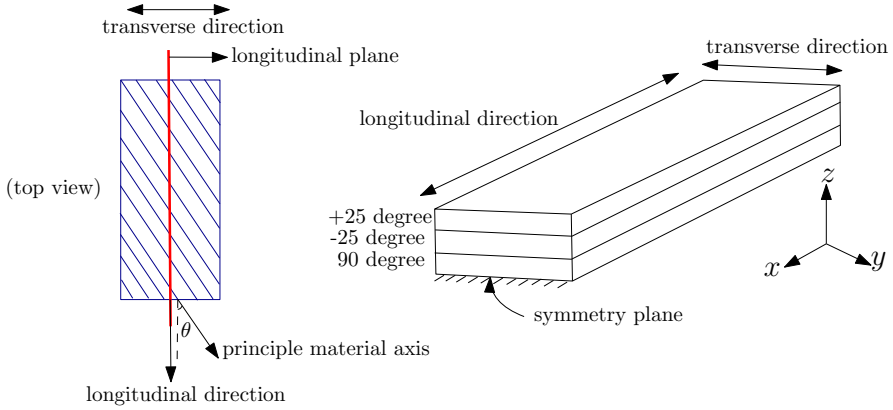

Figure 6.3: No symmetry across longitudinal plane (top view)

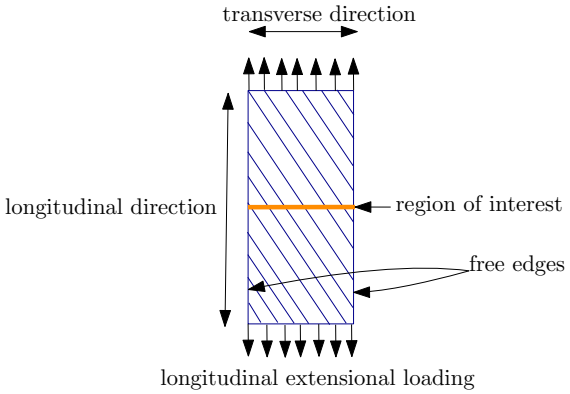

Figure 6.4: Region of interest for free edge stress analysis in $[\pm 25/90]_s$ laminate (top view)

The material properties listed in table 6.1 are the properties for T300/934 material [9]. These properties have been chosen for modelling the homogeneous layers of the $[\pm 25/90]_s$ laminate's model.

Table 6.1: Material constants for unidirectional ply of T300/934 material from literature [9]

Properties	Values
E_x (GPa)	144.8
E_y (GPa)	11.7
E_z (GPa)	11.7
ν_{xy}	0.3
ν_{xz}	0.3
ν_{yz}	0.54
G_{yz} (GPa)	3.5
G_{xz} (GPa)	6.5
G_{xy} (GPa)	6.5

The mesh in longitudinal direction is biased towards the transverse central region of interest as shown in figure 6.4. further, the mesh in transverse direction is biased towards the free edges in y direction. Figure 6.5 represents mesh on the model.

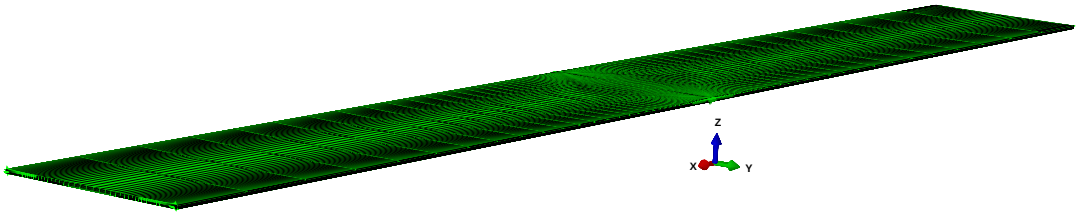

Figure 6.5: Mesh generation with biasing towards transverse mid-section

The mesh in the free edge region at interface between ninety-ninety layers in the region of interest has been shown in a detailed manner in figure 6.6.

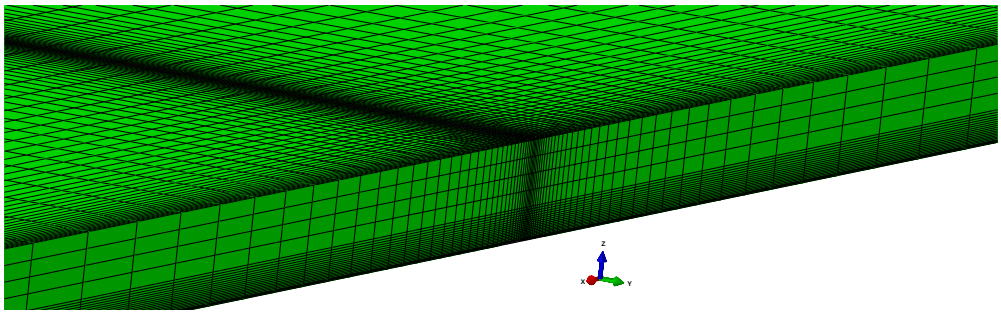

Figure 6.6: Refined view of discretisation at transverse mid-section

The idea through this model is to arrive at a converged average stress value along the transverse (y) direction. As shown later in the chapter, the comparison of stresses between two models, one with smallest element size in transverse direction of 0.01 mm and the other with smallest element size in transverse direction of 0.02 mm prove sufficient for arriving at converged average stress results. The model corresponding to smallest element size of 0.01 mm results in a mesh with 326898 elements while the mesh with the smallest element size of 0.02 mm results in a mesh with a total of 273812 elements (C3D8R).

Plots of interlaminar stresses σ_z, τ_{yz} and τ_{xz} are obtained in the transverse direction at the interface between ninety-ninety degree layers. The results presented for first analysis have been obtained for 273812 elements (C3D8R) with smallest element size of 0.02 mm along transverse (y) direction. As mentioned earlier, these results have been obtained at a strain loading of 0.61 %. Figure 6.7 shows a combined plot of all three interlaminar stresses obtained. Since the width of the laminate modelled in this case is not a multiple of layer thickness, the distance along interface in transverse direction is not represented in terms of ply thickness. Rather the distance is directly represented in mm.

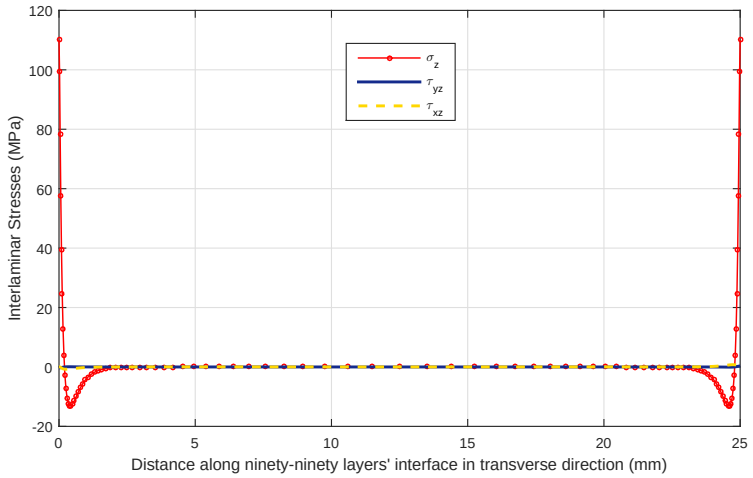

Figure 6.7: Interlaminar stresses at interface between ninety-ninety layers in transverse direction for 273812 elements

It has been observed that the σ_z shows a high gradient in vicinity of the free edge while other two stress components, τ_{yz} and τ_{xz} are comparatively negligible to σ_z. The observance of high gradient in σ_z prompts to further investigation of its behaviour through discretisation with finer elements. The discretisation is refined to a finer mesh with smallest element size of 0.01 mm along transverse direction. Thus, analysis with comparatively finer mesh comprising of 326898 elements (C3D8R) is conducted and the results obtained are presented in figure 6.8.

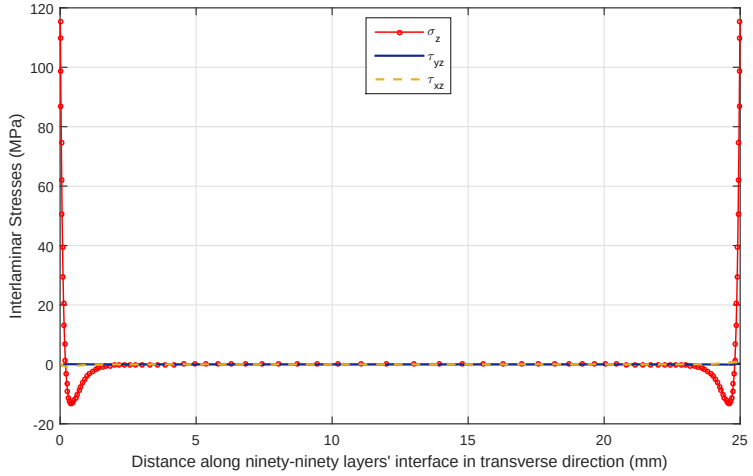

Figure 6.8: Interlaminar stresses at interface between ninety-ninety layers in transverse direction for 326898 elements

It has been found that for the mesh with 273812 elements, the peak σ_z stress at free edge in the region of interest is 110.2 MPa, while that in the case of 326898 elements, the peak σ_z stress changes to 115.3 MPa. The difference between the peak stresses is less than 5 %. The high gradient stress in the free edge vicinity makes a case to investigate free edge

stress delamination initiation at the interface between ninety-ninety degree plies. Further, it is notable from figures 6.7 and 6.8 that σ_z would play a dominant role among the three interlaminar stresses in delamination initiation prediction through QDC.

Unlike in the case of cross-ply laminates discussed in previous chapters where only the quarter symmetric part was modelled, this $[\pm 25/90]_s$ model is built with half symmetric part with entire width of the laminate (25 mm wide) in transverse (y) direction. Hence free edge effect on both ends in transverse direction is observed.

As the QDC incorporates averaged values of interlaminar stresses, the average stress plots of the three interlaminar stresses are presented in figure 6.9.

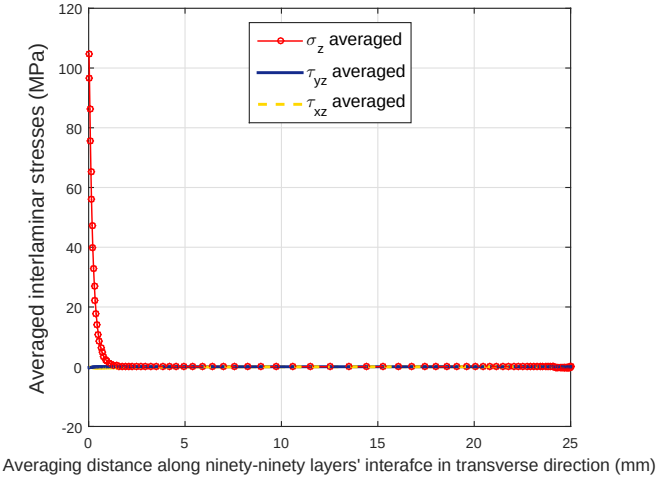

(a) Transversely averaged interlaminar stresses for 273812 elements

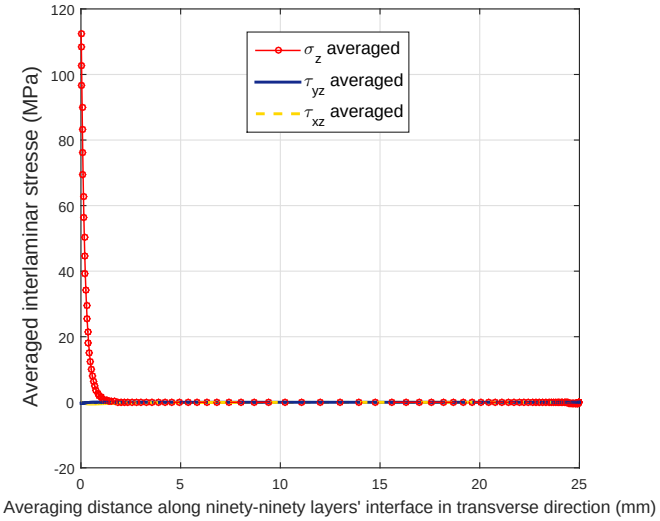

(b) Transversely averaged interlaminar stresses for 326898 elements

Figure 6.9: Transversely averaged interlaminar stresses along the ninety-ninety layer interface

Since, the average stress value is to be used in QDC, it is imperative that the two plots converge with each other. Figure 6.10 shows a comparison of the two averaged stress plots.

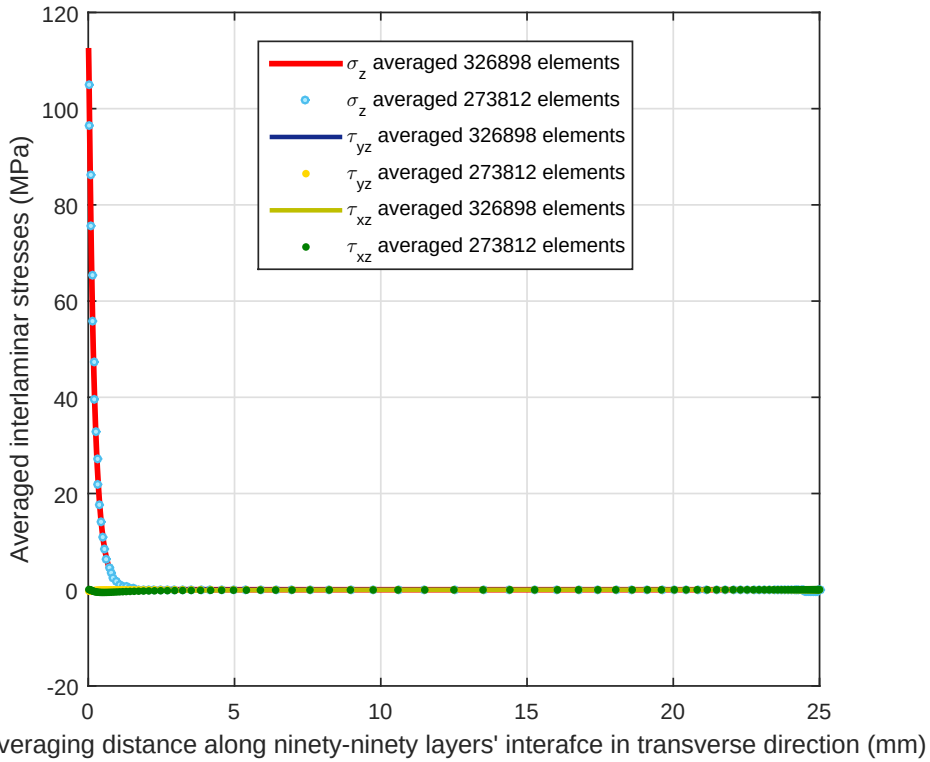

Figure 6.10: Comparison of averaged interlaminar stresses for 326898 and 273812 elements at interface between ninety-ninety layers

It is observed that the averaged stresses for the two meshes converge with each other (almost right from the free edge). This paves way for a use of a definitive average stress value corresponding to an averaging distance from free edge. The free edge is the zero abscissa in figure 6.10).

At this stage, the average stress values across the entire width of the laminate is available through plots in figure 6.10. The only parameter which is required to predict the initiation of delamination through QDC is the averaging distance from the free edge. The approach mentioned earlier in this chapter will now be used to determine the averaging distance for the interface between ninety-ninety degree layers of $[\pm 25/90]_s$ laminate. Since the averaging distance is required at the ninety-ninety layers' interface of $[\pm 25/90]_s$ laminate, the determination of averaging distance has been done at the ninety-ninety degree layers' interface of $[0/90]_s$ cross-ply laminate.

6.4 Determination of averaging distance at interface between ninety-ninety layers of $[0/90]_s$ cross-ply laminate

Since the application of averaging distance is made on $[\pm 25/90]_s$ laminate made of T300/934 material, the averaging distance also needs to be found out on the $[0/90]_s$ cross-ply laminate made of T300/934 material. Interlaminar stress analysis has been conducted at the interface between ninety-ninety degree layers of the $[0/90]_s$ cross-ply laminate. The analysis has

been conducted on both heterogeneous and homogeneous layer models made of T300/934 material. The procedure described for determination of the averaging distance in section 6.2 has been followed with stresses obtained at the ninety-ninety degree layers' interface of $[0/90]_s$ laminate. The surface plots are used to eventually determine the average stresses in transverse direction. Then, periodic homogenisation of the UC modelled with T300/934 material has been carried out to extract homogenised properties. The deformation states and relevant plots obtained for the homogenisation procedure in this chapter are reported in appendix A. The homogeneous engineering constants obtained upon homogenisation is used to build homogeneous layer $[0/90]_s$ cross-ply laminate and stress analysis is conducted at the interface between ninety-ninety degree layers. Averaged values of stresses are obtained at the interface in transverse direction in both homogeneous and heterogeneous models. Finally, the correlation of necessary average stress values has been carried out between plots obtained for homogeneous and heterogeneous models to determine averaging distance for T300/934 material. Eventually, this averaging distance is used on the plot shown in figure 6.10 to find average stress values at the characteristic averaging distance and subsequently predict delamination initiation through QDC. It is to be mentioned that because the averaging distance is independent of strain, analyses in the cross-ply models have been carried out at a strain of 0.01 (unlike at 0.0061 strain for stress analysis in $[\pm 25/90]_s$ laminate).

Interlaminar stress analysis in heterogeneous model

Like in section 4.3, the heterogeneous quarter symmetric part with width $10h$ ($h = 0.134mm$) in transverse direction of $[0/90]_s$ laminate made of T300/934 material is loaded under a tensile strain of 0.01 and a linear analysis is conducted in Abaqus. The material constants for fibre and matrix for T300/934 combination is shown in table 6.2.

Table 6.2: Material properties for T300/934 fibre-matrix combination [11]

Properties	T300 fibre	934 matrix
E_{xf} (GPa)	233.04	-
E_{yf} (GPa)	23.10	-
E_{zf} (GPa)	23.10	-
ν_{xyf}	0.2	-
ν_{xzf}	0.2	-
ν_{yzf}	0.4	-
G_{yzf} (GPa)	8.27	-
G_{xzf} (GPa)	8.96	-
G_{xyf} (GPa)	8.96	-
$E_m(GPa)$	-	4.34
ν_m	-	0.37

The tensile strain has been applied through PBC using displacement difference between front and rear boundaries corresponding to a strain of 0.01. The plots obtained at the ninety-ninety degree layers' interface are shown in figure 6.11.

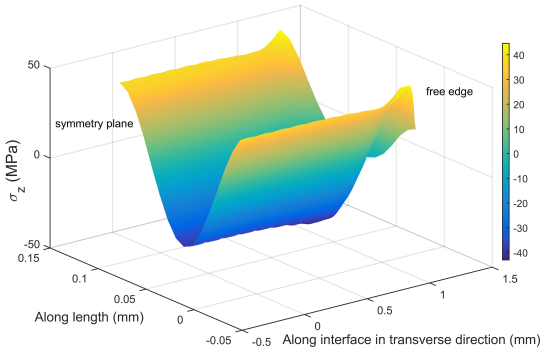

(a) σ_z at ninety-ninety layers' interface surface

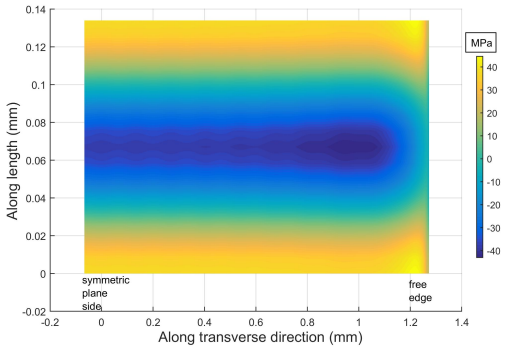

(b) Projection of σ_z on ninety-ninety layers' interface surface

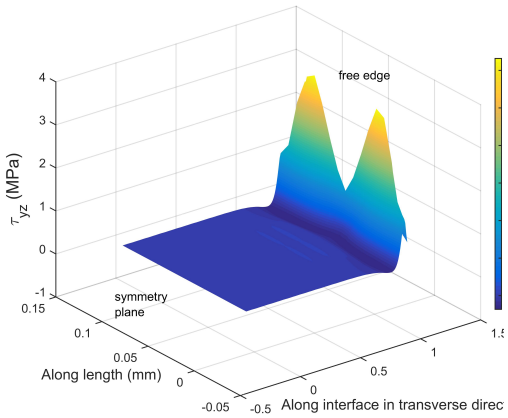

(c) τ_{yz} at ninety-ninety layers' interface surface

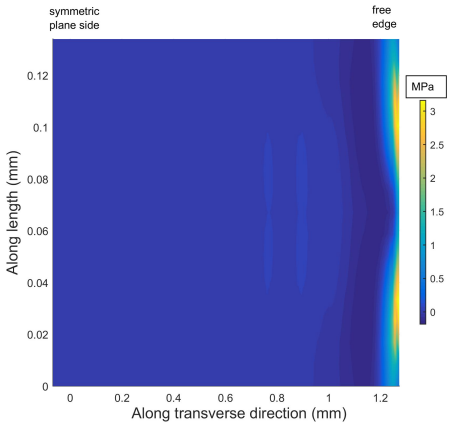

(d) Projection of τ_{yz} on ninety-ninety layers' interface surface

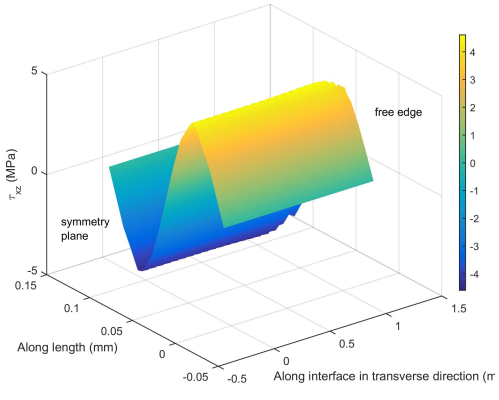

(e) τ_{xz} at ninety-ninety layers' interface surface

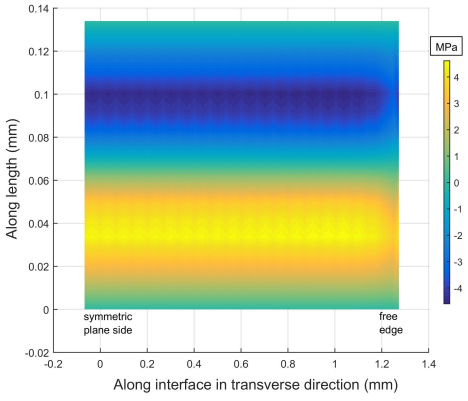

(f) Projection of τ_{xz} on ninety-ninety layers' interface surface

Figure 6.11: Interlaminar stresses at ninety-ninety interface of T300/934 $[0/90]_s$ laminate

Like plots at ninety-ninety layers' interface of heterogeneous model made of graphite-epoxy material in figure 4.24, the plots obtained for T300/934 material in figure 6.11 suggests that the distribution of σ_z is same on the front and rear surfaces of the strip with high gradient near the free edge. High gradient is also observed for τ_{yz} near the free edge but the magnitude of distribution is comparatively lower than that of σ_z. Distribution of τ_{xz} in longitudinal direction suggests that the longitudinal average of stresses would be negligible. The average of these surface stresses in longitudinal direction are obtained as mentioned in chapter 4. Upon averaging the stresses along the length in figure 6.11, the longitudinally averaged stresses are obtained which are plotted in transverse direction as shown in figure 6.12.

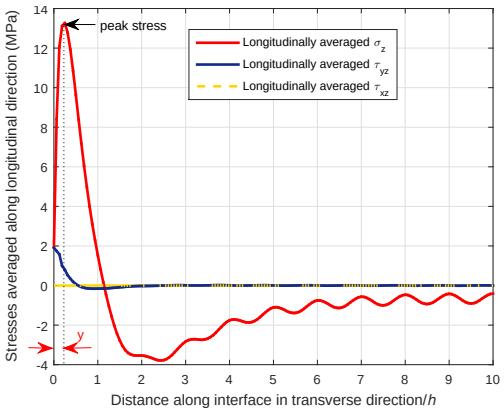

Figure 6.12: Longitudinally averaged interlaminar stresses at interface between ninety-ninety layers

It is observed that there is a tendency of the interlaminar stresses to approach to zero value at distance far away from the free edge. Hence, as expected, the free edge effect fades out as the distance from free edge increases. Now that the stresses are averaged in longitudinal direction, the longitudinally averaged stresses can be averaged in transverse direction starting from the free edge. The averaged stresses in transverse direction are shown in figure 6.13.

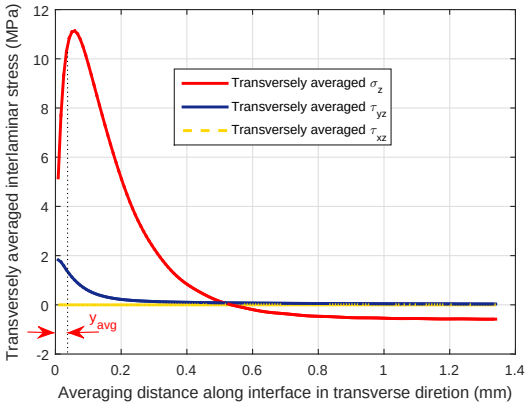

Figure 6.13: Transversely averaged interlaminar stresses at interface between ninety-ninety layers

While average plots for τ_{yz} and τ_{xz} settle to zero away from free edge in figure 6.13, plot for

average σ_z is expected to approach zero in figure 6.13 with increase in distance in transverse direction. This is expected because of tendency of longitudinally averaged σ_z in figure 6.12 to reach zero value as distance from free edge increases.

From figure 6.13, it is clear that in the free edge vicinity average σ_z attains the highest value among the three stresses. τ_{xz} is negligible and could hence be neglected for now. For T300/934 material, as reported in section 6.2, the interlaminar normal strength is 50 MPa while the interlaminar shear strength is 112 MPa. Hence, from perspective of QDC, the square of ratio of average σ_z (in transverse direction) to corresponding strength i.e. $(\frac{<\sigma_z>}{50})^2$ is considerably higher than the square of ratio of average τ_{yz} (in transverse direction) to corresponding strength i.e. $(\frac{<\tau_{yz}>}{112})^2$ near the free edge. Thus, σ_z plays a dominant role in delamination initiation through QDC.

Now that the dominant stress component is identified in σ_z, the correlation of transversely averaged σ_z can be done between the homogeneous and heterogeneous models for T300/934 material at the ninety-ninety layers' interface to determine the averaging distance. We can therefore refer back to figure 6.12. It is worthwhile to note the distance from free edge at which the peak stress value is obtained for σ_z in figure 6.12. It has been found in figure 6.12 that the peak value of 13.26 MPa occurs at a distance $y = 0.25h$ or at 0.0335 mm where, $h = 0.134$ mm for heterogeneous $[0/90]_s$ model from free edge. Therefore, to determine the average of σ_z until 0.0335 mm from free edge in transverse direction, the transversely averaged σ_z plot in figure 6.13 is referred to.

At $y_{avg} = 0.0335$ mm from free edge, the average σ_z value in transverse direction is found to be 10.3 MPa on plot shown in figure 6.13. This averaged value of 10.3 MPa (obtained after two dimensional averaging, first in longitudinal then in transverse direction) is to be correlated with transversely averaged value of σ_z of homogeneous layer $[0/90]_s$ laminate made of T300/934 material at ninety-ninety degree layers' interface.

For this purpose homogenisation of the heterogeneous UC is carried out this time around using T300/934 material through the procedure using PBC described in chapter 5. The FEA results of homogenisation procedure is reported in appendix A. The homogenised material properties obtained thereafter are listed in table 6.3 as follows:

Table 6.3: Derived material constants for unidirectional ply of T300/934 material upon homogenisation

Properties	Values
E_x (GPa)	141.61
E_y (GPa)	13.21
E_z (GPa)	13.21
ν_{xy}	0.2613
ν_{xz}	0.2613
ν_{yz}	0.4437
G_{yz} (GPa)	3.6757
G_{xz} (GPa)	4.2684
G_{xy} (GPa)	4.2684

Interlaminar stress analysis in homogeneous model

Now that the homogenised properties are obtained through homogenisation on T300/934 material UC, FEA of homogeneous layer $[0/90]_s$ laminate is conducted for the same strain as that in heterogeneous $[0/90]_s$ model case i.e. at 0.01 strain in Abaqus. Hence, a symmetric quarter slice model of $[0/90]_s$ has been built through material properties listed in table 6.3. C3D8 elements have been used for discretisation and interlaminar stress analysis has been done at interface between ninety-ninety layers. Thus, a linear analysis with a longitudinally extensional strain of 0.01 is conducted.

Interlaminar stresses at the ninety-ninety layers' interface of the homogeneous $[0/90]_s$ cross-ply laminate built from homogenised T300/934 material properties is shown in figure 6.14. For the first analysis, 29412 elements have been used from a perspective of capturing high gradient free edge stresses at ninety-ninety layers' interface. The smallest element size in this mesh while biasing the mesh in transverse direction is 1 micron. The mesh is further refined along the interface in transverse direction to study the free edge stresses with smallest element size of 0.5 microns in transverse direction. The finer mesh resulted in a total of 36292 elements. The results obtained are shown in figure 6.14b. It has been observed from the analysis in figure 6.14 that σ_z has emerged as the dominant free edge stress analogous to the case of heterogeneous layer model plot in figure 6.12. Thus, compared to other stress components which are comparatively negligible, σ_z averaged in transverse direction would play the most dominant role in delamination initiation prediction through QDC as visible in figure 6.13.

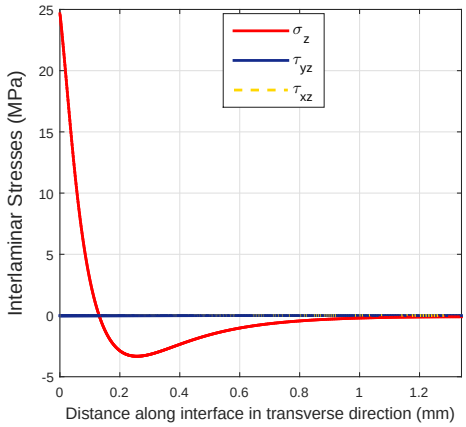

(a) Interlaminar stresses for 29412 elements

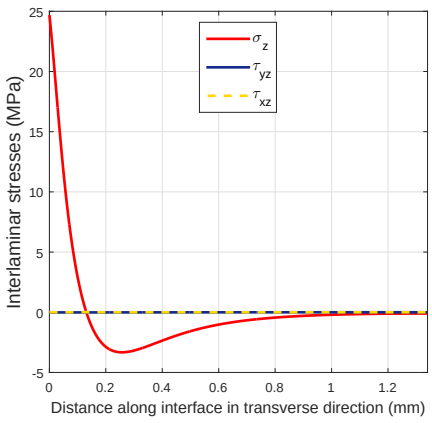

(b) Interlaminar stresses for 36292 elements

Figure 6.14: Interlaminar stresses at interface between ninety-ninety layers of $[0/90]_s$ homogeneous layer cross-ply laminate made of homogenised T300/934 material properties

The peak stress values obtained at the interface between ninety-ninety layers is 24.65 MPa and 24.68 MPa for meshes with 29412 and 36292 elements respectively. When compared to the longitudinally averaged interlaminar stress plots at the same interface of heterogeneous model in figure 6.12, it is observed that the peak stress of 24.68 MPa in homogeneous layer model with 326898 elements is much higher than 13.26 MPa in heterogeneous model, and hence, the higher gradient in homogeneous layer model is attributable to consideration of homogeneous layers while modelling the $[0/90]_s$ laminate. Therefore, an averaging distance determined at

ninety-ninety interface of $[0/90]_s$ laminate, would be used for determining average stresses at ninety-ninety interface of $[\pm 25/90]_s$ laminate.

For getting the correlation between transversely averaged stress until 0.0335 mm in heterogeneous model with that of transversely averaged stress of homogeneous layer model, the transversely averaged stress plots for homogeneous layer model are generated. Figure 6.15 presents the transversely averaged plots at ninety-ninety layers' interface.

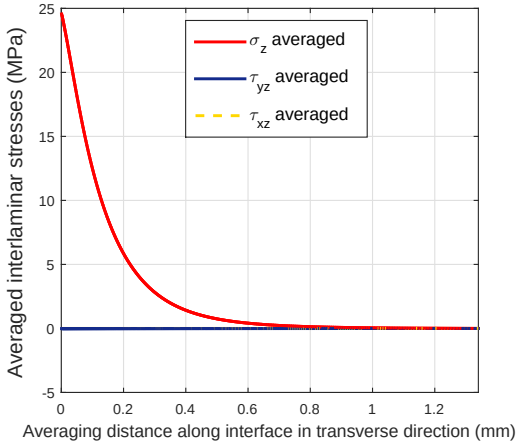

(a) Average interlaminar stresses for 29412 elements

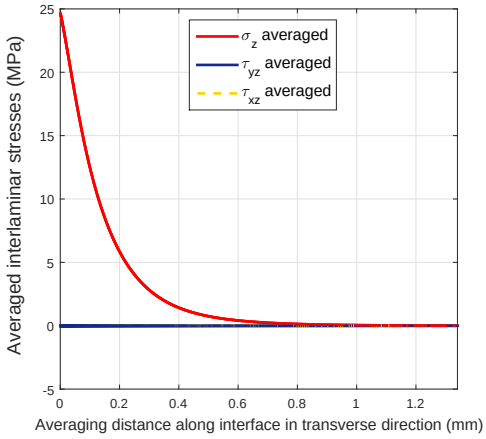

(b) Average interlaminar stresses for 36292 elements

Figure 6.15: Average interlaminar stresses at ninety-ninety interface surface of homogeneous $[0/90]_s$ laminate made of homogenised T300/934 material properties in transverse direction

A comparison of average stress components σ_z, τ_{yz} and τ_{xz} for 29412 and 36292 elements is shown in figure 6.16. The comparisons in figure 6.16 show that the three stress components converge with each other (τ_{xz} is negligible for both meshes). Hence, it can be inferred that the average stress value for the mesh with 36292 elements could be used safely for correlation with corresponding average stress value of heterogeneous model at the same interface.

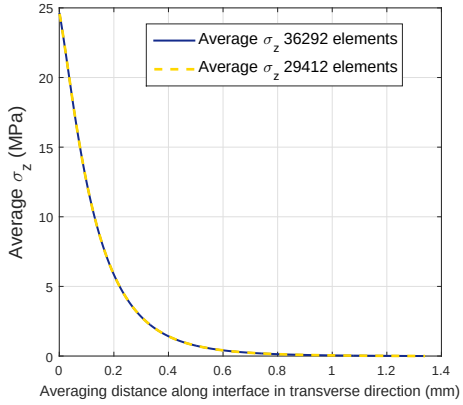

(a) Comparison of average σ_z

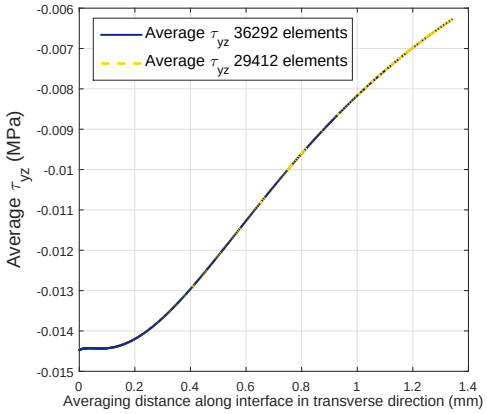

(b) Comparison of average τ_{yz}

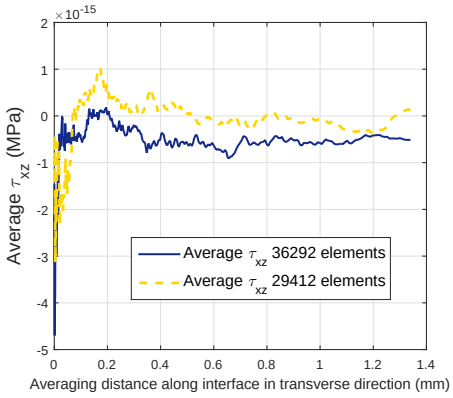

(c) Comparison of average τ_{xz}

Figure 6.16: Comparison of average interlaminar stresses for 29412 and 36292 elements

As it has been pointed out before, since σ_z has appeared to be the most dominant of the three stress components, the converged transverse direction average σ_z plot in figure 6.16a

has been used for correlating the transversely averaged stress value of 10.3 MPa obtained from the heterogeneous model at the same interface. Upon correlating the value of 10.3 MPa with the plot in figure 6.16a, the averaging distance of 0.125 mm has been found. This is illustrated in figure 6.17

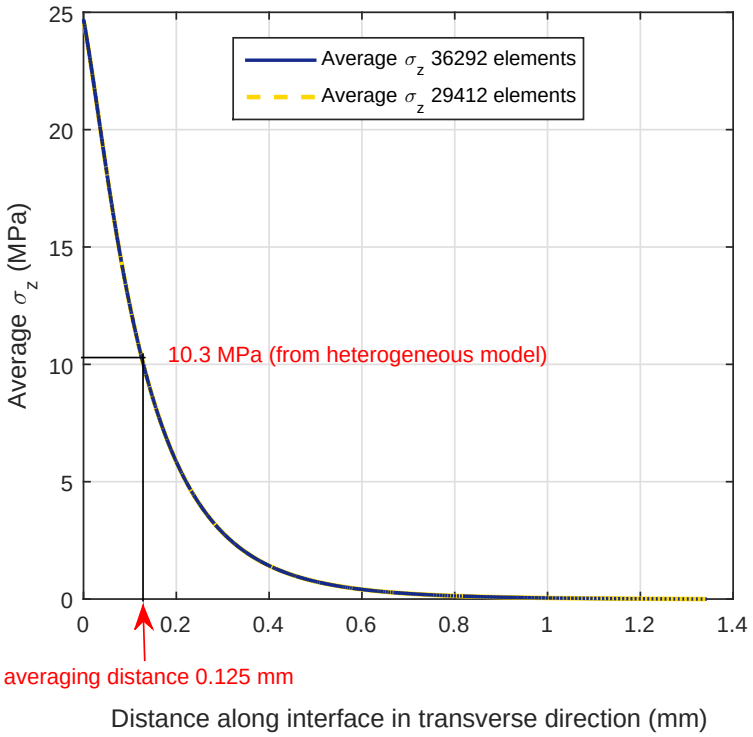

Figure 6.17: Correlation of average σ_z of 10.3 MPa from heterogeneous $[0/90]_s$ model with converged average σ_z plot of homogeneous layer $[0/90]_s$ model made of T300/934 material

The determined averaging distance of 0.125 mm at interface between ninety-ninety degree layers' interface can now be comprehensively used to determine average stress values for predicting delamination initiation at interface between ninety-ninety layer interface of homogeneous $[\pm 25/90]_s$ laminate.

6.5 Application of averaging distance for predicting delamination initiation

The converged values of average interlaminar stresses at every point along the transverse direction at interface between ninety-ninety layers of $[\pm 25/90]_s$ laminate are already obtained as shown in figure 6.10. Using the determined averaging distance of 0.125 mm, the average values of all three stress components are obtained. Since the analysis of $[\pm 25/90]_s$ laminate is conducted at a strain of 0.0061 (which is the upper limit of experimentally determined range for delamination initiation in $[\pm 25/90]_s$ laminate made of T300/934 material), use of

QDC with the determined averaging distance of 0.125 mm is expected to predict delamination initiation. Hence the value of criterion's index (left hand side) is expected to be $\geqslant 1$. The QDC is reproduced here as equation (6.1) for convenience.

$$(\frac{<\tau_{xz}>}{Z^{s1}})^2 + (\frac{<\tau_{yz}>}{Z^{s2}})^2 + (\frac{<\sigma_z^t>}{Z^t})^2 + (\frac{<\sigma_z^c>}{Z^c})^2 = 1 \tag{6.1}$$

where,
Z^t = tensile interlaminar normal strength;
Z^c = compressive interlaminar normal strength;
Z^{s1} = interlaminar shear strength for τ_{xz} stress and
Z^{s2} = interlaminar shear strength for τ_{yz} stress

The three average stress components, σ_z, τ_{yz} and τ_{xz} in figure 6.10 are normalised by their respective strength parameters. Average σ_z component is normalised by 50 MPa while average τ_{yz} and τ_{xz} components are normalised by 112 MPa respectively [12]. The square of ratio of average stress components to their respective strengths is added to obtain the index of QDC and plotted along the ninety-ninety layer interface along transverse direction. The plot is shown in figure 6.18. The plot 6.18 shows the index value at every averaging distance along the ninety-ninety layer interface in transverse direction. Since, the average stress plots in figure 6.10 are already converged, the data from finer mesh (with 326898 elements) has been used for obtaining the plot in figure 6.18.

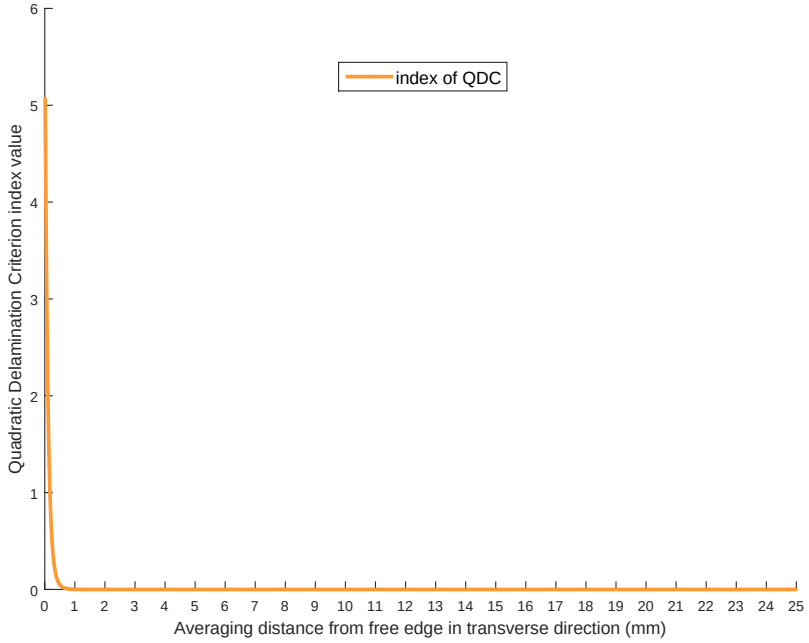

Figure 6.18: Index of QDC across the ninety-ninety layers' interface from the free edge

The sum of squares of average stress components at 0.125 mm from free edge normalised by their respective strengths represents the left-hand side value (or index) of the QDC at

the averaging distance of 0.125 mm. Since the applied strain of 0.0061 must already initiate delamination according to experimental findings [9], the value of index must be $\geqslant 1$ at a distance of 0.125 mm from free edge if the validity of determined averaging distance of 0.125 mm is to be verified.

A closer view of the plot in figure 6.18 is presented in figure 6.19 for analysis of index value at the determined averaging distance of 0.125 mm.

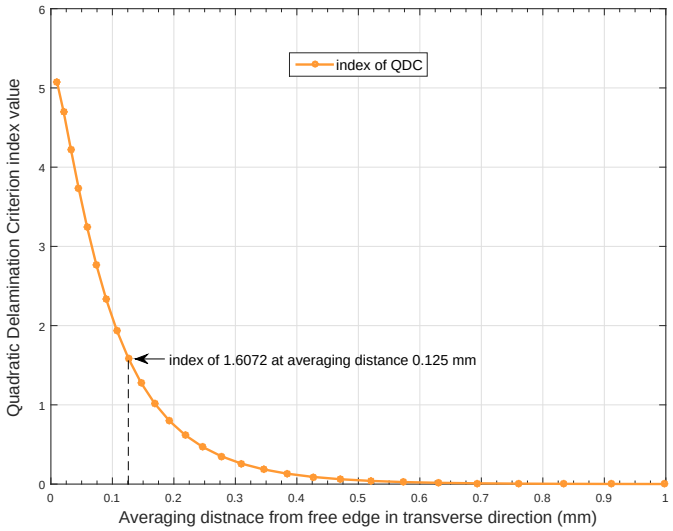

Figure 6.19: Closer view near free edge of index of QDC along the ninety-ninety layers' interface from the free edge

From the plot in figure 6.19, the value of index at 0.125 mm from free edge is found to be 1.607. A linear interpolation is used to arrive correctly at the index value of 1.607 at 0.125 mm from the plot in figure 6.19. The index of 1.607 suggests that at a strain of 0.0061, delamination initiation would occur according to QDC. This observation is in line with experimentally observed delamination initiation at the strain of 0.0061.

As the lower limit of reported experimental strain for initiating delamination is 0.0058, the index value at a strain of 0.0058 is calculated at 0.125 mm. This is done by considering only σ_z stress component out of the three components in the QDC. This is because average plots of other components, τ_{yz} and τ_{xz} are negligible (as seen in figure 6.10) and hence the square of ratio of average of these components at 0.125 mm after normalisation by their respective strengths would lead to negligible contribution in the QDC index. This leads to an effective form of the QDC as shown in equation (6.2) at the interface between ninety-ninety degree layers of $[\pm 25/90]_s$ laminate at a strain of 0.0061.

$$\left(\frac{< \sigma_z^t >}{Z^t}\right)^2 = 1.607 \tag{6.2}$$

For a linear analysis, $< \sigma_z^t >$ can be represented as a product of a constant c and the corresponding strain. Hence at 0.125 mm for a strain of 0.0061, equation (6.3) can be written.

$$(\frac{< \sigma_z^t >}{Z^t})^2 = (\frac{c \times 0.0061}{Z^t})^2 = 1.607 \tag{6.3}$$

Since Z^t is considered to be 50 MPa, the value of constant c can be determined from equation (6.3).

$$c = 10390.77 \quad \mathrm{N}^2/\mathrm{mm}^4 \tag{6.4}$$

Hence, for a strain of 0.0058, equation (6.3) can be written as

$$(\frac{< \sigma_z^t >}{Z^t})^2 = (\frac{10390.77 \times 0.0058}{50})^2 = 1.4528 \tag{6.5}$$

Hence, the value of QDC index at 0.0058 strain at averaging distance 0.125 mm is 1.4528. This means that at the averaging distance of 0.125 mm, QDC index value of higher than one will be obtained for both 0.0058 and 0.0061 strains which are the limits of experimentally reported delamination initiation strain range of 0.0058 to 0.0061.

Hence, at the averaging distance of 0.125 mm from free edge, table 6.4 could be charted.

Table 6.4: QDC index values corresponding to reported strain range at averaging distance of 0.125 mm

strain	Index value
0.0061	1.6072
0.0058	1.4528

Thus, it has been shown that when the approach for determining averaging distance described in this chapter is used to determine the averaging distance at ninety-ninety layers' interface of $[0/90]_s$ laminate, then the averaging distance of 0.125 mm is found for T300/934 material. Further, when the determined averaging distance of 0.125 mm is implemented in the QDC for predicting delamination initiation at ninety-ninety layers' interface of $[\pm 25/90]_s$ laminate in the experimentally reported strain range for delamination initiation at this interface, then the determined averaging distance has been verified to predict delamination initiation successfully.

It is further observed that the averaging distance of 0.125 mm is a conservative value because for the strain range of 0.0058 to 0.0061, the index values obtained are 1.6072 and 1.4528 respectively which are clearly above 1. However, the primary motive of a successful verification of the proposed approach for determining the averaging distance has been achieved through the course of this thesis. This concludes the results obtained in this thesis.

Computational efficiency through average stress approach

For high gradient stresses near the free edge, it could be worthwhile to compare the difference in analysis time when the convergence of actual stresses is studied compared to the convergence of average of the actual stresses. This comparison has been conducted for the

analysis carried out on ninety-ninety layers' interface of $[\pm 25/90]_s$ laminate model whose general meshing strategy is shown in figures 6.5 and 6.6. As seen through figures 6.7 and 6.8, σ_z is identified as the high gradient stress near the free edge as the other two stress components are comparatively negligible. To be able to reach a convergence in σ_z at the free edge, with the meshing approach followed, the two meshes consisted of 273812 elements and 326898 elements. The smallest element size in the transverse direction at ninety-ninety layers' interface on which the graphs are plotted is 20 microns for 273712 elements' mesh and 10 microns for 326898 elements' mesh. With these element sizes at the free edge, the difference between peak stresses came within the range of 5 % difference (as the peak stresses are 110.2 MPa and 115.3 MPa corresponding to smallest element size in transverse direction of 20 microns and 10 microns respectively). Figure 6.20 below shows a view of σ_z distribution at free edge.

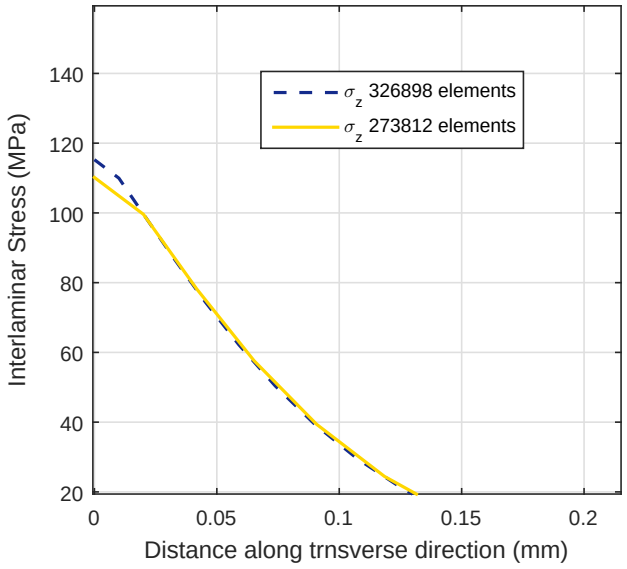

Figure 6.20: Distribution of σ_z at free edge for 273812 and 326898 elements

The comparison of analysis time is made for a CPU configuration with four Giga Bytes random access memory and 3.20 Giga Hertz processor. The analysis time required for the converged σ_z through mesh consisting of 326898 elements has been found to be 1264.3 seconds (21.07 minutes) in terms of CPU time.

In this chapter, the averaging distance at ninety-ninety layers' interface of $[\pm 25/90]_s$ laminate made of T300/934 material is found to be 0.125 mm. Hence a converged average stress data is required at this averaging distance from the free edge. By coarsening the mesh by reducing element size in transverse direction by a factor of two, the coarsest mesh for which a converged average stress plot for σ_z is obtained. The smallest element size in transverse direction at free edge on the ninety-ninety layers' interface is found to be 40 microns for which a converged average stress plot is obtained at 0.125 mm from free edge. The mesh consists of 229108 elements. The figure 6.21 shows a comparison of average stress plots with meshes consisting of smallest element sizes of 10 microns and 40 microns.

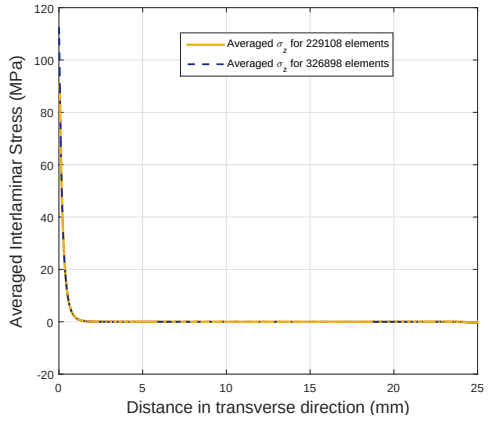

Figure 6.21: Comparison of average stress plots for mesh with 326898 elements and 229108 elements

A distribution of the stresses keeping in mind the averaging distance of 0.125 mm is shown in figure 6.22. The average value of σ_z is found to converge around 63 MPa at 0.125 mm from free edge.

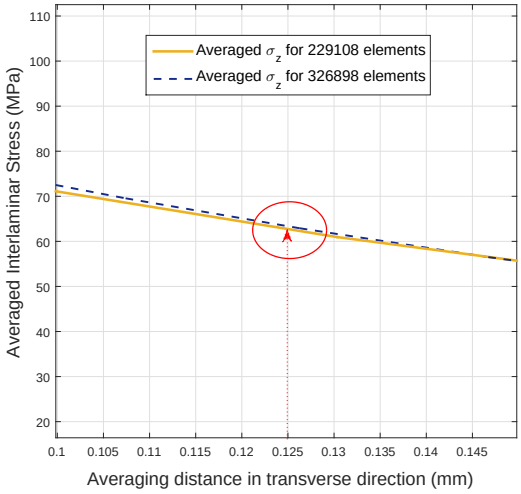

Figure 6.22: Distribution of average σ_z at 0.125 mm from free edge for 229108 and 326898 elements

The analysis time with the use of the same CPU for conducting the analysis with 229108 elements which has smallest element size in transverse direction of 40 microns at free edge is 845.20 seconds (14.08 minute) in terms of CPU time.

The difference in analysis time for obtaining a converged actual σ_z stress at free edge of ninety-ninety layers' interface of $[\pm 25/90]_S$ laminate and converged average σ_z stress at 0.125 mm from free edge is therefore found to be 6.99 minutes in terms of CPU time. The difference in the analysis time is therefore considerable and hence, the analysis requiring converged average stresses is computationally more efficient. Hence, when dealing with high gradient free edge stresses, employment of a criterion involving average stresses could prove to be computationally efficient.

Table 6.5 summarises a comparison of computational time required for the convergence of σ_z at free edge and for convergence of average of σ_z ($< \sigma_z >$) at 0.125 mm from free edge (the determined averaging distance) for the homogeneous $[\pm 25/90]_s$ model.

Table 6.5: Comparison of computational time for convergence of high gradient interlaminar stress and convergence of average of the stress through coarsest mesh

Parameter	Coarsest mesh for convergence	CPU time (minutes)
σ_z (at free edge)	326898 elements	21.07
$< \sigma_z >$ (at 0.125 mm)	229108 elements	14.08
Difference	97790 elements (29.9 %)	6.99 (33.17 %)

It is to be mentioned that the meshing strategy adopted for the results in table 6.5 may not be the optimum mesh for the analysis. However, since the strategy followed for both meshes is similar, a comparison is reported.

Scope for further verifications

It has been observed so far that proposed averaging distance of 0.125 mm at the ninety-ninety layers' interface of $[\pm 25/90]_s$ laminate has predicted delamination initiation positively via application of QDC with indices 1.6072 and 1.4528 for strains 0.0061 and 0.0058 respectively. This means that there is a scope for increasing the averaging distance so as to predict an index value which is either equal to or marginally higher than 1.0 compared to 1.6072 or 1.4528 (for the respective strains of 0.0061 and 0.0058). Back tracing the data in the plot shown in figure 6.19, it has been found that an averaging distance of 0.16 mm from free edge corresponds to an index of 1.12 at 0.0061 strain. Using the approach mentioned from equation (6.2) to (6.5), it has been calculated that at a strain of 0.0058, the averaging distance of 0.16 mm would correspond to an index of 1.006. Thus, the averaging distance of 0.16 mm would predict delamination positively for experimentally reported delamination initiation strain range of 0.0058 to 0.0061 (corresponding to indices 1.006 and 1.12 respectively).

Therefore, as an observation it can be proposed that the range of averaging distance 0.125 mm to 0.16 mm from the free edge would successfully predict delamination initiation through QDC for experimentally proposed delamination initiation strain range of 0.0058 to 0.0061. However, the averaging distance of 0.16 mm has not been determined directly through the approach described in this thesis and hence is not being reported as a result of this thesis.

There is a scope in future works for verifying the validity of the range of 0.125 mm to 0.16 mm or the mean between the two through other laminates made of T300/934 material as suitable averaging distance or range of averaging distance. In literature the reported averaging distance for $[\pm 25/90]_s$ laminate made of T300/934 material is 0.145 mm [12]. Since the mean of 0.125 mm and 0.16 mm would be 0.1425 mm, there is a close correlation between the two values and hence there is a scope to work towards verifying the validity of averaging distance range of 0.125 mm to 0.16 mm or the mean of the range 0.1425 mm at corresponding interface of T300/934 material laminates.

Chapter 7

Conclusion and Recommendations

7.1 Conclusions

Through the course of this research, various investigations have been conducted to arrive at important conclusions pertaining to analysis of free edge stresses in homogeneous and heterogeneous layer fibre reinforced composite laminates which motivate the proposal of an approach to predict free edge stress induced delamination initiation. The work in this thesis starts with the study of interlaminar stresses in homogeneous layer $[0/90]_s$ cross-ply laminate. In an attempt to avoid sudden material discontinuity at interface between dissimilar layers of the homogeneous layer laminate, a heterogeneous layer $[0/90]_s$ cross-ply laminate is modelled with incorporation of constituent material properties of fibre and matrix. Interlaminar stress analysis is conducted in the heterogeneous layer model and differences in stress profiles have been observed when compared to results obtained from homogeneous layer model. The findings from this comparison motivate the proposal of an approach by which the interlaminar stresses in the free edge region of the two models could be correlated. The correlation of stresses between the two models yields an averaging distance from the free edge which when used with QDC for predicting delamination initiation in a $[\pm 25/90]_s$ homogeneous layer laminate, proves to give positive results with reference to experimentally determined delamination initiation data for $[\pm 25/90]_s$ laminate.

As a key highlight, it has been observed that unlike in the case of homogeneous layer models, where the presence of high gradient free edge stresses has been found, sometimes even to an effect of a singularity, comparatively no such high gradient stresses have been observed in heterogeneous layer model. However, apart from the free edge region, the overall profile of interlaminar stresses in heterogeneous layer model has been found to be analogous to those in the corresponding homogeneous layer model. This finding indicates that the presence of comparatively steeper gradients which pose difficulties in convergence analysis of free edge stresses in homogeneous layer models is a sign of a mathematical artefact. Therefore, based on this finding, it becomes possible to propose an approach by which the difficulties posed by interlaminar stresses due to their computationally expensive requirement of convergence studies with a perspective of studying delamination initiation could rather be avoided by the

use of average of interlaminar stresses, the convergence of which is found to be comparatively much convenient.

The major conclusions derived to the best of knowledge during the course of this thesis are as follows:

- The slice model has been found to be working adequately in terms of capturing high gradient interlaminar stresses near free edge of homogeneous layer laminates. The results obtained are found to be correlating well when compared with results published in literature. The convergence of high gradient interlaminar stresses near free edge is found to be computationally expensive. Particularly at the interface between zero and ninety degree layers of $[0/90]_s$ cross-ply laminate, the stresses interlaminar normal stress is found to be increasing by more than 5 % with every mesh refinement. The mesh has been refined by reducing the size of the element at free edge of an interface in a manner by which the DoF particularly in transverse direction is increased.

- The optimum width of quarter portion of cross-ply homogeneous layer laminate (in transverse direction) under tensile longitudinal strain for analysis of interlaminar stresses has been investigated by determining the convergence of average stresses for different widths while keeping the same number of elements in a mesh. With variation in width, when the average stresses overlap with each other, then it indicates that a sufficient width for the quarter symmetric model is attained for which average stresses are converged. A further increase in size for a given mesh would therefore be a redundant increase in size. A width equal to ten times the ply thickness for the quarter portion of homogeneous laminate has been found to be a sufficiently wide and computationally affordable model.

- Linear FEA of interlaminar stresses at interfaces of heterogeneous $[0/90]_s$ cross-ply laminate under longitudinal tensile strain simulated through PBC reveals that comparatively there is no tendency of interlaminar stress components to rise in a high gradient manner near the free edge like in the case of homogeneous layer model. However, the general nature of interlaminar stresses (except at the free edge) has been found analogous to those in homogeneous layer model. This correlation in nature of stresses between homogeneous and heterogeneous models indicates that the existence of such high gradient stresses at free edge (sometimes even to an extent of a singularity), is a sign of a mathematical artefact.

- QDC has been identified as a suitable criterion for predicting delamination initiation due to free edge region interlaminar stresses with high gradients. For this purpose, an averaging distance has been determined corresponding to a given material and interface through a proposed correlation. The correlation involves comparison of average stresses between $[0/90]_s$ laminate's heterogeneous layer model and $[0/90]_s$ homogeneous model of equivalent stiffness at corresponding interface. This is obtained through homogenisation on heterogeneous UC through PBC. A correlation for T300/934 graphite-epoxy combination at interface between ninety-ninety degree layers (symmetric mid-plane) of $[0/90]_s$ cross-ply laminate reveals an averaging distance of 0.125 mm from free edge (in transverse direction).

- A linear FEA of $[\pm 25/90]_s$ laminate under longitudinal tensile strain reveals the presence of high gradient interlaminar stress component σ_z near free edges at interface between ninety-ninety degree layers. The reported experimentally determined longitudinal extensional strain range for initiating delamination in $[\pm 25/90]_s$ laminate is 0.0058 to 0.0061. At a strain of 0.0061, a prediction of delamination initiation at ninety-ninety layers' interface through determined averaging distance of 0.125 mm from free edge reveals a QDC index value of 1.6072. For the same averaging distance at a strain of 0.0058, the QDC index value has been found to be 1.4528. Hence, a positive result towards predicting delamination initiation at interface between ninety-ninety degree layers is obtained through determined averaging distance of 0.125 mm for T300/934 material by the use of QDC.

- A comparison of analysis time for studying convergence of high gradient free edge σ_z stress with analysis time required for studying convergence of the average of the σ_z at the averaging distance of 0.125 mm at the ninety-ninety layers' interface of $[\pm 25/90]_s$ laminate (at which delamination initiation is reported experimentally) reveals a difference in CPU time of 6.99 minutes. This analysis shows that indeed obtaining converged average stresses is computationally less expensive and thus prediction of delamination initiation through incorporation of average stresses of high gradient free edge stresses in QDC is a proof to the concept of an efficient prediction approach.

Through the current research, the primary objectives of studying free edge stresses in homogeneous and heterogeneous models comparatively and proposing an approach by which a suitable averaging distance could be successfully determined has been realised. The evaluation of averaging distance allows determination of average stresses which averts the need for high computational requirements in dealing with high gradient stresses or singular stresses near the free edge. The application of determined averaging distance has revealed positive outcomes when used through QDC, a criterion which takes account of average interlaminar stresses near the free edge for predicting delamination initiation.

7.2 Recommendations for future work

The current research has been conducted under a limited time frame and hence, there are scopes for futuristic works to be done in some areas of the research. Some of the primary recommendations which could be suggested at this stage include ideas on modelling methods and application of obtained results on other suitable scenarios for further verification of proposed approach. In this light, the following recommendations are proposed:

- In the current work, heterogeneous $[0/90]_s$ cross-ply laminate has been built for carrying out correlation with results obtained from a homogeneous $[0/90]_s$ cross-ply laminate of equal stiffness. However, the heterogeneous model cross-ply laminate is modelled in such a way that there is one fibre across the thickness of a ply where the ply thickness is the same as that considered for the homogeneous layer model. This heterogeneous model is capable of overcoming the problem of very high gradients in interlaminar stresses near the free edge because the intersection of free edge and interface between layers

is modelled with same material (matrix material). However, it might not necessarily capture the state of stresses at micromechanical scale in the free edge region. Since, the micromechanical scale model could be a more idealistic representation of the fibre reinforced composite laminate, it would be interesting to carry out the proposed approach for correlation of stresses between the $[0/90]_s$ micromechanical model and a homogeneous $[0/90]_s$ model of equal stiffness for the purpose of determining the averaging distance.

- In the current work, the RVE consists of one UC for the purpose of homogenisation through PBC. This is because the heterogeneous layer is modelled with one fibre across the thickness of layer. Upon homogenisation using one UC in RVE, it is observed that specially the shear moduli are under predicted when compared to homogeneous lamina properties reported in literature. If the heterogeneous layer is modelled with multiple fibres across its thickness, then there is a scope to consider a larger RVE with multiple UCs for carrying out the homogenisation. A larger RVE would enable prediction of shear moduli in closer approximation to experimentally reported properties because the deformation state of the larger RVE upon use of PBC would be in closer approximation to homogeneous deformation state and hence the magnitude of predicted shear moduli upon homogenisation through PBC would increase.

- Results for averaging distance reported in literature [12] suggests the use of a statistically averaged averaging distance for a combination of laminates for the same material. This has encouraged the determination of averaging distance on a simpler laminate like a cross-ply laminate, while the application of averaging distance has been made on a $[\pm 25/90]_s$ laminate for predicting delamination initiation. Considering the constraints during the research, modelling of a heterogeneous $[\pm 25/90]_s$ laminate for carrying out the correlation has not been possible and hence, there is a scope to determine the averaging distance through the approach proposed in the current work through a straight forward comparison of interlaminar stresses between homogeneous model $[\pm 25/90]_s$ laminate and heterogeneous model $[\pm 25/90]_s$ laminate. Further, the averaging distance determined from this modelling approach could be compared with the determined averaging distance of 0.125 mm in the current work for T300/934 material.

- Finally, the last recommendation addresses the conservative value of determined averaging distance (0.125 mm). In the current work, the application of determined averaging distance of 0.125 mm has been made on a $[\pm 25/90]_s$ laminate. Although the results obtained from this averaging distance towards predicting delamination initiation are positive for $[\pm 25/90]_s$ laminate case, it would be interesting to verify the applicability of this averaging distance on laminates with other configurations made of the same material (T300/934). Also, as reported in section 6.5, there is a scope to verify if application of the range of 0.125 mm to 0.16 mm or the mean of the range 0.1425 mm would result in successful prediction of delamination initiation in other suitable laminates made of T300/934 material. For the $[\pm 25/90]_s$ laminate, the range of 0.125 mm to 0.16 mm gives positive delamination initiation indices in experimentally reported range for the laminate's delamination initiation. Thus, it remains to be seen whether the application of this range or mean of the range is able to successfully predict delamination initiation on other suitable laminates in the strain range for their delamination initiation.

This concludes the recommendations that have been identified as of now for future course of work in this area of research. Carrying out studies based on these recommendations can help in further verification of results proposed during the course of this thesis.

References

[1] C Mittelstedt and W Becker. Free-edge effects in composite laminates. *Applied Mechanics Reviews*, 60(5):217–245, 2007.

[2] R Byron Pipes and NJ Pagano. Interlaminar stresses in composite laminates under uniform axial extension. *Journal of Composite Materials*, 4(4):538–548, 1970.

[3] LB Lessard, AS Schmidt, and MM Shokrieh. Three-dimensional stress analysis of free-edge effects in a simple composite cross-ply laminate. *International journal of solids and structures*, 33(15):2243–2259, 1996.

[4] AH Puppo and HA Evensen. Interlaminar shear in laminated composites under generalized plane stress. *Journal of composite materials*, 4(2):204–220, 1970.

[5] F Ellyin, Z Xia, and Y Chen. Viscoelastic micromechanical modeling of free edge and time effects in glass fiber/epoxy cross-ply laminates. *Composites Part A: Applied Science and Manufacturing*, 33(3):399–409, 2002.

[6] P Suquet. Elements of homogenization for inelastic solid mechanics. *Homogenization techniques for composite media*, 272:193–278, 1987.

[7] Z Xia, Y Zhang, and F Ellyin. A unified periodical boundary conditions for representative volume elements of composites and applications. *International Journal of Solids and Structures*, 40(8):1907–1921, 2003.

[8] MW Hyer. *Stress analysis of fiber-reinforced composite materials*. DEStech Publications, Inc, 2009.

[9] ASD Wang, NN Kishore, and CA Li. Crack development in graphite-epoxy cross-ply laminates under uniaxial tension. *Composites Science and Technology*, 24(1):1–31, 1985.

[10] JCJ Schellekens and R De Borst. Nonlinear analysis of propagation of delamination near free edges. In *Composites; Proceedings of the 8th International Conference on Composite Materials (ICCM/8), Honolulu, HI; 15-19 July 1991, 28-E-1-28-E-11.(1991)*. Society for the Advancement of Material and Process: Engineering, 1991.

[11] Z Ran, Y Yan, J Li, Z Qi, and L Yang. Determination of thermal expansion coefficients for unidirectional fiber-reinforced composites. *Chinese Journal of Aeronautics*, 27(5):1180–1187, 2014.

[12] JC Brewer and PA Lagace. Quadratic stress criterion for initiation of delamination. *Journal of composite materials*, 22(12):1141–1155, 1988.

[13] EF Rybicki. Approximate three-dimensional solutions for symmetric laminates under inplane loading. *Journal of Composite Materials*, 5(3):354–360, 1971.

[14] ASD Wang and FW Crossman. Some new results on edge effect in symmetric composite laminates. *Journal of Composite Materials*, 11(1):92–106, 1977.

[15] IS Raju and JH Crews. Interlaminar stress singularities at a straight free edge in composite laminates. *Computers & Structures*, 14(1):21–28, 1981.

[16] JD Whitcomb, IS Raju, and JG Goree. Reliability of the finite element method for calculating free edge stresses in composite laminates. *Computers & Structures*, 15(1):23–37, 1982.

[17] T Kant and K Swaminathan. Estimation of transverse/interlaminar stresses in laminated composites–a selective review and survey of current developments. *Composite structures*, 49(1):65–75, 2000.

[18] NJ Salamon. An assessment of the interlaminar stress problem in laminated composites. *Journal of composite materials*, 14(1):177–194, 1980.

[19] J Lindemann and W Becker. Analysis of the free-edge effect in composite laminates by the boundary finite element method. *Mechanics of composite materials*, 36(3):207–214, 2000.

[20] CL Nailadi, DF Adams, and DO Adams. An experimental and numerical investigation of the free edge problem in composite laminates. *Journal of reinforced plastics and composites*, 21(1):3–39, 2002.

[21] VT Nguyen and JF Caron. A new finite element for free edge effect analysis in laminated composites. *Computers & structures*, 84(22):1538–1546, 2006.

[22] SS Ramesh, CM Wang, JN Reddy, and KK Ang. A higher-order plate element for accurate prediction of interlaminar stresses in laminated composite plates. *Composite Structures*, 91(3):337–357, 2009.

[23] RL Spilker. A traction-free-edge hybrid-stress element for the analysis of edge effects in cross-ply laminates. *Computers & Structures*, 12(2):167–179, 1980.

[24] Z Tian, F Zhao, and Q Yang. Straight free-edge effects in laminated composites. *Finite Elements in Analysis and Design*, 41(1):1–14, 2004.

[25] RB Pipes and NJ Pagano. Interlaminar stresses in composite laminates-an approximate elasticity solution. *Journal of Applied Mechanics*, 41(3):668–672, 1974.

[26] C Kassapoglou and PA Lagace. An efficient method for the calculation of interlaminar stresses in composite materials. *Journal of Applied Mechanics*, 53(4):744–750, 1986.

[27] M Tahani and A Nosier. Free edge stress analysis of general cross-ply composite laminates under extension and thermal loading. *Composite Structures*, 60(1):91–103, 2003.

[28] N Dhanesh, S Kapuria, and GGS Achary. Accurate prediction of three-dimensional free edge stress field in composite laminates using mixed-field multiterm extended kantorovich method. *Acta Mechanica*, pages 1–25, 2016.

[29] B Peng, J Goodsell, RB Pipes, and W Yu. Generalized free-edge stress analysis using mechanics of structure genome. *Journal of Applied Mechanics*, 83(10):101013, 2016.

[30] NJ Pagano and RB Pipes. The influence of stacking sequence on laminate strength. *Journal of composite materials*, 5(1):50–57, 1971.

[31] C Kassapoglou and PA Lagace. Closed form solutions for the interlaminar stress field in angle-ply and cross-ply laminates. *Journal of Composite Materials*, 21(4):292–308, 1987.

[32] JM Whitney and RL McCullough. Micromechanical material modelling, delawarecomposites design encyclopaedia. technomicpub. co, 1990.

[33] J Aboudi. *Mechanics of composite materials: a unified micromechanical approach*, volume 29. Elsevier, 2013.

[34] R Hill. Elastic properties of reinforced solids: some theoretical principles. *Journal of the Mechanics and Physics of Solids*, 11(5):357–372, 1963.

[35] ND Cristescu, EM Craciun, and Eugen S. *Mechanics of elastic composites*. CRC Press, 2003.

[36] Ver Abaqus. 6.14 documentation. *Dassault Systemes Simulia Corporation*, 2014.

[37] HP Langtangen. *Python scripting for computational science*, volume 3. Springer, 2006.

[38] Z Xia, C Zhou, Q Yong, and X Wang. On selection of repeated unit cell model and application of unified periodic boundary conditions in micro-mechanical analysis of composites. *International Journal of Solids and Structures*, 43(2):266–278, 2006.

[39] W Wu, J Owino, A Al-Ostaz, and L Cai. Applying periodic boundary conditions in finite element analysis. In *SIMULIA community conference, providence, RI*, pages 707–719, 2014.

[40] CT Herakovich. Edge effects and delamination failures. *The Journal of Strain Analysis for Engineering Design*, 24(4):245–252, 1989.

[41] TK O'Brien. Characterization of delamination onset and growth in a composite laminate. In *Damage in Composite Materials: Basic Mechanisms, Accumulation, Tolerance, and Characterization*. ASTM International, 1982.

[42] PJ Davis and P Rabinowitz. *Methods of numerical integration*. Courier Corporation, 2007.

[43] Y Chen, Z Xia, and F Ellyin. Evolution of residual stresses induced during curing processing using a viscoelastic micromechanical model. *Journal of composite materials*, 35(6):522–542, 2001.

Appendix A

Appendix 1: FEA results for homogenisation on T300/934 material

A.1 Abaqus output database (odb) results

The equal and opposite distribution of nodal forces has been shown through the odb results obtained through FEA in Abaqus. The pair of surfaces on which PBC have been simulated through displacement difference are shown for every deformation mode. The fibres and matrix of the UC are modelled using T300/934 material as listed in table 6.2. The homogenisation is carried out in a similar way as described in section 5.2. Further, the distribution of nodal forces and displacements on surfaces subjected to PBCs are found to be in compliance with requirements of PBC. The nodal forces are equal and opposite and the displacement difference on opposite surfaces are constant (resulting in displacement continuity) across the two opposite boundary surfaces.

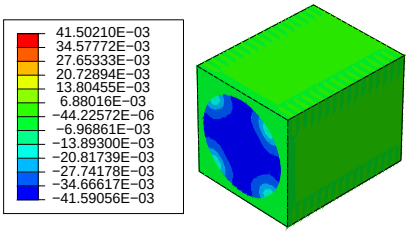

(a) Nodal force distribution in x direction on front surface

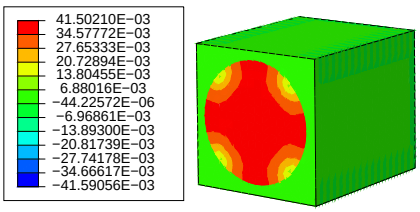

(b) Nodal force distribution in x direction on rear surface

Figure A.1: Periodic nodal force distribution for ϵ_x strain

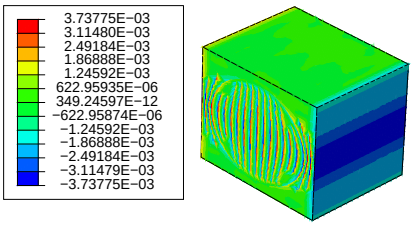

(a) Nodal force distribution in y direction on right surface

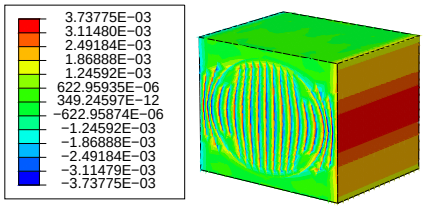

(b) Nodal force distribution in y direction on left surface

Figure A.2: Periodic nodal force distribution for ϵ_y strain

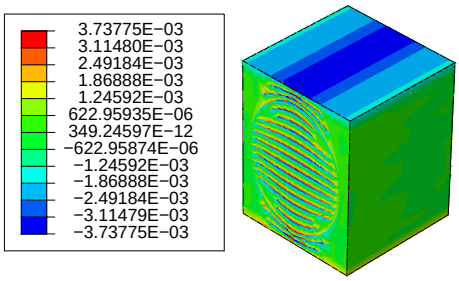

(a) Nodal force distribution in z direction on top surface

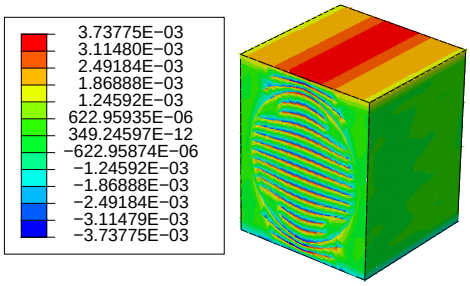

(b) Nodal force distribution in z direction on bottom surface

Figure A.3: Periodic nodal force distribution for ϵ_z strain

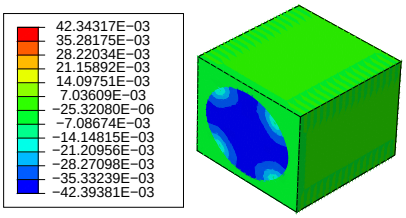

(a) Nodal force distribution in x direction on front surface

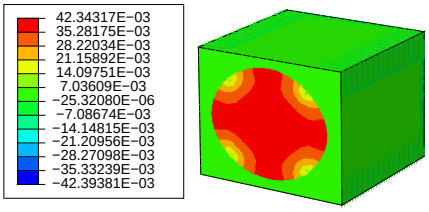

(b) Nodal force distribution in x direction on rear surface

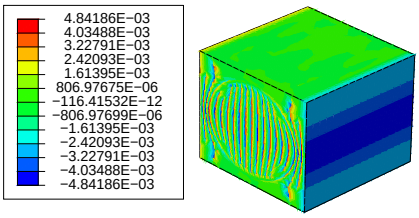

(c) Nodal force distribution in y direction on right surface

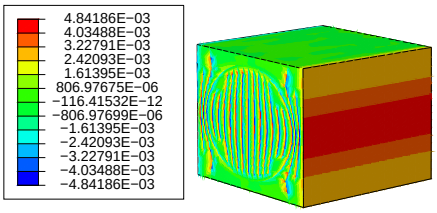

(d) Nodal force distribution in y direction on left surface

Figure A.4: Periodic nodal force distribution for combined ϵ_x and ϵ_y strains

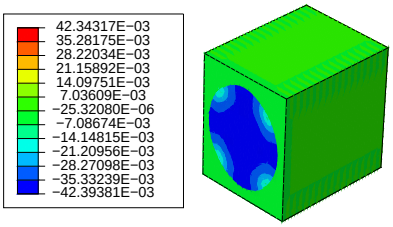

(a) Nodal force distribution in x direction on front surface

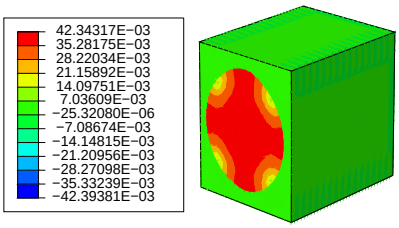

(b) Nodal force distribution in x direction on rear surface

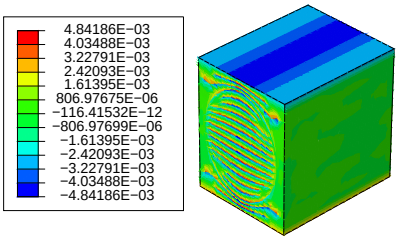

(c) Nodal force distribution in z direction on top surface

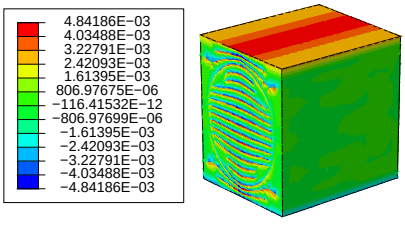

(d) Nodal force distribution in z direction on bottom surface

Figure A.5: Periodic nodal force distribution for combined ϵ_x and ϵ_z strains

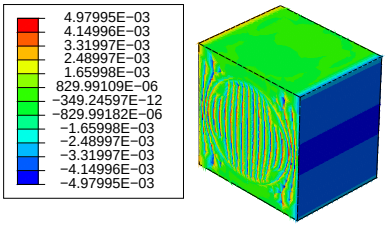

(a) Nodal force distribution in y direction on right surface

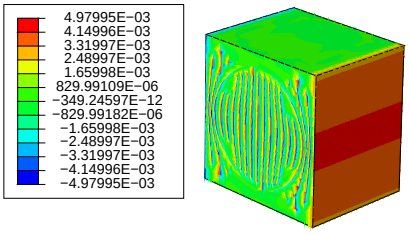

(b) Nodal force distribution in y direction on left surface

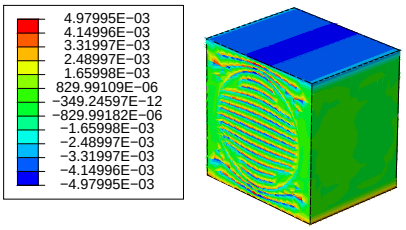

(c) Nodal force distribution in z direction on top surface

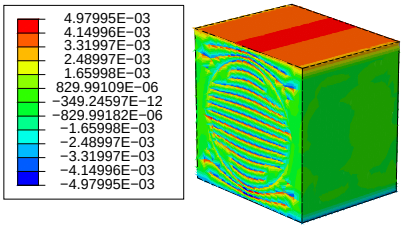

(d) Nodal force distribution in z direction on bottom surface

Figure A.6: Periodic nodal force distribution for combined ϵ_y and ϵ_z strains

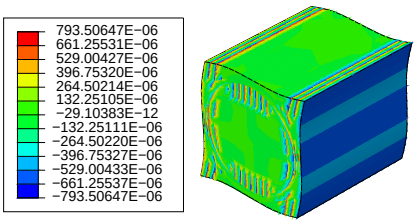

(a) Nodal force distribution in z direction on right surface

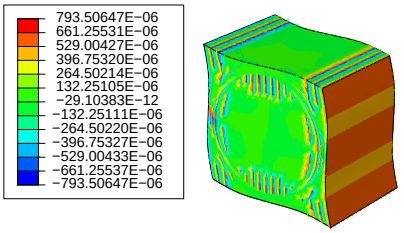

(b) Nodal force distribution in z direction on left surface

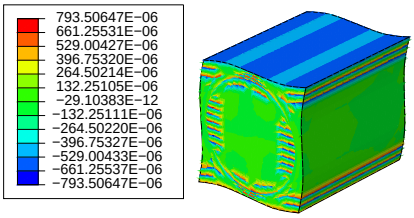

(c) Nodal force distribution in y direction on top surface

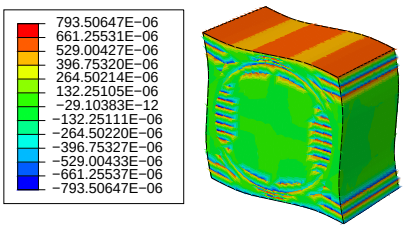

(d) Nodal force distribution in y direction on bottom surface

Figure A.7: Periodic nodal force distribution for γ_{yz}

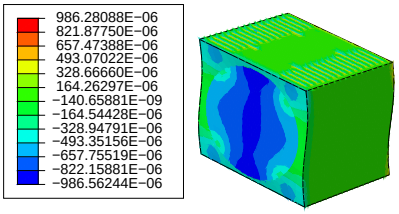

(a) Nodal force distribution in z direction on front surface

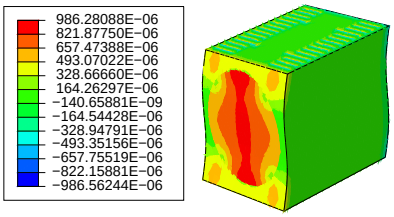

(b) Nodal force distribution in z direction on rear surface

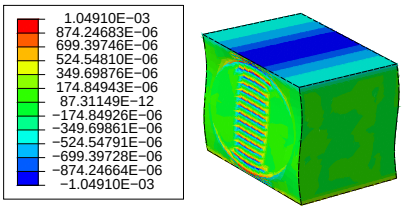

(c) Nodal force distribution in x direction on top surface

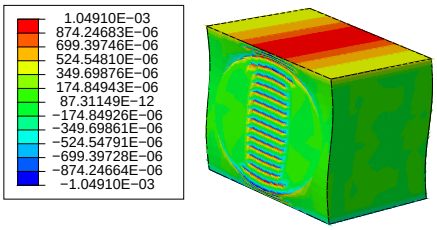

(d) Nodal force distribution in x direction on bottom surface

Figure A.8: Periodic nodal force distribution for γ_{xz}

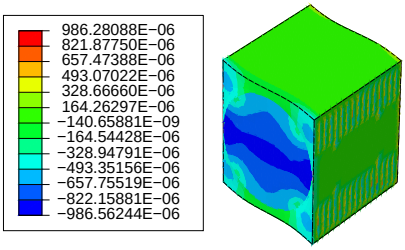

(a) Nodal force distribution in y direction on front surface

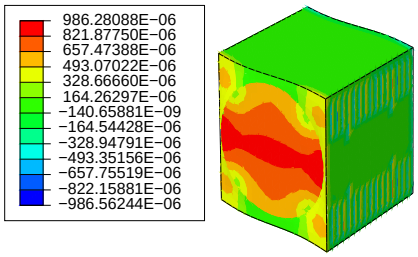

(b) Nodal force distribution in y direction on rear surface

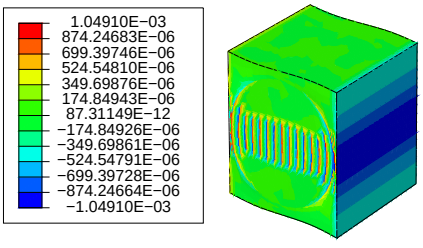

(c) Nodal force distribution in x direction on right surface

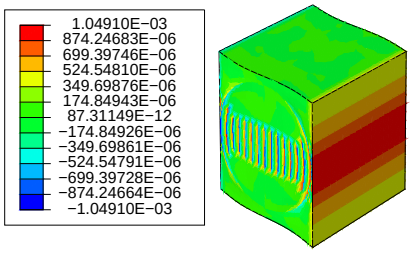

(d) Nodal force distribution in x direction on left surface

Figure A.9: Periodic nodal force distribution for γ_{xy}

A.2 Plots for nodal forces and displacements on application of PBC

The deformation states shown in section A.1 visually suggest that the distribution of nodal forces are equal and opposite on opposite boundary surfaces. However, plots of nodal forces and displacements on opposite boundary surfaces would present state of equal and opposite nodal forces and continuity of displacement across opposite boundary surfaces more clearly.

Plots for all unidirectional normal strain deformation states (ϵ_x, ϵ_y and ϵ_z) and all (engineering) shear strain components (γ_{yz}, γ_{xz} and γ_{xy}) are shown from figure A.10 to A.15. Plots for deformation states in which combination of normal strains have been applied together are not sown because plots for unidirectional normal strains are sufficient to represent the distribution of nodal forces and displacements on respective boundaries when combination of unidirectional normal strains are applied.

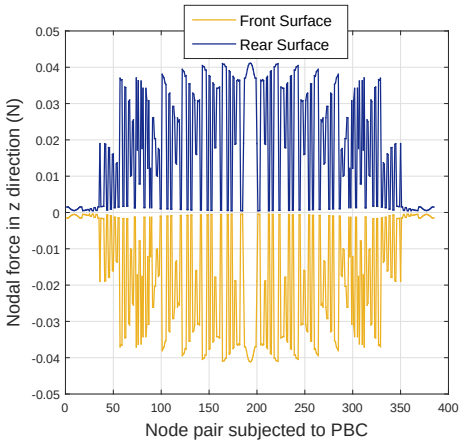

(a) Nodal force distribution in x direction on front and rear surfaces

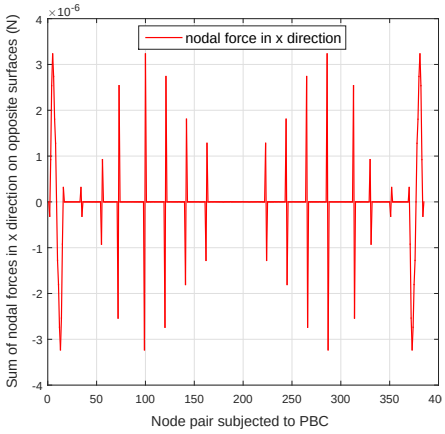

(b) Nodal force sum in x direction on front and rear surfaces

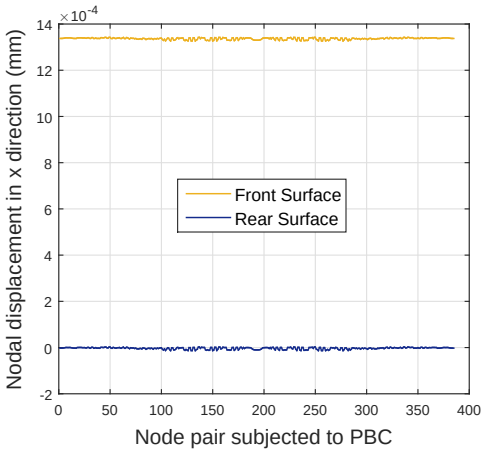

(c) Nodal displacement distribution in x direction on front and rear surfaces

Figure A.10: Representation of nodal forces and displacements on front and rear surfaces for ϵ_x

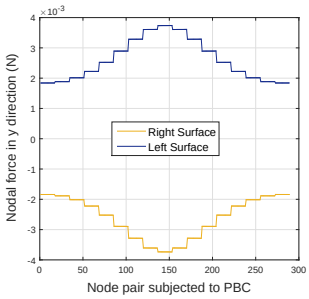

(a) Nodal force distribution in y direction on right and left surfaces

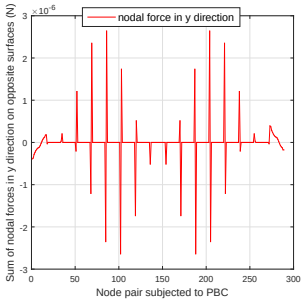

(b) Nodal force sum in y direction on right and left surfaces

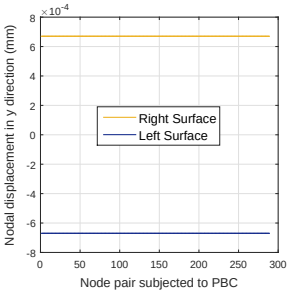

(c) Nodal displacement distribution in y direction on right and left surfaces

Figure A.11: Representation of nodal forces and displacements on right and left surfaces for ϵ_y

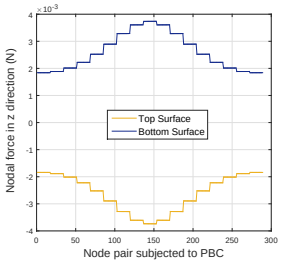

(a) Nodal force distribution in z direction on top and bottom surfaces

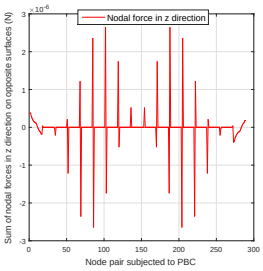

(b) Nodal force sum in z direction on top and bottom surfaces

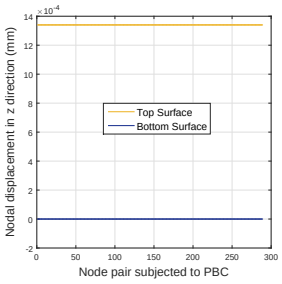

(c) Nodal displacement distribution in z direction on top and bottom surfaces

Figure A.12: Nodal forces and displacements on top and bottom surfaces for ϵ_z

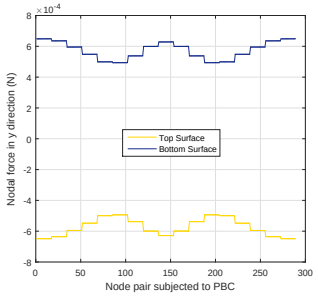

(a) Nodal force distribution in y direction on top and bottom surfaces

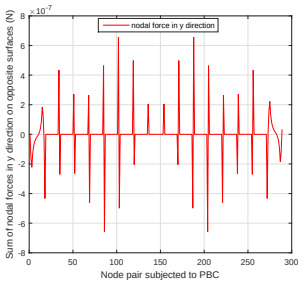

(b) Nodal force sum in y direction on top and bottom surfaces

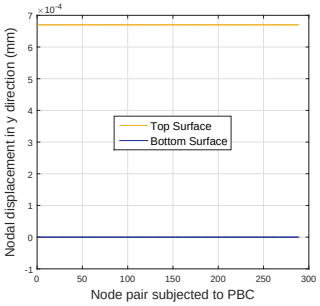

(c) Nodal displacement distribution in y direction on top and bottom surfaces

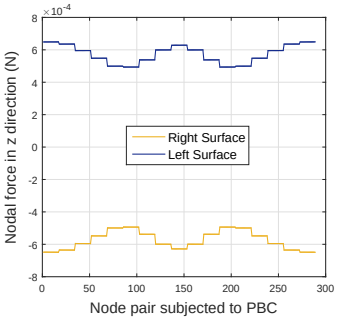

(d) Nodal force distribution in z direction on right and left surfaces

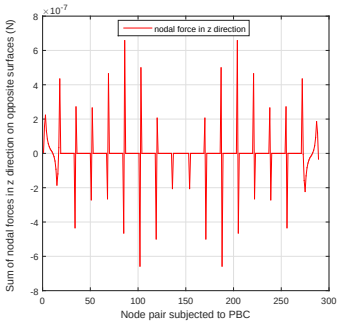

(e) Nodal force distribution in z direction on right and left surfaces

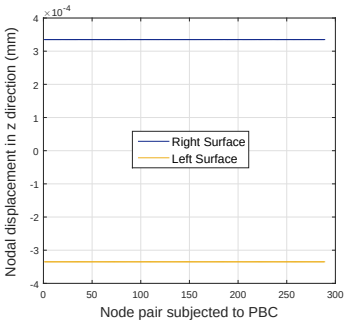

(f) Nodal displacement distribution in z direction on right and left surfaces

Figure A.13: Nodal force and displacement distributions for γ_{yz}

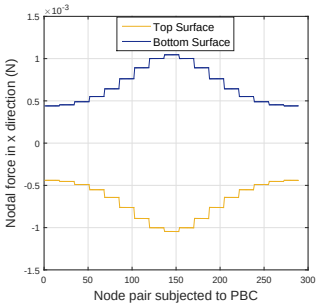

(a) Nodal force distribution in x direction on top and bottom surfaces

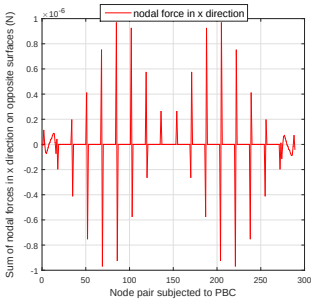

(b) Nodal force sum in x direction on top and bottom surfaces

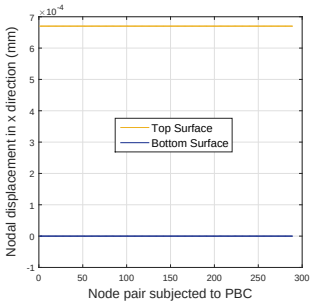

(c) Nodal displacement distribution in x direction on top and bottom surfaces

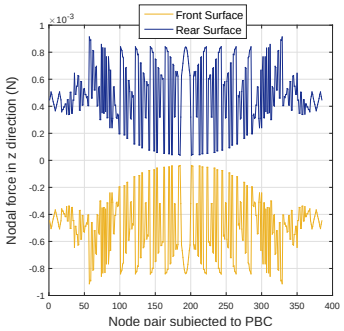

(d) Nodal force distribution in z direction on front and rear surfaces

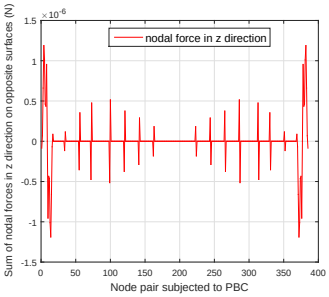

(e) Nodal force sum in z direction on front and rear surfaces

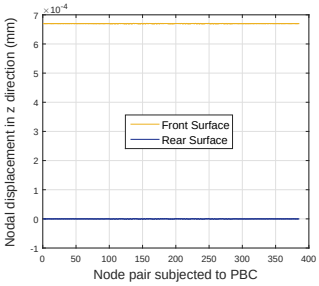

(f) Nodal displacement distribution in z direction on front and rear surfaces

Figure A.14: Nodal force and displacement distributions for γ_{xz}

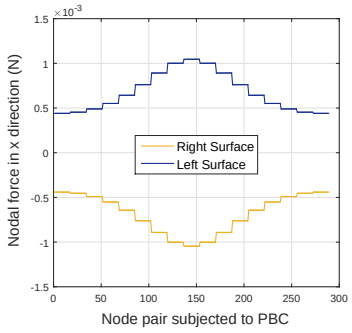

(a) Nodal force distribution in x direction on right and left surfaces

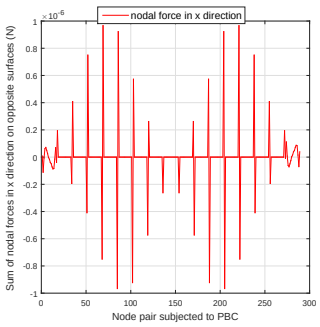

(b) Nodal force sum in x direction on right and left surfaces

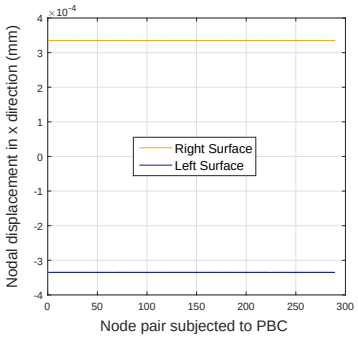

(c) Nodal displacement distribution in x direction on right and left surfaces

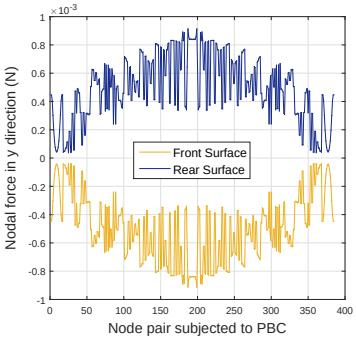

(d) Nodal force distribution in y direction on front and rear surfaces

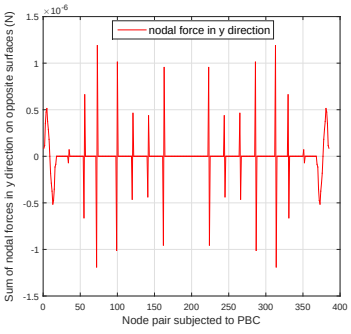

(e) Nodal force sum in y direction on front and rear surfaces

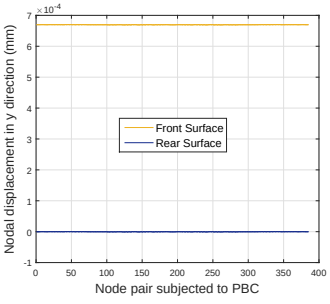

(f) Nodal displacement distribution in y direction on front and rear surfaces

Figure A.15: Nodal force and displacement distributions for γ_{xy}

Appendix B

Appendix 2: Scripts for modelling and post-processing

B.1 Script for pre-processing data

The FEA of homogeneous and heterogeneous layer models involved scripting of models through Abaqus Scripting Interface for generation of *cae* models with the help of Abaqus user manual [36] and *Langtangen* (2006) [37]. Particularly, for running analysis in the case of heterogeneous $[0/90]_s$ cross-ply laminate, the data is extracted through input file primarily for generation of suitable node sets for application of desired boundary conditions.

Application of PBC on 3D UC

An example Matlab script used for applying PBC nodal constraint equations on nodes belonging to opposite boundary surfaces is presented in this subsection. In the script l,t, and z represent the longitudinal, transverse and through-thickness directions respectively. The script has been written to simulate a normal strain (for which displacement needs to be applied on respective dummy node in Abaqus input file). It has been ensured that none of the nodes is over constrained.

```
1  %% Example script for writing nodal constraint equations for applying
       normal strain:
2  % l, t and z represent longitudinal, transverse and through-thickness
3  % directions respectively.
4  %%
5  dof_l=1;
6  dof_t=2;
7  dof_z=3;
8
9  fileID_PBC_E_tt = fopen('PBC_equations_E_tt.inp','w');
10 terms_t=3; % represents number of terms in constraint equation (linear)
```

```
11 coeff_1_t=1.; % represents coefficient on a face with normal vector along
       the positive axis direction
12 coeff_2_t=-1.; % represents coefficient on a face with normal vector
      along the negative axis direction
13 coeff_3_t=-1.; % represents coefficient of dummy node which decides the
      dummy node's displacement direction. Since the dummy node is expressed
       on L.H.S of equation, '-' coefficient means displacement along +ve
      axis direction and vice-versa
14 dummy_node_t = 2000000;
15 for v=1:length(Paired_nodes_for_PBC_left_right)
16     fprintf(fileID_PBC_E_tt,'%d\n%4s%7d%1s%d%1s%1.0f%1s%4s%7d%1s%d%1s%1.0
          f%1s%7d%1s%d%1s%1.0f\n',terms_t,'Set-',
          Paired_nodes_for_PBC_left_right(v,1),',',dof_t,',',coeff_1_t,',','
          Set-',Paired_nodes_for_PBC_left_right(v,2),',',dof_t,',',coeff_2_t
          ,',',dummy_node_t,',',dof_t,',',coeff_3_t);
17 end
18 fclose(fileID_PBC_E_tt);
19
20 fileID_PBC_E_zz = fopen('PBC_equations_E_zz.inp','w');
21 terms_z=3;
22 coeff_1_z=1.;
23 coeff_2_z=-1.;
24 coeff_3_z=-1.;
25 dummy_node_z=3000000;
26 for v=1:length(Paired_nodes_for_PBC_bottom_top)
27     fprintf(fileID_PBC_E_zz,'%d\n%4s%7d%1s%d%1s%1.0f%1s%4s%7d%1s%d%1s%1.0
          f%1s%7d%1s%d%1s%1.0f\n',terms_z,'Set-',
          Paired_nodes_for_PBC_bottom_top(v,1),',',dof_z,',',coeff_1_z,',','
          Set-',Paired_nodes_for_PBC_bottom_top(v,2),',',dof_z,',',coeff_2_z
          ,',',dummy_node_z,',',dof_z,',',coeff_3_z);
28 end
29 fclose(fileID_PBC_E_zz);
30
31 fileID_PBC_E_ll = fopen('PBC_equations_E_ll.inp','w');
32 terms_l=3;
33 coeff_1_l=1.;
34 coeff_2_l=-1.;
35 coeff_3_l=-1.;
36 dummy_node_l=1000000;
37 for v=1:length(Paired_nodes_for_PBC_front_rear)
38     fprintf(fileID_PBC_E_ll,'%d\n%4s%7d%1s%d%1s%1.0f%1s%4s%7d%1s%d%1s%1.0
          f%1s%7d%1s%d%1s%1.0f\n',terms_l,'Set-',
          Paired_nodes_for_PBC_front_rear(v,1),',',dof_l,',',coeff_1_l,',','
          Set-',Paired_nodes_for_PBC_front_rear(v,2),',',dof_l,',',coeff_2_l
          ,',',dummy_node_l,',',dof_l,',',coeff_3_l);
39 end
40 fclose(fileID_PBC_E_ll);
41
42 fileID_PBC_E_zl = fopen('PBC_equations_E_zl.inp','w');
43 terms_zl=3;
44 coeff_1_zl=1.;
45 coeff_2_zl=-1.;
46 coeff_3_zl=-1.;
```

```
47 dummy_node_z_zl=5000000;
48 dummy_node_l_zl=4000000;
49 for v=1:length(Paired_nodes_for_PBC_front_rear) % To avoid
       overconstraining front face's top edge:
50     if  inp_file_nodes(find(inp_file_nodes(:,1) ==
           Paired_nodes_for_PBC_front_rear(v,1)),3)~= 0.067000001700000 %
           column index 3 means the through-thickness coordinate
51         fprintf(fileID_PBC_E_zl,'%d\n%4s%7d%1s%d%1s%1.0f%1s%4s%7d%1s%d%1s
               %1.0f%1s%7d%1s%d%1s%1.0f\n',terms_zl,'Set-',
               Paired_nodes_for_PBC_front_rear(v,1),',',dof_z,',',coeff_1_zl,
               ',','Set-',Paired_nodes_for_PBC_front_rear(v,2),',',dof_z,',',
               coeff_2_zl,',',dummy_node_l_zl,',',dof_z,',',coeff_3_zl);
52     end
53 end
54 for v=1:length(Paired_nodes_for_PBC_bottom_top) % To avoid
       overconstraining top face's front edge:
55     if inp_file_nodes(find(inp_file_nodes(:,1) ==
           Paired_nodes_for_PBC_bottom_top(v,1)),4)~= 0.134000003000000 %
           column index 4 means the longitudinal coordinate
56         fprintf(fileID_PBC_E_zl,'%d\n%4s%7d%1s%d%1s%1.0f%1s%4s%7d%1s%d%1s
               %1.0f%1s%7d%1s%d%1s%1.0f\n',terms_zl,'Set-',
               Paired_nodes_for_PBC_bottom_top(v,1),',',dof_l,',',coeff_1_zl,
               ',','Set-',Paired_nodes_for_PBC_bottom_top(v,2),',',dof_l,',',
               coeff_2_zl,',',dummy_node_z_zl,',',dof_l,',',coeff_3_zl);
57     end
58 end
59 fclose(fileID_PBC_E_zl);
60
61 fileID_PBC_E_tl = fopen('PBC_equations_E_tl.inp','w');
62 terms_tl=3;
63 coeff_1_tl=1.;
64 coeff_2_tl=-1.;
65 coeff_3_tl=-1.;
66 dummy_node_t_tl=6000000;
67 dummy_node_l_tl=7000000;
68 for v=1:length(Paired_nodes_for_PBC_front_rear) % To avoid
       overconstraining front face's right edge:
69     if inp_file_nodes(find(inp_file_nodes(:,1) ==
           Paired_nodes_for_PBC_front_rear(v,1)),2)~= 0.067000001700000 %
           column index 2 means the transverse coordinate
70         fprintf(fileID_PBC_E_tl,'%d\n%4s%7d%1s%d%1s%1.0f%1s%4s%7d%1s%d%1s
               %1.0f%1s%7d%1s%d%1s%1.0f\n',terms_tl,'Set-',
               Paired_nodes_for_PBC_front_rear(v,1),',',dof_t,',',coeff_1_tl,
               ',','Set-',Paired_nodes_for_PBC_front_rear(v,2),',',dof_t,',',
               coeff_2_tl,',',dummy_node_l_tl,',',dof_t,',',coeff_3_tl);
71     end
72 end
73 for v=1:length(Paired_nodes_for_PBC_left_right) % To avoid
       overconstraining right face's front edge and right face's top edge:
74     if inp_file_nodes(find(inp_file_nodes(:,1) ==
           Paired_nodes_for_PBC_left_right(v,1)),4)~= 0.134000003000000 &&
           inp_file_nodes(find(inp_file_nodes(:,1) ==
           Paired_nodes_for_PBC_left_right(v,1)),3)~= 0.067000001700000
```

```
75          fprintf(fileID_PBC_E_tl,'%d\n%4s%7d%1s%d%1s%1.0f%1s%4s%7d%1s%d%1s
                %1.0f%1s%7d%1s%d%1s%1.0f\n',terms_l,'Set-',
                Paired_nodes_for_PBC_left_right(v,1),',',dof_l,',',coeff_1_tl,
                ',','Set-',Paired_nodes_for_PBC_left_right(v,2),',',dof_l,',',
                coeff_2_tl,',',dummy_node_t_tl,',',dof_l,',',coeff_3_tl);
76      end
77  end
78  fclose(fileID_PBC_E_tl);
79
80  fileID_PBC_E_tz = fopen('PBC_equations_E_tz.inp','w');
81  terms_tz=3;
82  coeff_1_zl=1.;
83  coeff_2_zl=-1.;
84  coeff_3_zl=-1.;
85  dummy_node_t_12=8000000;
86  dummy_node_z_12=9000000;
87  for v=1:length(Paired_nodes_for_PBC_left_right) % To avoid
        overconstraining right face's top edge and right face's front edge:
88      if inp_file_nodes(find(inp_file_nodes(:,1) ==
            Paired_nodes_for_PBC_left_right(v,1)),3)~= 0.067000001700000 &&
            inp_file_nodes(find(inp_file_nodes(:,1) ==
            Paired_nodes_for_PBC_left_right(v,1)),4)~= 0.134000003000000
89          fprintf(fileID_PBC_E_tz,'%d\n%4s%7d%1s%d%1s%1.0f%1s%4s%7d%1s%d%1s
                %1.0f%1s%7d%1s%d%1s%1.0f\n',terms_tz,'Set-',
                Paired_nodes_for_PBC_left_right(v,1),',',dof_z,',',coeff_1_zl,
                ',','Set-',Paired_nodes_for_PBC_left_right(v,2),',',dof_z,',',
                coeff_2_zl,',',dummy_node_t_tz,',',dof_z,',',coeff_3_zl);
90      end
91  end
92  for v=1:length(Paired_nodes_for_PBC_bottom_top) % To avoid
        overconstraining top face's right edge and top face's front edge:
93      if inp_file_nodes(find(inp_file_nodes(:,1) ==
            Paired_nodes_for_PBC_bottom_top(v,1)),2)~= 0.067000001700000 &&
            inp_file_nodes(find(inp_file_nodes(:,1) ==
            Paired_nodes_for_PBC_bottom_top(v,1)),4)~= 0.134000003000000
94          fprintf(fileID_PBC_E_tz,'%d\n%4s%7d%1s%d%1s%1.0f%1s%4s%7d%1s%d%1s
                %1.0f%1s%7d%1s%d%1s%1.0f\n',terms_tz,'Set-',
                Paired_nodes_for_PBC_bottom_top(v,1),',',dof_t,',',coeff_1_zl,
                ',','Set-',Paired_nodes_for_PBC_bottom_top(v,2),',',dof_t,',',
                coeff_2_zl,',',dummy_node_z_tz,',',dof_t,',',coeff_3_zl);
95      end
96  end
97  fclose(fileID_PBC_E_tz);
```

B.2 Script for post-processing of data

Post-processing scripts have been written in Matlab and Python tools through the course of this thesis to reach desired results. Some of the scripts used for crucial results such as for the purpose of homogenisation on UC and for calculation of average of stresses have been shown in this section.

Scripts for extraction of nodal forces and displacement from Abaqus output database

Python scripts are written with the help of Abaqus user manual [36] and *Langtangen* (2006) [37] for extracting the nodal force and displacement data on desired surfaces of the output database model. For this purpose, suitable node sets are created and incorporated in the scripts for extraction of data. Example scripts used for extraction nodal forces and displacements on front and rear surfaces of a heterogeneous UC shown in figure 4.3 are shown in this subsection.

The example Python script for extraction of nodal force data on front and rear surfaces of the UC is as follows:

```
## FOR NODAL FORCES:

from abaqusConstants import *
from viewerModules import *
from odbAccess import *
import os

odb_1h = session.openOdb(name='heterogeneous_UC.odb')
odbRootA=odb_1h.rootAssembly

os.chdir(r"path")
session.viewports['Viewport: 1'].setValues(displayedObject=odb_1h)
frames = odb_1h.steps['Step-BC'].frames
no_of_frames = len(frames)
instance = odb_1h.rootAssembly.instances['PART-MERGE-1']
node_region = instance.nodeSets['SET-REAR_NODES']
nodes = node_region.nodes
no_of_nodes = len(nodes)

outPutFileName_forces_rear_front = 'EXTRACTED_NODAL_FORCES_REAR_FRONT.txt
    '

Nforce3_values_rear = odb_1h.steps['Step-BC'].frames[1].fieldOutputs['
    NFORC3'].getSubset(region=instance.nodeSets['SET-REAR_NODES']).values
Nforce2_values_rear = odb_1h.steps['Step-BC'].frames[1].fieldOutputs['
    NFORC2'].getSubset(region=instance.nodeSets['SET-REAR_NODES']).values
Nforce1_values_rear = odb_1h.steps['Step-BC'].frames[1].fieldOutputs['
    NFORC1'].getSubset(region=instance.nodeSets['SET-REAR_NODES']).values

Nforce3_values_front = odb_1h.steps['Step-BC'].frames[1].fieldOutputs['
    NFORC3'].getSubset(region=instance.nodeSets['SET-FRONT_NODES']).values
Nforce2_values_front = odb_1h.steps['Step-BC'].frames[1].fieldOutputs['
    NFORC2'].getSubset(region=instance.nodeSets['SET-FRONT_NODES']).values
Nforce1_values_front = odb_1h.steps['Step-BC'].frames[1].fieldOutputs['
    NFORC1'].getSubset(region=instance.nodeSets['SET-FRONT_NODES']).values

size_force_rear = len(Nforce3_values_rear)
size_force_front = len(Nforce3_values_front)

```

```
directory=os.path.split(odb_1h.path)[0]
with open(os.path.join(directory,outPutFileName_forces_rear_front),"w")
    as file:
     for i in range(0,size_force_rear):
         file.write("%20s %20s %20s %20s %20s %20s %20s %20s" % (
             Nforce1_values_rear[i].nodeLabel, Nforce1_values_rear[i].data,
               Nforce2_values_rear[i].data,  Nforce3_values_rear[i].data,
             Nforce1_values_front[i].nodeLabel, Nforce1_values_front[i].
             data,  Nforce2_values_front[i].data,  Nforce3_values_front[i].
             data))
         file.write("\n")

odb_1h.close()
```

The example Python script for extraction of nodal displacement data on front and rear surfaces of the UC is as follows:

```
## FOR NODAL DISPLACEMENTS:

from abaqusConstants import *
from viewerModules import *
import os

odb_1h = session.openOdb(name='heterogeneous_UC.odb')
odbRootA=odb_1h.rootAssembly
os.chdir(r"path")
session.viewports['Viewport: 1'].setValues(displayedObject=odb_1h)

frames = odb_1h.steps['Step-BC'].frames
no_of_frames = len(frames)
my_instance = odb_1h.rootAssembly.instances['PART-MERGE-1']
node_region = my_instance.nodeSets['SET-REAR_NODES']
nodes = node_region.nodes
no_of_nodes = len(nodes)

outPutFileName_displacement_rear_front = '
    EXTRACTED_NODAL_DISPLACEMENTS_REAR_FRONT.txt'

displacement_rear = odb_1h.steps['Step-BC'].frames[1].fieldOutputs['U'].
    getSubset(region=my_instance.nodeSets['SET-REAR_NODES']).values
displacement_front = odb_1h.steps['Step-BC'].frames[1].fieldOutputs['U'].
    getSubset(region=my_instance.nodeSets['SET-FRONT_NODES']).values

size_displacement_rear = len(displacement_rear)
size_displacement_front = len(displacement_front)

directory=os.path.split(odb_1h.path)[0]

with open(os.path.join(directory,outPutFileName_displacement_rear_front),
    "w") as file:
     for i in range(0,size_displacement_rear):
```

```
31          file.write("%20s %20s %20s %20s %20s %20s %20s %20s" % (
                displacement_rear[i].nodeLabel, displacement_rear[i].data[0],
                displacement_rear[i].data[1], displacement_rear[i].data[2],
                displacement_front[i].nodeLabel, displacement_front[i].data
                [0], displacement_front[i].data[1], displacement_front[i].data
                [2]))
32          file.write("\n")
33
34  odb_1h.close()
```

Averaging of numerical stress data

This subsections illustrates through a Matlab script, the procedure that has been adopted throughout this work to calculate numerical average stress values. The averages are calculated such that the changes in mesh are accounted for. The example script is shown as follows:

```
1  % index starts with 2 to include first interval to the start calculation
       with
2
3  for j=2:length(X_Grid_Array_From_Free_Edge)
4      Sz_Integrated_Average(1,(j-1)) = trapz((X_Grid_Array_From_Free_Edge
           (1,1:j)),Sz_Data_From_Free_Edge(1,1:j))/(
           X_Grid_Array_From_Free_Edge(1,j)-X_Grid_Array_From_Free_Edge(1,1))
           ;
5  end
6
7  % 'Sz_Integrated_Average' has a dimension one less than that of the
8  % original array because the first value of integration is obtained at a
9  % distance of one element width and hence at second distance point of the
       array
```

Appendix C

Appendix 3: Comparison of homogeneous properties

During the course of this work, homogenised properties are determined through homogenisation of UC by using PBC. As a comparison, the homogenised engineering properties obtained from this approach are matched against those published in literature experimentally. Table C.1 shows the values obtained for T300/934 material from the two approaches.

Table C.1: Comparison of homogenised engineering constants for unidirectional ply of T300/934 material from homogenisation through PBC and experimental findings

Properties	Homogenisation (through PBC)	Experimental results in literature [9]
E_x (GPa)	141.61	144.8
E_y (GPa)	13.21	11.7
E_z(GPa)	13.21	11.7
ν_{xy}	0.2613	0.3
ν_{xz}	0.2613	0.3
ν_{yz}	0.4437	0.54
G_{yz} (GPa)	3.6757	3.5
G_{xz} (GPa)	4.2684	6.5
G_{xy} (GPa)	4.2684	6.5

A comparison of effective engineering properties from the two approaches suggests that the longitudinal shear moduli (G_{xy} and G_{xz}) are found to be under predicted by a comparatively larger difference when compared with experimental results. The small size of the RVE with a single UC considered during homogenisation through PBC is believed to be the reason for the under predicted shear moduli. The other properties are found to be comparing with each other with a relatively lower difference than the longitudinal shear moduli.